CALIFORNIA INSTITUTE OF TECHNOLOGY

EARTHQUAKE ENGINEERING RESEARCH LABORATORY
Center for Research on the Prevention of Natural Disasters

ANALYSIS OF THE EARTHQUAKE RESPONSE OF A NINE-STORY STEEL FRAME BUILDING DURING THE SAN FERNANDO EARTHQUAKE

by
John H. Wood

EERL 72-04

A Report on Research Conducted under Grants
from the National Science Foundation and
the Earthquake Research Affiliates Program
at the California Institute of Technology

Pasadena, California
October, 1972

CALIFORNIA INSTITUTE OF TECHNOLOGY
EARTHQUAKE ENGINEERING RESEARCH LABORATORY

ANALYSIS OF THE EARTHQUAKE RESPONSE OF A NINE-STORY STEEL FRAME BUILDING DURING THE SAN FERNANDO EARTHQUAKE

by

John H. Wood

Report No. EERL 72-04

A Report on Research Conducted under Grants
from the National Science Foundation and
the Earthquake Research Affiliates Program
at California Institute of Technology

Pasadena, California

October, 1972

ABSTRACT

A study has been made of the earthquake response of the nine-story steel frame Building 180, located at the C. I. T. Jet Propulsion Laboratory, Pasadena, during the San Fernando earthquake of February 9, 1971. The study was motivated by the likelihood that an earthquake similar to the February 9, 1971, shock could occur close to the JPL grounds with consequent very strong ground shaking. It was, therefore, judged desirable to make a thorough study of the response of the building to the moderately strong ground shaking during the February 9, 1971 event. The analysis throws light on the actual dynamical properties of the building during the earthquake, and also demonstrates that it is possible to make accurate calculations of building motions during earthquakes when the ground motion is specified.

Methods of evaluating the lower mode periods and damping ratios from the earthquake records are described and these values are compared with values obtained by dynamic testing before and after the earthquake and with the periods computed from structural models of the building. Although no structural damage, as a result of the earthquake motions, was detected, and computed stresses in the frame were less than yield stresses, the ambient test periods after the earthquake were approximately 10% higher than the pre-earthquake test values. The maximum periods during the earthquake were found to be about 30% higher than the post-earthquake ambient test values, and it is believed that this significant increase was mainly the result of the non-linear behavior of the concrete encased steel columns. The periods computed from the structural models based on two different assumptions regard-

ing the influence of the composite concrete agreed within 5% of the post-earthquake ambient test results and within 10% of the earthquake periods.

The model roof acceleration responses were computed using the recorded base motions as inputs. Good agreement was obtained between the recorded and computed roof responses confirming that the elastic response computation method currently used in the earthquake design of buildings gives satisfactory stress predictions.

A stress analysis of the lower stories of the model gave a maximum total steel stress during the earthquake of 34 Kips/in^2. This maximum value occurred in the second story columns and was computed by adding to the gravity load stresses the root-mean-square sum of the two horizontal earthquake stress components.

The Fourier amplitude spectra of the recorded horizontal base motions were found to contain peaks corresponding closely with a number of the lower mode natural frequencies. A study was undertaken to determine whether these peaks could have resulted from soil-structure interaction. It was concluded that soil-structure interaction would be unlikely to have produced significant changes to the horizontal free-field motions. The influence of soil-structure interaction in the vertical direction was found to be rather more significant, producing a peak and a dip in the Fourier amplitude spectrum close to the fundamental vertical frequency.

TABLE OF CONTENTS

1. INTRODUCTION

The California Institute of Technology, Jet Propulsion Laboratory is located at the base of the San Gabriel Mountains, 16 miles southeast of the Pacoima Dam which was near the center of energy release of the February 9, 1971 San Fernando earthquake (Fig. 1). The easternmost extent of the ground breakage resulting from the faulting causing this magnitude 6.5 earthquake terminated some 9 miles from the Laboratory. A description of the earthquake and a detailed account of its effects has been presented by Jennings[7]*.

After the earthquake, while excavating for a bridge foundation, an east-west trending fault plane was exposed, which traversed the northern portion of the JPL grounds. Figure 2 shows an aerial photograph of the JPL buildings and the fault location as determined by Converse, Davis and Associates[3], consulting geologists. This thrust fault appeared to dip downward to the north about 45^{o} under the San Gabriel mountains. At the excavation the fault had granite above, and geologically recent gravel beneath, which indicates that the fault should be classified active. The fault exposed on the JPL grounds was similar to the fault on which the San Fernando earthquake occurred and appeared to be an extension of this fault system. This raised the following question. How would the buildings at JPL behave if the San Fernando earthquake were to be followed by a similar event on the fault close to the JPL grounds? This question motivated the present study of how Build-

---

* Numbers in brackets designate References listed on page 130.

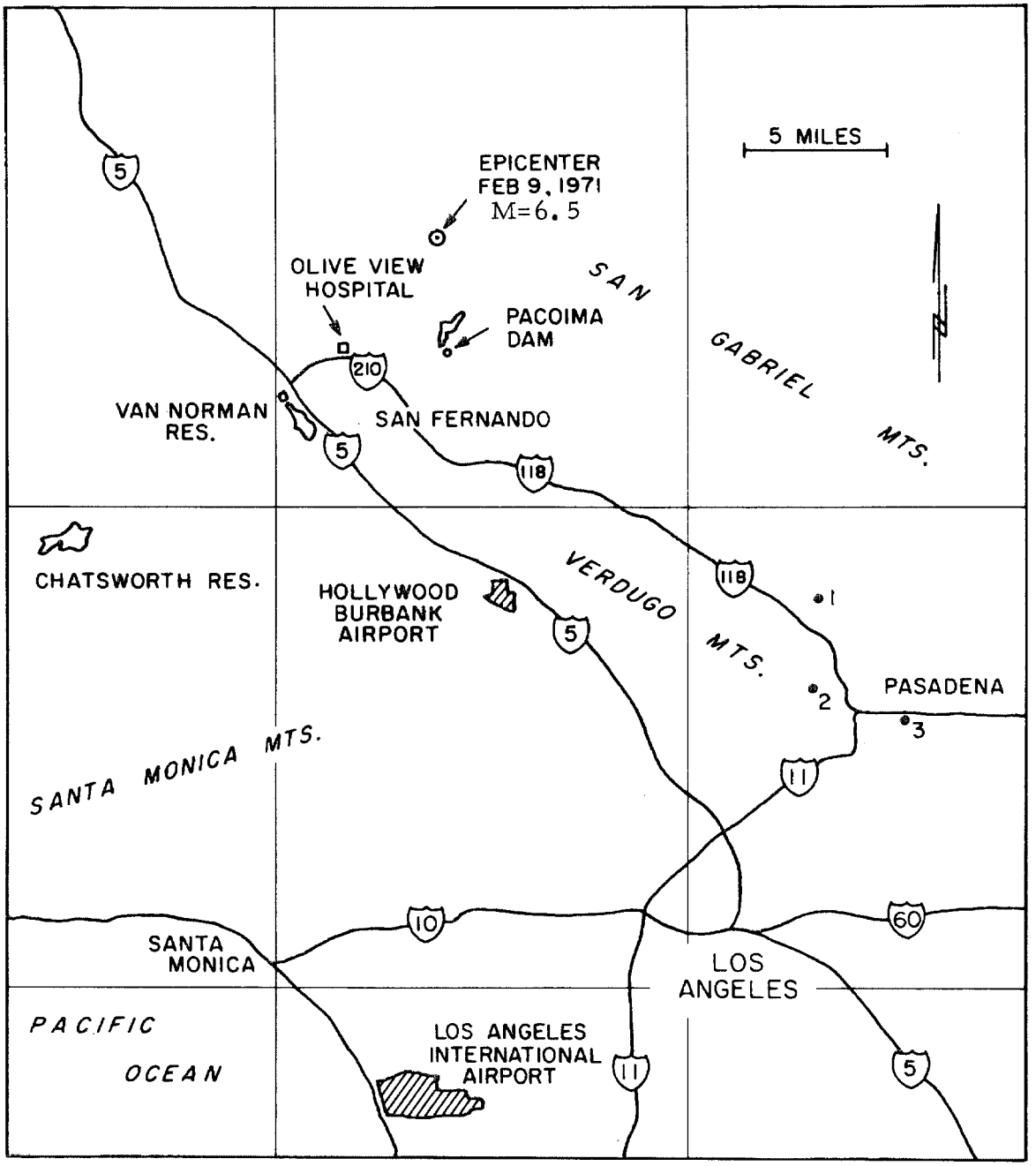

1. JET PROPULSION LABORATORY, BUILDING NO. 180.
2. SEISMOLOGICAL LABORATORY
3. CALTECH CAMPUS, MILLIKAN LIBRARY & ATHENAEUM.

LOCATION OF CALTECH ACCELEROGRAPHS

Figure 1.

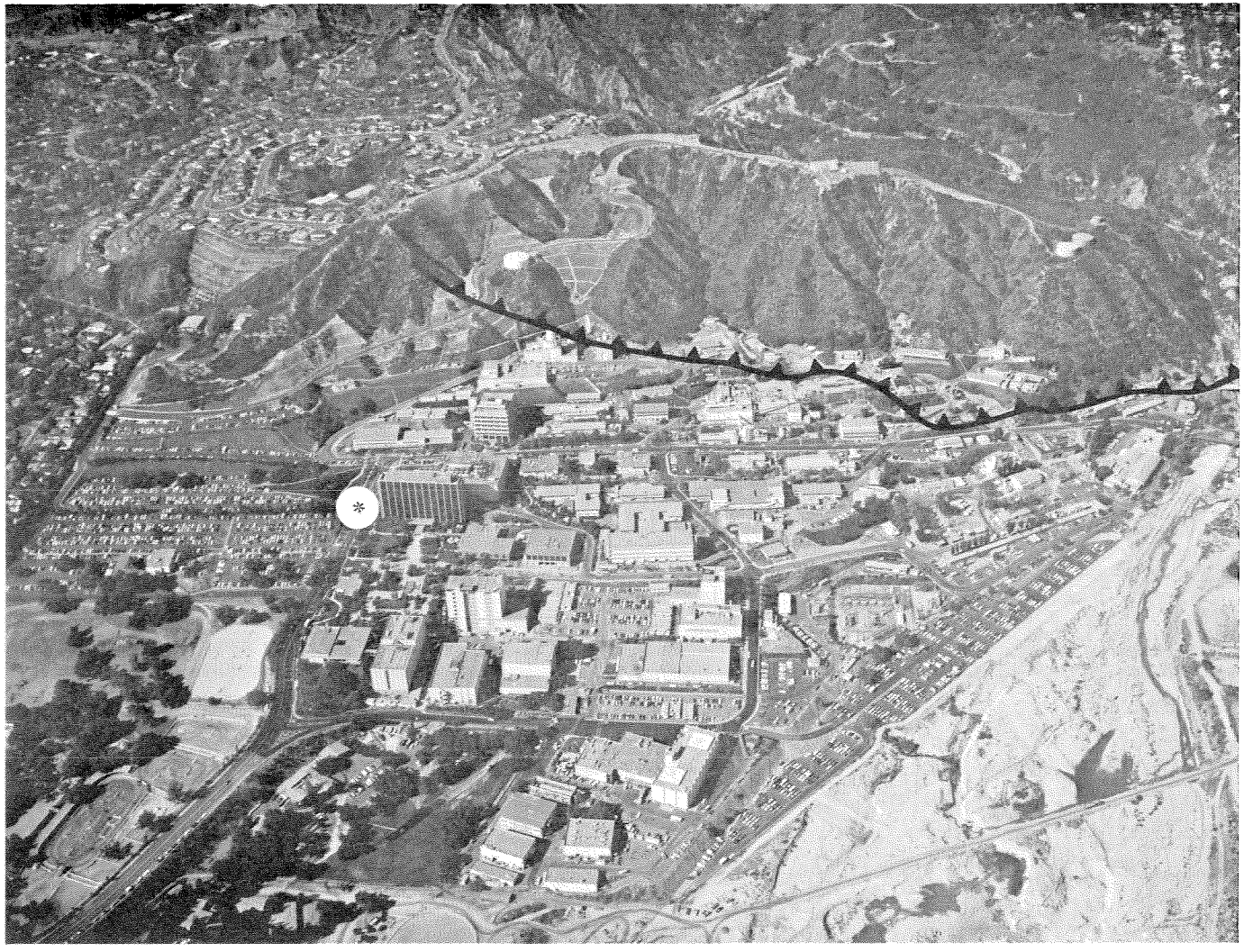

Figure 2. Aerial view of Jet Propulsion Laboratory showing fault trace as located by Converse, Davis and Associates. *Building 180.

ing 180 behaved during the San Fernando earthquake. This study is the first stage in answering the foregoing question.

Two RFT-250 strong-motion accelerographs were located at JPL in the Central Engineering Building, Building 180, and produced excellent records of the San Fernando earthquake motions. These instruments are part of a Caltech telephone line accelerograph system which links four instruments, separated by a maximum distance of about five miles, between the Jet Propulsion Laboratory, the Caltech Seismological Laboratory and the Millikan Library building on the main Caltech campus. The instruments are so arranged that the first to trigger simultaneously starts the other instruments. An accelerograph which is not connected to the telephone line system is located in the basement of the Athenæum building on the campus. The location of the network is shown in Figure 1. One of the instruments in Building 180 is located inside a mechanical equipment room on the concrete roof slab, and the other instrument is seated on the concrete floor slab which rests directly on the foundation soil. The plan location of the instruments in the building is shown in Figure 7.

1.1 BUILDING 180

Building 180 is an administrative building for the Jet Propulsion Laboratory with most of the floor space occupied by offices. Typical details and dimensions of the nine-story steel frame structure are shown in Figures 3 to 7. The north and south faces of the building are of glass curtain wall construction and the narrow east and west end walls consist of precast concrete panels supported by the steel frame.

Lateral loads in the north-south direction are resisted by the rigid frame action of the partly concrete encased steel columns and the welded steel trussed floor girders; in the east-west direction they are resisted by the action of the columns and the trussed spandrel girders. Earth retaining walls in the basement and first-story add appreciable stiffness to the frames in their lower sections. All the members in the east-west trusses are constructed of 8 in x 11.5 lb channel sections. The north-south trusses are constructed of a variety of T and angle sections and generally the section properties of the members decrease with height in the building. Both sets of trussed girders are bolted to the steel column sections. The 5 in thick lightweight concrete floor slabs are supported on east-west directed 12WF27 steel beams and on the north-south trusses.

The columns were originally designed as fully encased but were constructed with only the outer section of concrete in order to reduce the cost.

Figure 3. JPL Building 180. South face.

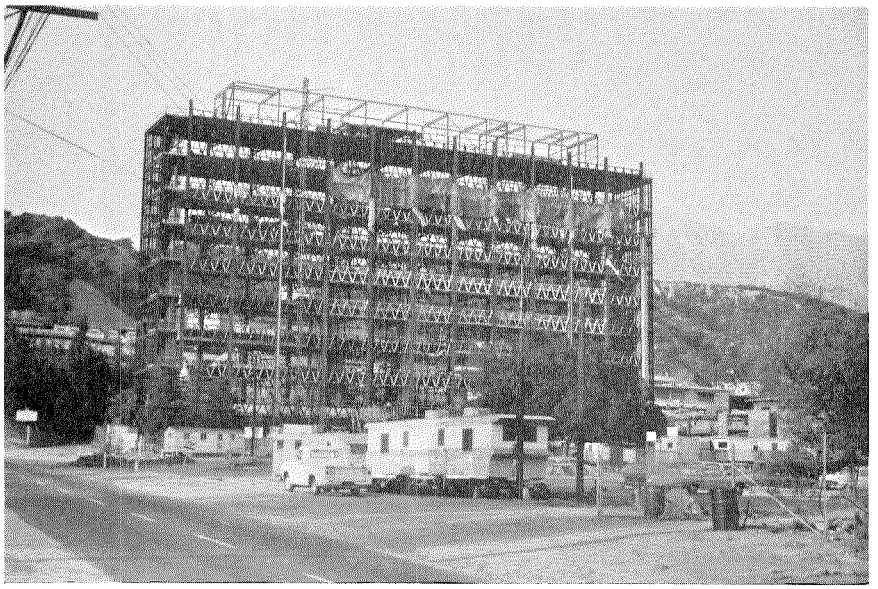

Figure 4. Building 180 under construction. South face.

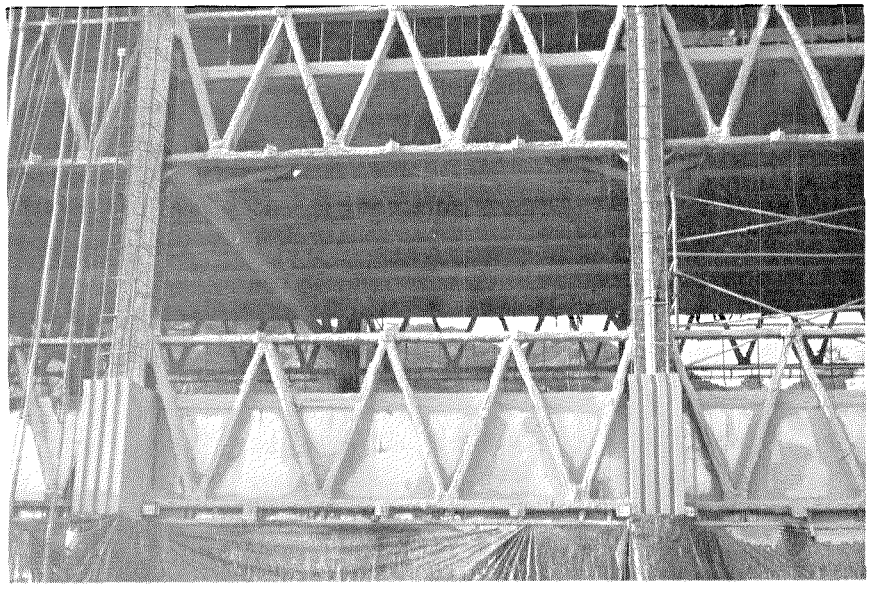

Figure 5. Building 180. E-W spandrel truss.

Figure 6. Building 180 under construction. Interior view.

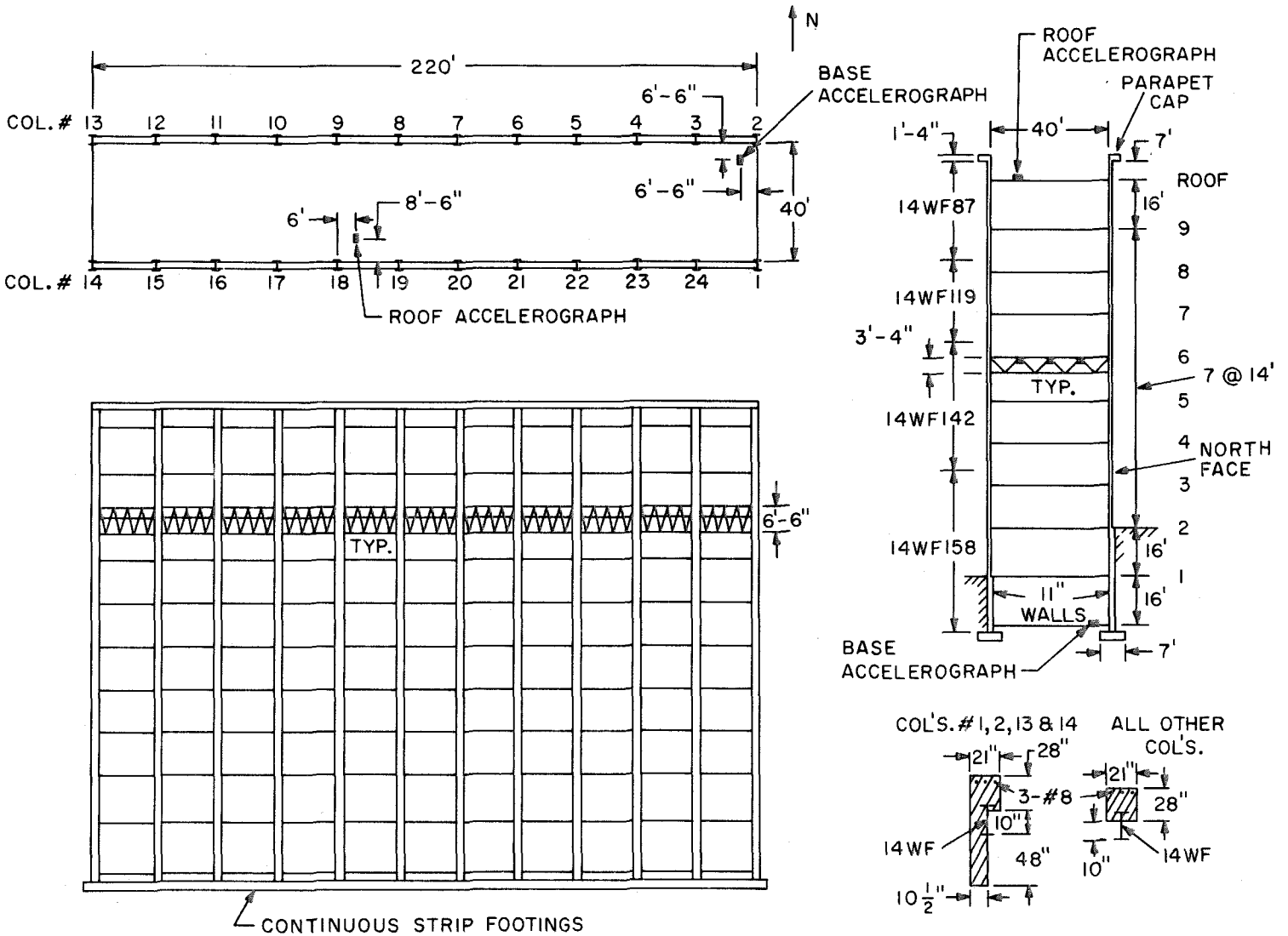

JPL BUILDING 180

Figure 7.

1.2 BUILDING 180 FOUNDATIONS AND SITE GEOLOGY

The building is located on a moderately sloping ancient alluvial flood plain about 1,000 feet from the intersection of the plain and the steeply rising San Gabriel Mountains. The foundation soil is a firm alluvium consisting of moderately dense sand, gravel and boulders with varying proportions of silt. A typical bore-hole log of the material at the building site, reproduced from the foundation investigation report[28], is shown in Figure 8. Water wells drilled downslope from the site suggest that the depth of alluvium covering the granitic basement rock in the vicinity of the building may be between 200 - 300 ft[3].

In an investigation of the fault on the JPL site, Converse, Davis and Associates[3], consulting geologists, measured the p-wave velocity of the ancient alluvium in a locality about 1,200 ft from the building and close to the base of the mountain slope to be 1,700 ft/sec at a depth below ground surface of 30 ft. It is believed that the alluvium in this locality is similar to the building foundation material.

The structural foundation consists of 7 ft wide continuous reinforced concrete spread footings around the perimeter of the building.

LOG OF BORINGS BORING NO. 2

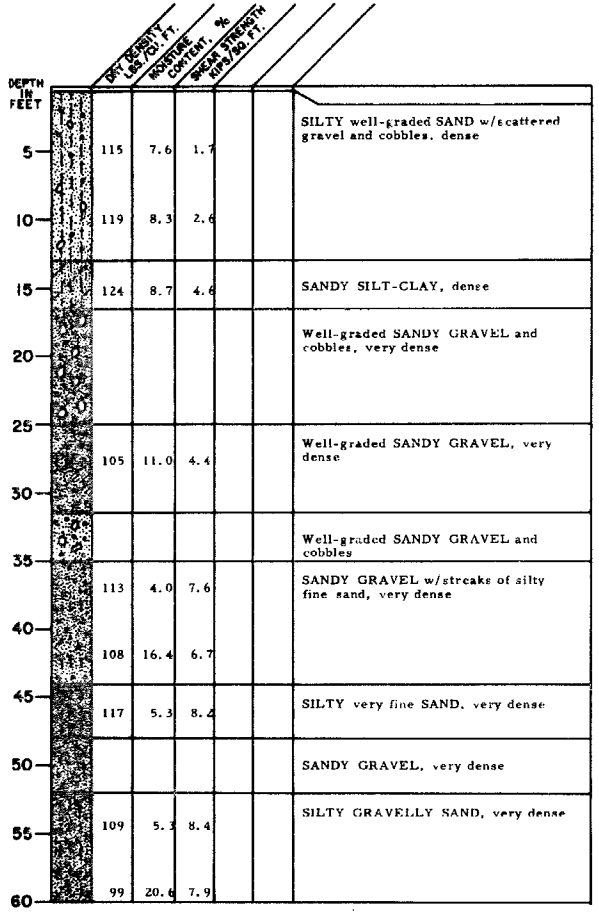

TYPICAL TEST BORING JPL BUILDING 180

LOG OF BORINGS BORING NO. 2

DEPTH IN FEET	PROFILE	CHARACTERISTICS			CODE CLASSIF.	DRIVE ENERGY FT. KIPS/FT.	FIELD MOIST. % DRY WT.	DRY DENSITY LB/CU FT.	SHEAR RESIST KIPS/SQ.FT.
5	Dry	Medium	Dark Brown	SILTY + 10% Gr. to 2"	SM	1.7	4.7	98.0	0.31
		Soft	Brown	SAND (Fine + 20% Gr. to 2" To + 30% Gr. to 3" Coarse) & occ. rock to 6"	SM	0.7 7.1	4.0 3.3	100.1 99.8	0.35 0.91
10		Medium	Light Brown	SAND + 40% Gr. Fine to Coarse + 20% Gr.	SW	1.8	2.6	105.6	0.88
		Loose M. Firm		SILTY SAND	SM				
15		Dense		SAND + 30% Gr. Fine to Coarse to 3"	SW	8.2	3.9	113.2	0.69
		Firm		SANDY SILT	ML				
20		Firm		SILTY SAND + 30% Gr. to 3"	SM	11.3	4.4	121.5	1.00
25		Dense		SAND + 40% Fine Gravel To To 3" & occ. rock Coarse to 6"	SW	12.0 13.2	2.3 3.0	112.3 119.4	1.13 1.80
30	Slightly moist			9" Sandy Silt Streak		10.5	7.1	105.2	2.39
35	Moist	Firm	Brown	Alt. Merging 1" - 3" Streaks Sandy Silt to Silty Sand	ML & SM	9.7	7.7	101.0	2.64
		Dense	Light Brown	SAND + 30% Gr. & Rock to 6" (Fine to Coarse) & occ. Silty Sand Streak	SW & SM				
40		Firm	Brown	SILTY SAND	SM				
				SANDY SILT	ML	5.9	2.2	105.6	3.04
45				SILTY Fine to Medium SAND - occ. Gravel + Alt.	SM & ML	15.0	9.4	113.8	3.66
50				Streaks of + Str. Sandy Silt of Sand + 20% Gr.	& SW	17.3	11.2	99.5	3.18
55		Dense	Light Brown Brown	SAND Fine to Coarse + 30% Gravel 7" Silty Sand Streak	SW	12.0	3.7	98.8	3.55

TYPICAL TEST BORING MILLIKAN LIBRARY

Figure 8.

1.3 MILLIKAN LIBRARY AND SEISMOLOGICAL LABORATORY SITES

The relatively close proximity of the Millikan Library and the Caltech Seismological Laboratory accelerographs to the Building 180 site enables some interesting deductions to be made regarding the influence of site geology on the ground motions. A comparison of the Building 180 records with the ground motions at the other stations was found to give some indication of whether soil-structure interaction significantly modified the Building 180 records.

The Seismological Laboratory is sited 3.4 miles due south of Building 180 and is located on an outcrop of granitic basement rock. The accelerograph foundation is seated directly on to rock and is isolated from any structural interference.

The Millikan Library is sited on the Caltech campus, 5.1 miles south-east of Building 180 and about 3 miles south of the intersection of the alluvial plain with the base of the San Gabriel Mountains. The Athenæum building is sited approximately 1,100 ft east of the Library. The alluvial material at the campus extends approximately 1,000 ft to bedrock and at the base of the structural foundation of the Library building consists of a dense sand with 40% gravel. A bore hole log taken at the Library site is shown in Figure 8.

The Library building is a nine-story reinforced concrete structure. Lateral load resistance in the north-south direction is provided by reinforced concrete shear walls and in the east-west direction by a central reinforced concrete elevator tower. The north and south façades consist of precast concrete grill window wall panels located

between reinforced concrete columns. The frame action between the panels and the columns provides additional lateral stiffness to the structure. The shear walls, central tower and exterior columns have reinforced concrete inter-connected strip footings. A foundation plan of the building is shown in Figure 9.

During the final stages of construction in 1966-1967 the Library building was subjected to an extensive dynamic test study. Details of the building and the test results are given by Jennings and Kuroiwa[8].

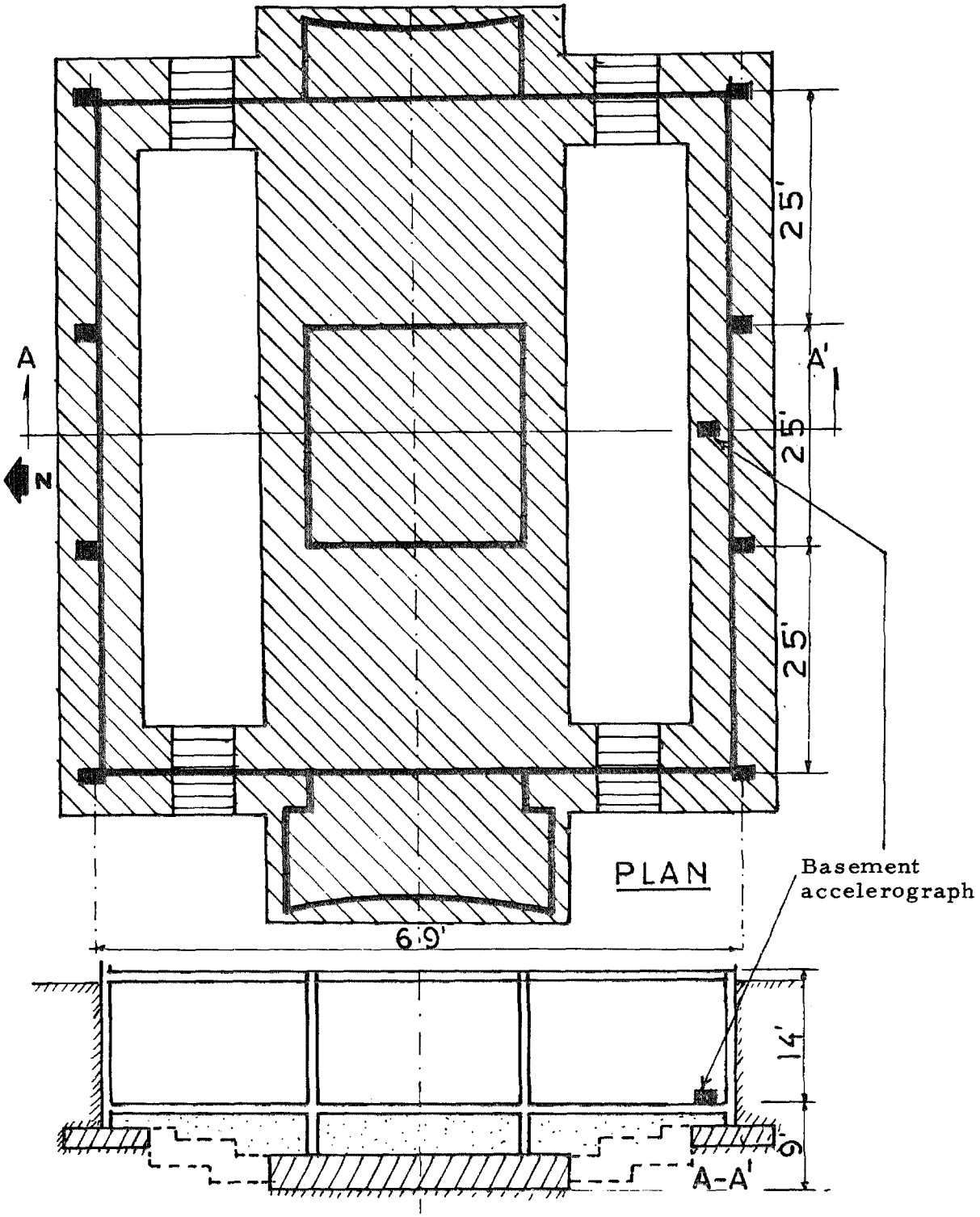

Figure 9. Millikan Library foundation details.

2. DYNAMIC TESTING OF BUILDING 180

Building 180 was subjected to forced and man-excited dynamic testing by Nielsen[18] during and after the completion of construction in 1963. Tests of particular interest to this study were a forced vibration test conducted on the completed structure before the windows, partitions and other architectural work was placed and a man-excited test performed with all the architectural work complete and the building ready for occupancy.

In July 1971 (after the San Fernando earthquake) Teledyne Geotech West[25] was engaged to measure natural frequencies and mode shapes in an ambient vibration survey of the building.

Natural frequencies were determined by a further series of man-excited tests conducted by Teledyne and Nielsen[25] in February 1972.

The measured values of the horizontal translation mode periods are compared in Tables 1 and 2 with the values obtained by the other methods described in this study.

Periods of two well defined torsional modes and a floor slab free-free beam mode were also measured during the tests. Values of interest are given in Table 3.

TABLE 1

JPL BUILDING N - S DIRECTION

COMPARISON OF MEASURED AND COMPUTED PERIODS

	PERIODS SEC			FREQUENCY RATIOS		
	T_1	T_2	T_3	f_1	f_2	f_3
Man-excited test, 1963 - Nielsen	0.88	0.29	-	1.0	3.1	-
Forced vibration test, 1963 - Nielsen (Architectural work not complete)	1.03	0.31	0.16	1.0	3.3	6.4
Ambient test, July 1971 - Teledyne	1.11	0.35	0.16	1.0	3.2	7.0
Man-excited test, Feb. 1972 - Teledyne, Nielsen	1.15	0.31	-	1.0	3.7	-
Computed using full composite column model	1.16	0.34	0.17	1.0	3.4	7.0
From Fourier spectrum Feb. 9, 1971 EQ record (0.-40. sec.)	1.44	0.44	0.24	1.0	3.3	6.1
Computed using partial composite column model. free at floor 2	1.46	0.47	0.26	1.0	3.1	5.6
Computed using partial composite column model, held at floor 2	1.29	0.41	0.22	1.0	3.2	5.9

TABLE 2

JPL BUILDING E - W DIRECTION

COMPARISON OF MEASURED AND COMPUTED PERIODS

	PERIODS SEC			FREQUENCY RATIOS		
	T_1	T_2	T_3	f_1	f_2	f_3
Man-excited test, 1963 - Nielsen	0.91	0.29	-	1.0	3.1	-
Forced vibration test, 1963 - Nielsen (Architectural work not complete)	0.99	0.33	0.20	1.0	3.0	5.0
Ambient test, July 1971 - Teledyne	1.05	0.33	0.20	1.0	3.2	5.2
Man-excited test, Feb. 1972 - Teledyne, Nielsen	1.00	0.30	-	1.0	3.3	-
Computed using full composite column model	1.09	0.36	0.21	1.0	3.0	5.1
From Fourier spectrum Feb. 9, 1971 EQ record (0.-40. sec.)	1.29	0.42	0.26	1.0	3.1	5.0
Computed using partial composite column model	1.21	0.42	0.26	1.0	2.9	4.7

TABLE 3

TORSION AND FREE-FREE BEAM PERIODS

Test	Periods Sec		
	First Torsion	Second Torsion	Free-free Beam
Man excited test, 1963, Nielsen	0.73	0.26	-
Forced vibration test, 1963, Nielsen	0.92	0.27	0.20
Ambient test, July 1971, Teledyne	0.91	0.28*	0.20*
Man excited test, Feb. 1972, Teledyne-Nielsen	0.93	-	0.28

* The typical mode shapes were not positively identified in this test.

3. STRONG MOTION RECORDS

The first 40 sec. of the Building 180 San Fernando records are presented in Figures 10, 11 and 12. For convenience in this report, the records are referred to as N-S and E-W but the more precise orientations of the instrument axes are S08W and S82E.

The instruments recorded the initial earthquake motions for a duration of approximately 100 sec. The recorded roof accelerations beyond 40 sec did not exceed 1.5% g and so can be considered as low amplitude motions in comparison with the strongest shaking which exceeded 20% g in all three components. A feature of interest in the records is the arrival of the first aftershock motion at about 31 sec.

The peak accelerations recorded in Building 180 are compared in Table 4 with peak values recorded at the other two telephone network localities and by the Athenæum basement instrument.

TABLE 4

LOCATION OF INSTRUMENT	PEAK ACCELERATION % g		
	N-S	E-W	Vert.
Building 180 Roof	21.7	38.7	27.4
Building 180 Basement	14.2	21.1	12.8
Millikan Library Basement	20.2	18.6	9.4
Athenæum Basement	9.5	11.1	9.5
Seismological Laboratory	9.1	18.2	8.0

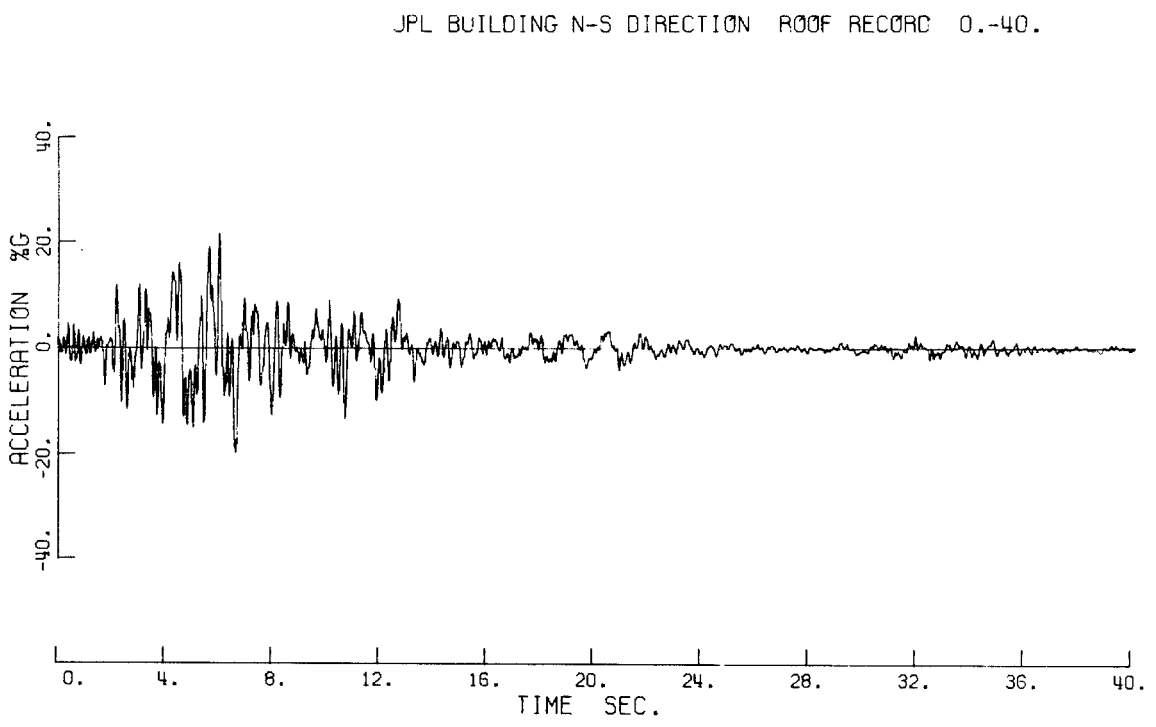

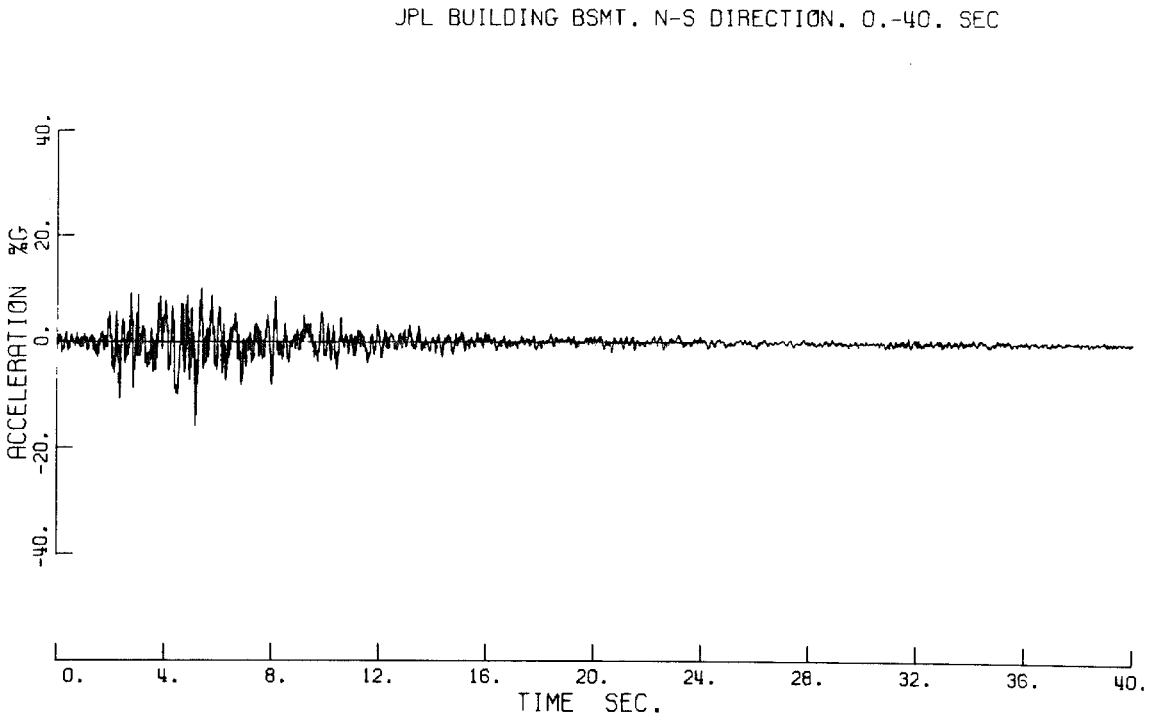

Figure 10. Recorded Accelerations.

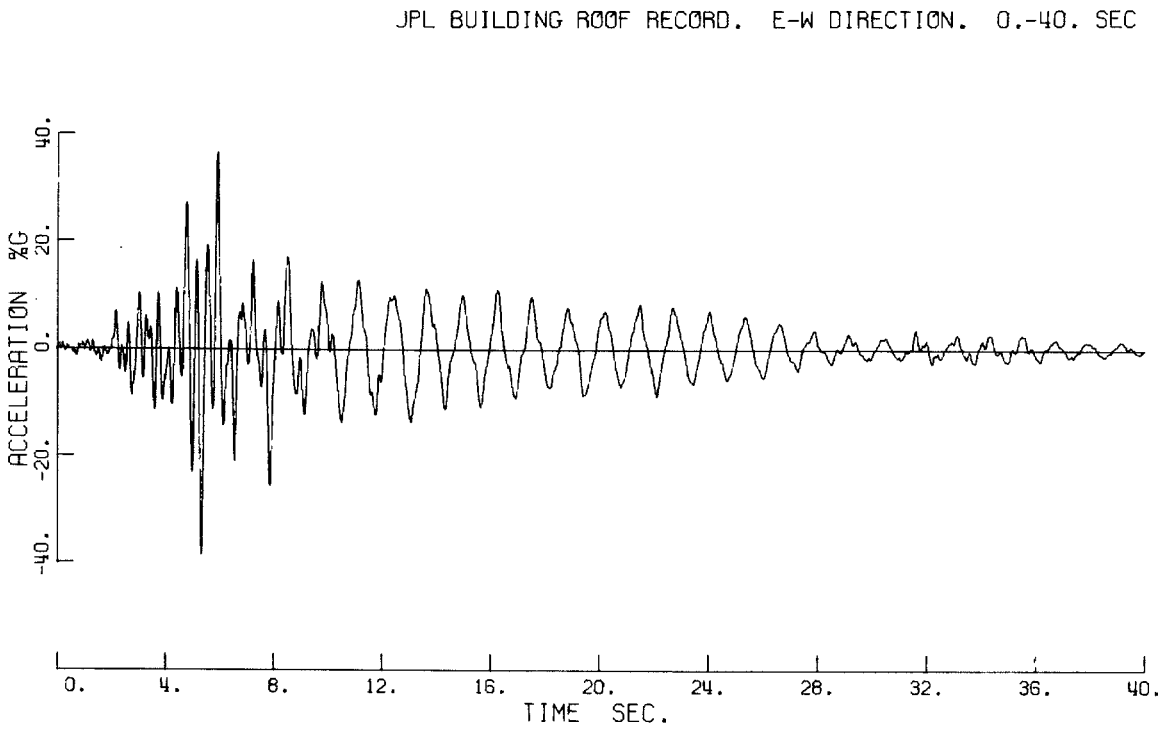

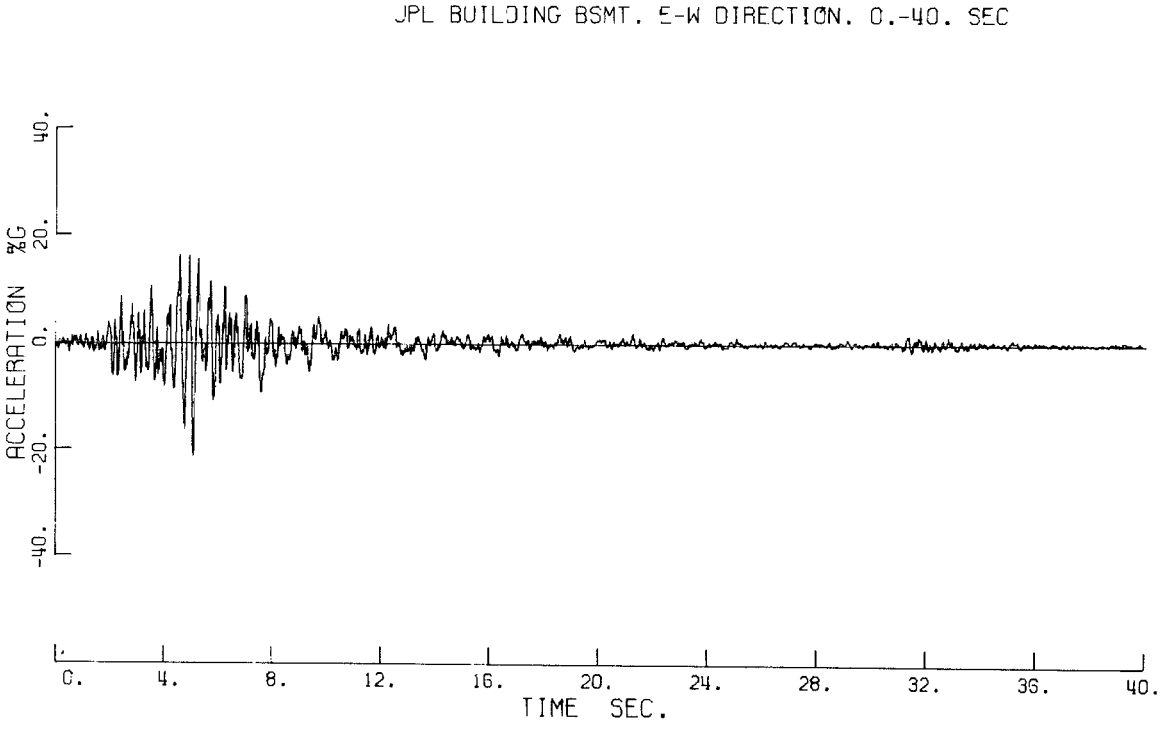

Figure 11. Recorded Accelerations.

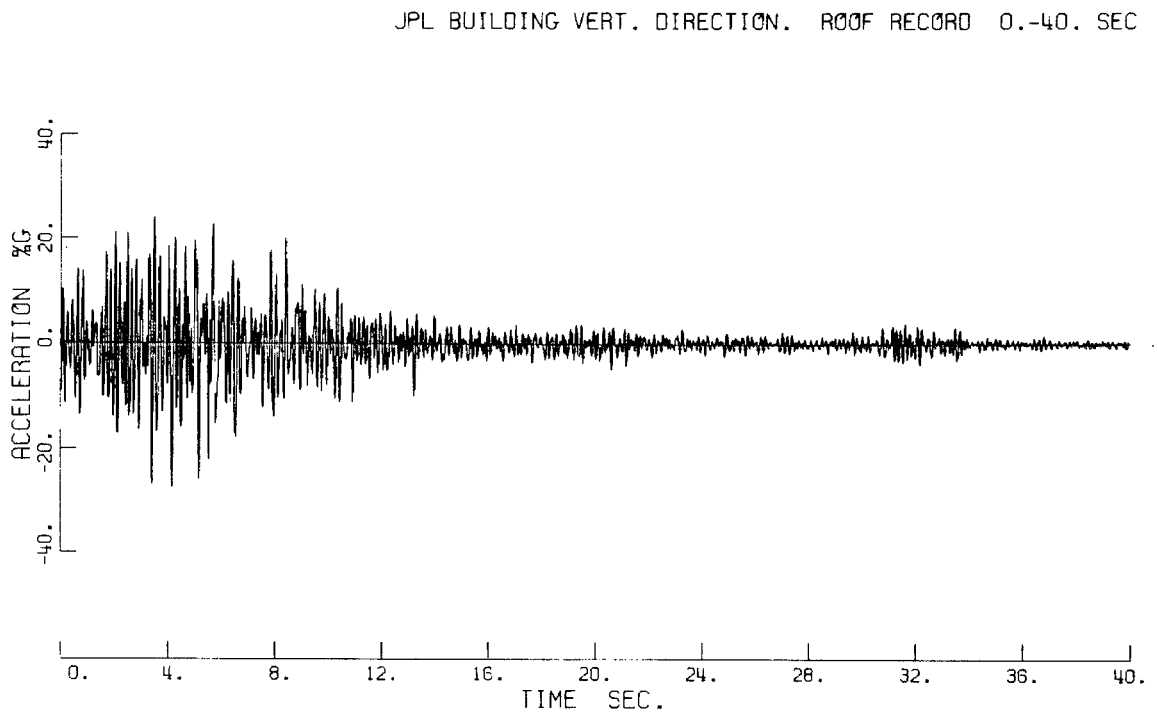

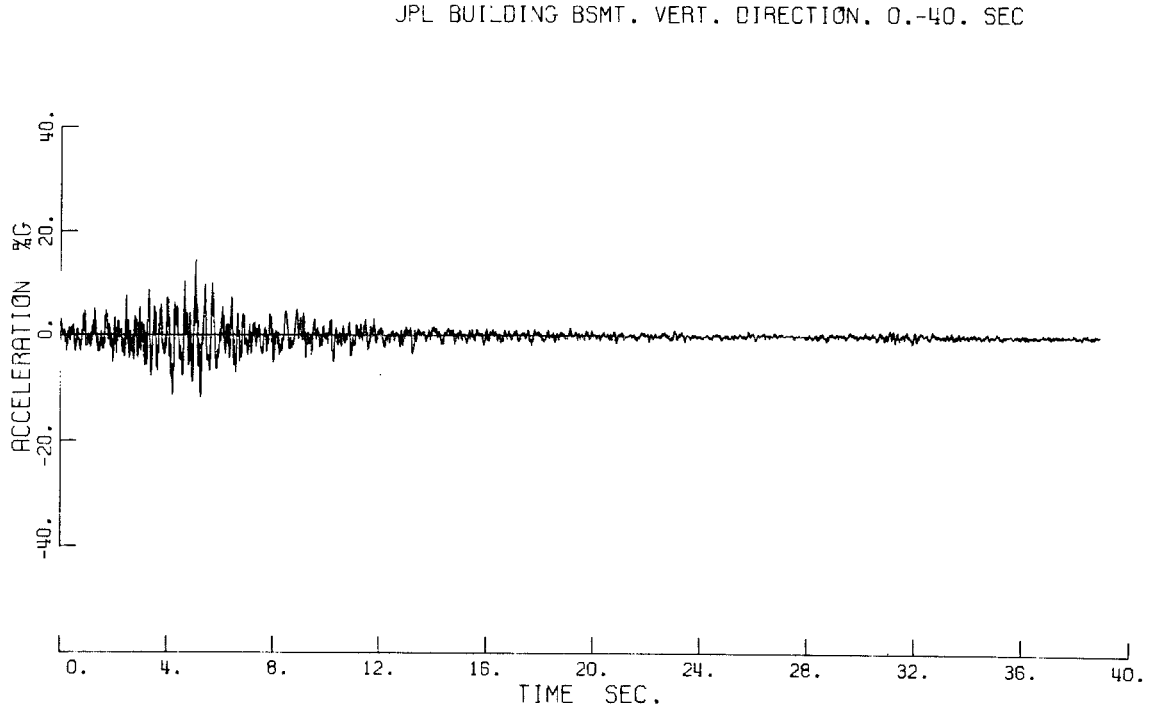

Figure 12. Recorded Accelerations.

It is not possible to attach any major significance to peak acceleration values but a general interpretation might be that there was no major dissimilarity in the intensity of shaking at the three localities. The peak horizontal accelerations recorded at the Millikan Library and Athenæum differ significantly, which is perhaps unexpected in view of the close proximity of the two buildings. A comparison by Hudson[10] of the relative velocity response spectra computed from the recorded accelerograms at both buildings showed significant differences over the frequency range of 0.3 to 3.0 hz. The Athenæum is a very rigid concrete structure with two stories and a basement. It is thought that soil-structure interaction did not have significant influence on the Athenaeum record but at present no detailed studies have been made to investigate this effect. A more detailed study of the Caltech accelerograms is given by Hudson[10] and a comparison of the Fourier amplitude spectra computed from some of the records is made in Section 10 below.*

The earthquake motions produced no visible damage to Building 180 although some cracking was observed in the elastomeric paint finish on the concrete encasing the columns. Cracking of a number of non-structural plaster walls surrounding the stairwells and the displacement of some of the suspended ceilings was reported by Brandow and Johnson Associates[2], consulting engineers.

Details of the maximum computed stresses occurring during the earthquake are given in Section 9 of this report. The stresses computed in the steel frame members were below yield stress.

* Complete plots of the Caltech accelerograms and listings of digital data obtained from the records are given in Reference 11a.

4. STRUCTURAL MODELS

To facilitate a study of the recorded building motions, it was found necessary to develop a number of simplified structural models. In this study, the three-dimensional frame was represented by three independent two-dimensional models; two translational and one vertical. This simplification excluded the possibility of directly studying the influence on the response of torsion, free-free slab and higher order vertical modes of vibration, but significantly reduced the amount of computation required in the dynamic analysis.

Some earthquake excitation of torsional modes of the building might be expected because, although the building is essentially structurally symmetric, the dynamic tests showed that the torsion natural frequencies were close to the horizontal translation mode frequencies. (A discussion of torsion in buildings with close translational and torsion periods has been presented by Skinner et al[24]). Because the torsional motion of the building cannot be determined from the accelerograph records and because this motion was considered to be of secondary importance, its effects have not been studied. It is unlikely that free-free slab and higher order vertical modes have significant participation under earthquake excitation and therefore it was considered unnecessary to study their effect.

From a study of the independent two-dimensional models it is frequently possible to find sufficient structural simplifications to permit the development and analysis of a simplified three-dimensional model. An alternative method of studying torsional effects is to include

a rotational degree of freedom as well as a translation degree of freedom at each floor level of the two-dimensional model. Either of the above approaches would be suitable for extending the analyses of Building 180 described in this report to include torsional effects.

Part of this study is concerned with the computation of roof accelerations using the recorded base motions as input to the building system. The recorded base motions are a superposition of the free-field earthquake translation motions and the relative translation movement of the base. Hence, the correct model for computing the roof responses from the records should have a base rigid in the translation sense but capable of rotational deformation about the horizontal axes. In general the rotation of the base is not recorded (except possibly as a component of the vertical record), but if the base rotation were known a model with a completely rigid base could be used to compute the building response. The influence of base rotation on the response of the building in the N-S direction was checked by undertaking a static analysis of both a rigid base and a flexible base structure with a base stiffness derived from the elastic soil parameters computed in Section 10. Under a static 100% g lateral load the top story deflection of the flexible base model was 3% greater than the rigid base model. Consequently it was concluded that base rotation would modify the N-S natural frequencies by less than 2% and that in the long E-W direction the influence of rotation would be considerably less significant. In view of the fact that a number of other necessary assumptions (for example the influence of the concrete encasement on the columns) were considered

to introduce considerably larger errors, the influence of base rotation was neglected.

The basic rigid base structural models were developed from the stiffness properties of the frame members and the calculated story weights. After completing a study of the earthquake response of these basic models, refined models were obtained by adjusting the periods of the lower modes to agree with the predominant periods found from an investigation of the recorded accelerograms. The three lowest periods of the horizontal models and the fundamental period of the vertical model were adjusted. The mode shapes (or participation factors) of the refined models were assumed to be the same as the shapes obtained from the analysis of the basic models. The error introduced by this assumption is small since in general it is found that mode shapes are relatively insensitive to changes in the frame member stiffnesses provided the changes are relatively uniform over the building height.

4.1 HORIZONTAL DIRECTION E-W MODEL

The E-W frames were simplified by summing the column and girder stiffness in each story to reduce the 12-bay frame to an equivalent single-bay frame. Because of the uniformity of the building along its length and the large number of bays this approximation gives rise to only small errors in the dynamic properties. One difficulty arises from the fact that the column axial deformations are accentuated by the large reduction in width of the frame. For the purpose of this study the axial deformations in the E-W equivalent single-bay frame were suppressed by increasing the column axial stiffnesses by an arbitrary factor of 10. On the assumption that column axial deformations do not occur in either the full 12-bay frame or the equivalent single-bay frame the error in the fundamental mode period resulting from the approximation was estimated to be less than 1%. This error tends to decrease with increasing mode number.

The basement and first-story walls provide significant stiffening to the E-W frames. In the dynamic tests no displacement was detected at or below the second floor level. On the basis of the test results and structural stiffness calculations the assumption was made that the E-W columns were held against translation at the second-floor level and fully fixed at the first floor. (Because of the difference in height of the concrete walls on the north and south sides of the building a somewhat more correct model could be achieved by considering two frames with different base fixity conditions).

A preliminary static analysis was made to study the possibility

of simplifying the frame by replacing the trussed girders with either rigid girders or equivalent uniform beams. The equivalent single-bay trussed girder model and the two simplified models are shown in Figure 13. The rigid girder model was formed by assuming that each trussed girder could be replaced by a single frame member having infinite flexural stiffness. In the equivalent uniform beam model the trusses were replaced by beams having moments of inertia computed from the sum of the top and bottom chord areas multiplied by the square of half the distance between the chords. In both simplified models the column heights were taken as the distance between floor slab centers.

The model static deflection curves resulting from the application of a 100% g horizontal loading are shown in Figure 13. The rigid girder assumption was found to be a poor approximation to the trussed girder model and the equivalent uniform-beam model was 10% stiffer than the trussed model. A more detailed examination of the trussed girder model revealed that axial deformations of the diagonal members allow the top and bottom chords of the truss to move relative to one another in a horizontal shearing like action. The deflected shape of the fifth-floor spandrel truss is shown in Figure 14. The truss "shearing" deformations accentuate the column rotations at each floor level with a resulting increase in frame flexibility.

In view of the results of the static analyses it was concluded that the more exact trussed girder model was required for the dynamic study.

The concrete encasement on the columns increases the bare

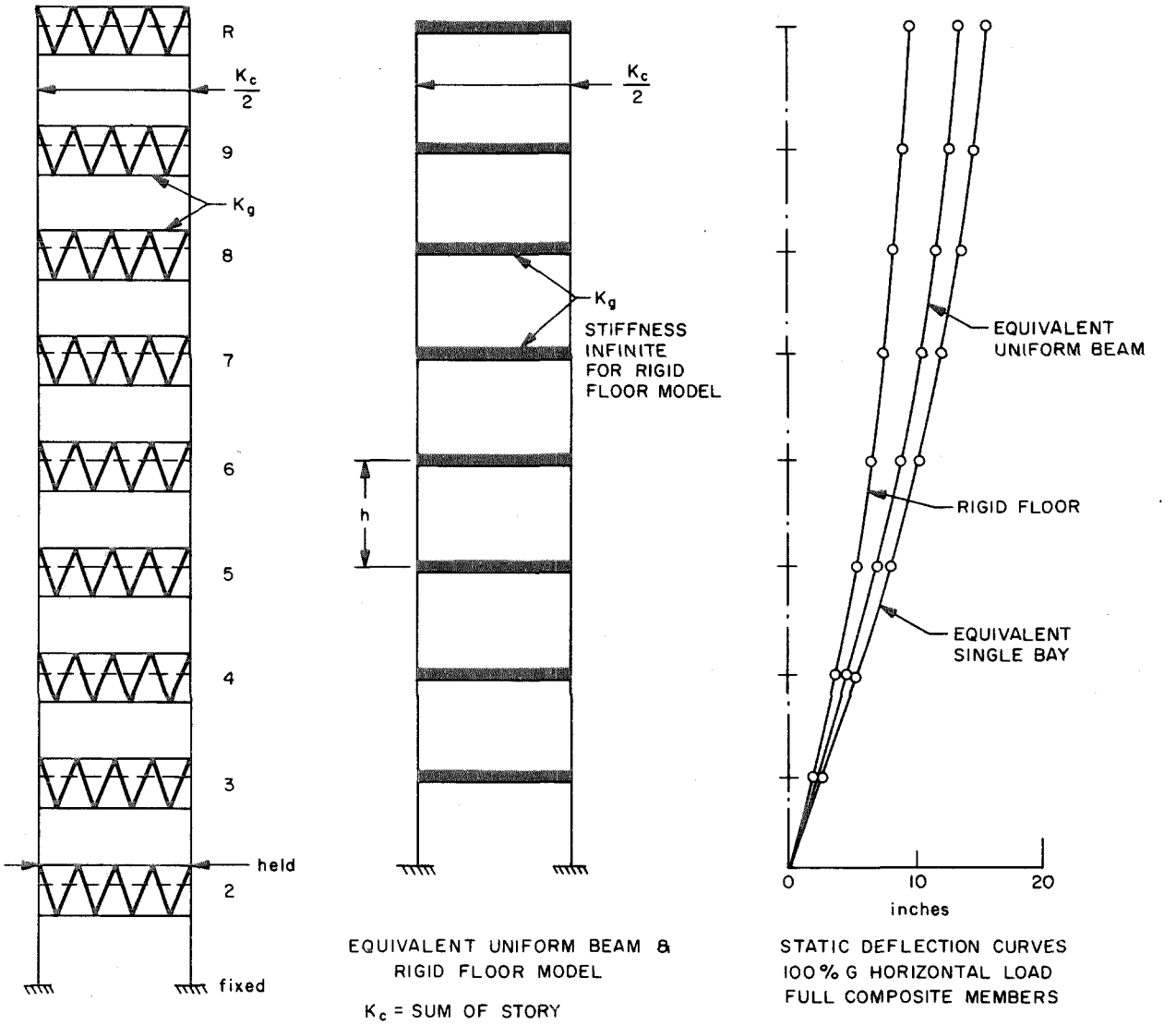

JPL BUILDING E-W MODELS

Figure 13.

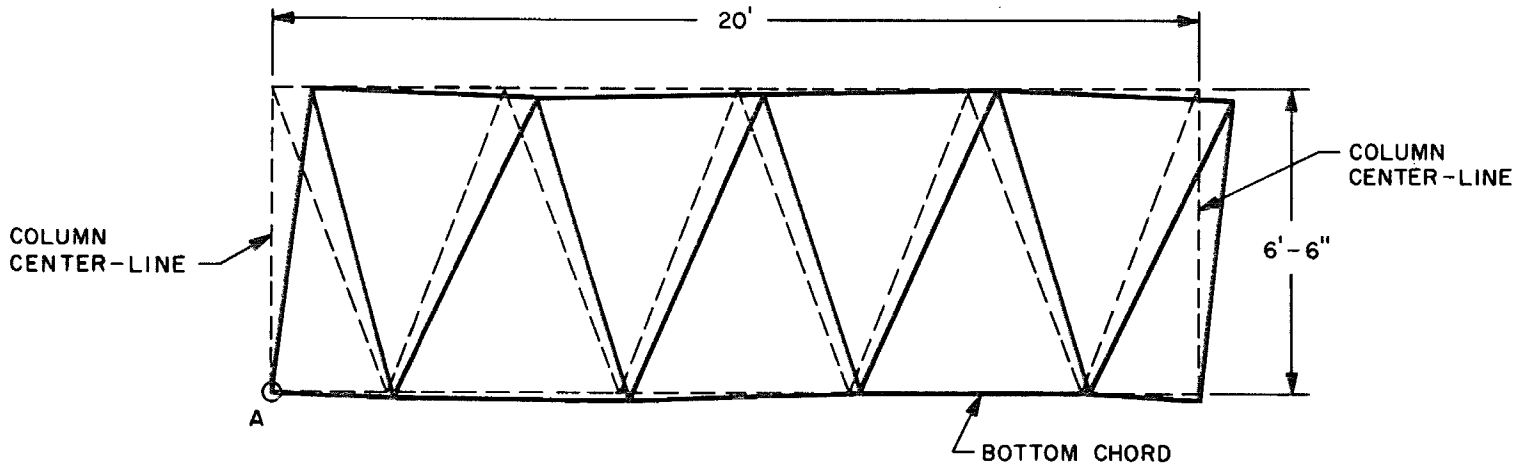

DEFLECTIONS OF FLOOR 5 E-W SPANDREL TRUSS

JPL BUILDING

Figure 14.

steel column moments of inertia in the E-W direction by approximately a factor of five. (The increase in the N-S direction is approximately a factor of eight). Both a full composite and a partial composite model were studied. In computing the full composite model column areas and moments of inertia, the total area of concrete encasement on the columns was used. The partial composite model was developed on the assumption that the concrete in the flexural tension zone of the columns (over the full height of the column) provided no flexural stiffness.

The partial composite column assumption was considered to give a reasonable estimate of the frame stiffness during the large amplitude motions occurring in the San Fernando earthquake. Approximately 75% of the building dead loads were transmitted to the steel column sections before the concrete encasement was added and consequently the dead and live load compressive stresses in the concrete section are low. The maximum earthquake induced column moments were of sufficient magnitude to produce concrete tension cracking over the end sections of all the columns. Without undertaking an experimental study it appears difficult to make a more exact estimate of the column stiffnesses under the earthquake loading. The assumption of full composite action appears appropriate for computing the building natural frequencies corresponding to the forced and ambient vibration tests where the forces in the structure are typically one to three orders of magnitude lower than the earthquake forces. The concrete sections would remain uncracked at these low force levels.

Story weights were assumed lumped at the floor levels and the

weight of the partitions and live-load was taken as 20 lb/ft^2. The total roof weight was estimated to be 1517 kips and all the lower floor weights were taken to have a weight of 1270 kips.

4.2 HORIZONTAL DIRECTION N-S MODEL

Both full composite and partial composite structural models were developed for the N-S (short) direction of the building. The member properties of the full composite model were computed using the full area of concrete on the columns and assuming that a 15 ft wide section of floor slab was composite with the truss top chords. The partial composite model was developed by assuming that the concrete in the flexural tension zone of the columns provided no flexural stiffness and that a 7.5 ft width of floor slab acted with the truss top chords. The concrete is located only on the outer faces of the columns, for architectural appearance, so that under earthquake loading the concrete at one end of the column is under flexural tension while at the other end it is subjected to flexural compression. A column moment of inertia that approximately satisfies the condition of no contribution from the concrete in the tension zone was obtained by taking an average of the bare steel section and the full composite section properties. Since flexural cracking of the concrete would develop over only about one-quarter of the column length at any particular time, the column areas were computed assuming full composite action.

Under the assumption of full composite action the end frame column members (Fig. 7) are approximately six times stiffer in flexure than the interior columns. Also, because the truss members are varied at several locations along the length of the building, the interior frames are not all identical; however, the variation in truss properties is relatively small. A total lateral stiffness matrix was developed for the full composite condition by an analysis of both an exterior frame and

a typical interior frame which was formed by summing the properties of the interior columns and trusses.

The analysis was simplified for the partial composite model by assuming that the exterior columns had identical properties to the interior columns and summing all the truss and column properties to give an equivalent single-frame. Because of the difficulty in predicting the exact stiffness behavior of the encased columns during the earthquake a more refined model was considered unwarranted.

The choice of the base fixity conditions is complicated by the presence of the basement walls and the soil restraint against the walls. The dynamic tests indicated that lateral displacements at and below the second floor level were small. Some of the displacements measured during the Teledyne ambient tests[25] are given in Table 5.

TABLE 5

FLOOR DISPLACEMENTS FROM AMBIENT TESTS

Floor	Displacement Ratio	
	N-S Mode 1	N-S Mode 2
R	1.00	-0.60
6	0.52	1.00
3	0.11	0.31
2	0.02	0.07
1	0.004	0.02
B	0.005	0.06

From structural stiffness considerations some horizontal displacement would be expected at floors 1 and 2. The simplified base

fixity conditions given below were assumed for this study but a more correct model could be obtained by including the soil restraint as a Winkler foundation and by adding the wall section to the column section properties.

The full composite model was assumed to be held against horizontal translation at floors 1 and 2 and the columns fully fixed at the foundation pad level. The same fixity condition was used for the partial composite model as well as the condition of no restraint at the floor 2 level. Periods were computed for the two cases and are given in Table 1. The model with no restraint at floor 2 gave periods that agreed more closely with the periods observed during the earthquake and so this condition was assumed for the detailed analyses described below. However, because of the uncertainty of the assumptions made regarding the column and truss stiffnesses it is not possible to conclude that this condition was a true indication of the building fixity during the earthquake.

4.3 VERTICAL DIRECTION MODEL

The vertical dynamic properties of the building were investigated using the N-S single-frame partial composite trussed girder model described in the previous section. The simplification to a two-dimensional model restricted the analysis to the consideration of only the mode shapes in which all the N-S girders along the length of the building moved in phase. A further reduction in the number of degrees of freedom of the model was made by considering only the mode shapes symmetrical about the E-W center-line of the building.

A correction was applied to the vertical translation flexibility matrix developed from the model properties to allow for the slab deformation between the N-S girders. The story weights were assumed to be lumped at five points; center-span, quarter-points and column points, on each floor level. The following distribution of dead load plus live load was assumed.

Roof level:

Weight at center-span and each quarter-point	=	329 kips
Weight at each column point	=	265 kips

All other floors:

Weight at center-span and each quarter-point	=	200 kips
Weight at each column point	=	335 kips

5. COMPUTATION OF MODEL NATURAL FREQUENCIES AND MODE SHAPES

The natural frequencies and mode shapes of the horizontal translation and vertical models were computed using standard techniques. The computational method used in this study is summarized below for the case of the horizontal models. A similar method was used to evaluate the vertical dynamic properties.

Two translational and one rotational degree of freedom were assumed at each frame joint of the model and the force displacement relationship (or element stiffness matrix) for each frame member was used to assemble the total frame force displacement relationship

$$\underline{p}^* = K^* \underline{u}^* \tag{5.1}$$

where $\underline{p}^*$ = a vector of nodal forces

K^* = the total frame stiffness matrix

$\underline{u}^*$ = a vector of nodal displacements (translations and rotations).

The lateral flexibility matrix F was computed by applying a unit horizontal load at each floor level in succession and solving equations (5.1).

Horizontal displacements and forces are related by:

$$\underline{u} = F \underline{p} \tag{5.2}$$

where $\underline{u}$ = a vector of horizontal displacements at the floor levels,

F = the lateral flexibility matrix,

$\underline{p}$ = a vector of horizontal loads applied at the floor levels.

By neglecting the influence of vertical and rotary inertia and assuming classical normal modes the undamped natural frequencies

and mode shapes can be computed by solving the horizontal equations of motion for free undamped vibrations. The horizontal equations of motion may be written as:

$$M\ddot{\underline{u}} + K\underline{u} = 0 \tag{5.3}$$

where M = a diagonal matrix of floor masses

$K = F^{-1}$, the lateral stiffness matrix.

Taking $\underline{u} = \underline{\Phi} e^{i\omega t}$ and rearranging, equation (5.3) becomes

$$\left[\lambda I - FM\right] \underline{\Phi} = 0 \tag{5.4}$$

where $\lambda = \frac{1}{\omega^2}$

ω = a natural angular frequency

$\underline{\Phi}$ = a mode shape

$i = \sqrt{-1}$

I = the unity matrix

Equation (5.4) is a standard form of the eigenvalue problem; however, in general the product FM is not symmetric.

Using the transformation

$\underline{\Phi} = M^{-\frac{1}{2}} \underline{\Psi}$ equation (5.4) becomes

$$\left[\lambda I - M^{\frac{1}{2}} F M^{\frac{1}{2}}\right] \underline{\Psi} = 0 \tag{5.5}$$

where the product $M^{\frac{1}{2}}FM^{\frac{1}{2}}$ is symmetric allowing equations (5.5) to be solved by a standard computer program to yield the natural frequencies and mode shapes.

The response of a building to earthquake ground accelerations may be conveniently computed by using the modal properties. The relative displacement response at the building roof level for a ground acceleration $\ddot{u}_g(t)$ and zero initial conditions is given by

$$u_r(t) = -\sum_{n=1}^{N} \frac{P_{n,r}}{\omega_n\sqrt{1-\zeta_n^2}} \int_0^t \ddot{u}_g(\tau) e^{-\omega_n(t-\tau)} \sin \omega_n\sqrt{1-\zeta_n^2}\,(t-\tau)\,d\tau \quad (5.6)$$

or,

$$u_r(t) = -\sum_{n=1}^{N} P_{n,r}\; D\;(t,\ \omega_n,\ \zeta_n) \quad (5.7)$$

where N = the number of floor masses above the base

$P_{n,r} = \Phi_{n,r} \dfrac{\underline{\Phi}_n^T \underline{M}}{\underline{\Phi}_n^T M \underline{\Phi}_n}$, the roof participation factor in mode n

$\Phi_{n,r}$ = the displacement in mode n at the roof level

$\underline{\Phi}_n$ = the mode shape in mode n

$\underline{M}$ = the vector of story masses

M = the diagonal matrix of story masses

ω_n = the undamped natural angular frequency in mode n

ζ_n = the fraction of critical damping in mode n

$D(t, \omega_n, \zeta_n)$ = the relative displacement response of a single degree of freedom oscillator with undamped natural frequency ω_n and fraction of critical damping ζ_n.

As shown in equation (5.7) the participation factors have been chosen to give a convenient relationship between the building response and the response of a single degree of freedom oscillator.

5.1 HORIZONTAL MODEL DYNAMIC PROPERTIES

The periods and participation factors of the first six modes of the horizontal models are presented in Tables 6 and 7.

TABLE 6

N-S HORIZONTAL MODE PROPERTIES

MODE No.	Full Composite Model		Partial Composite Model	
	Period sec.	Roof participation factor	Period sec.	Roof participation factor
1	1.163	1.322	1.457	1.306
2	0.338	-0.487	0.469	-0.460
3	0.165	0.253	0.259	0.242
4	0.095	-0.140	0.168	-0.139
5	0.061	0.077	0.118	0.079
6	0.044	-0.035	0.087	-0.042

TABLE 7

E-W HORIZONTAL MODE PROPERTIES

MODE No.	Full Composite Model		Partial Composite Model	
	Period sec.	Roof participation factor	Period sec.	Roof participation factor
1	1.089	1.288	1.209	1.303
2	0.361	-0.438	0.418	-0.463
3	0.213	0.234	0.257	0.240
4	0.147	-0.127	0.184	-0.113
5	0.108	0.065	0.142	0.047
6	0.084	-0.032	0.114	-0.018

Figs. 15 and 16 show comparisons of the mode shapes computed for the full composite models and the shapes determined by two of the dynamic tests.

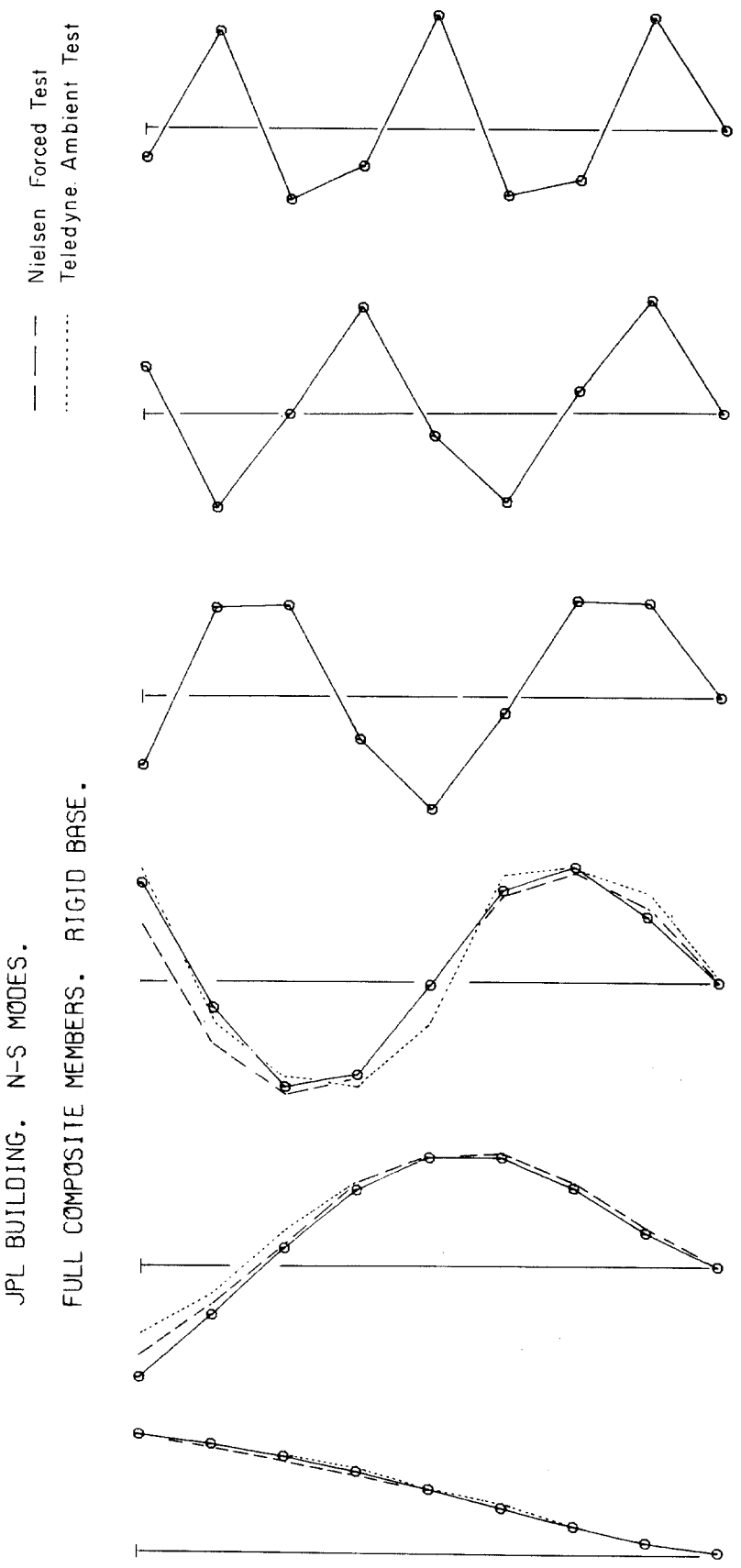

Figure 15. Computed and measured mode shapes.

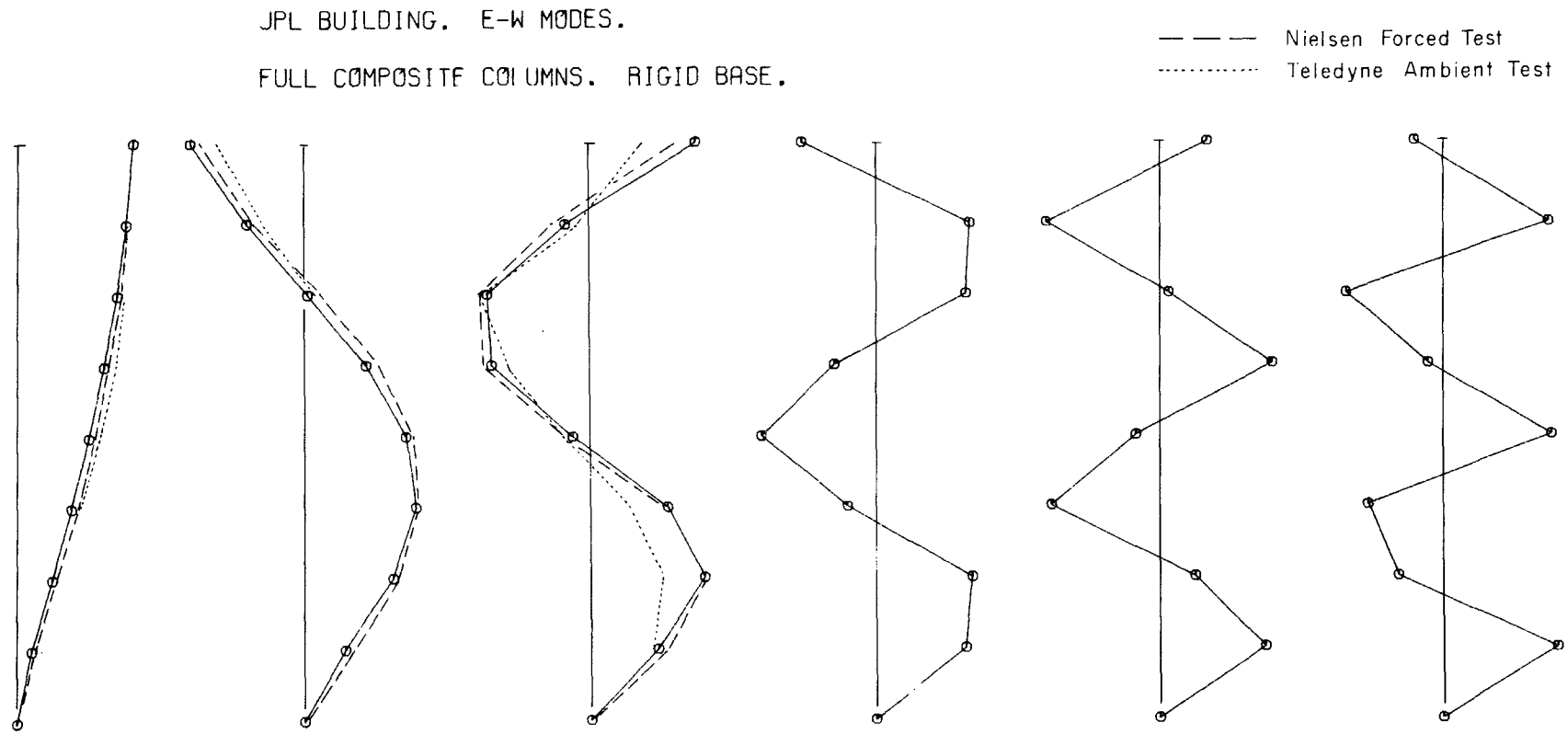

Figure 16. Computed and measured mode shapes.

5.2 VERTICAL MODEL DYNAMIC PROPERTIES

Periods and participation factors of the lowest 12 modes computed for the partial composite model are listed in Table 8. Participation factors are given for the center-span point of the roof and are defined in a similar manner to the factors for the horizontal modes.

TABLE 8

Mode No.	Period sec.	Roof Participation Factor
1	0.1622	2.309
2	0.1405	-0.653
3	0.1350	-0.094
4	0.1323	-0.066
5	0.1299	-0.036
6	0.1276	-0.044
7	0.1242	-0.016
8	0.1211	-0.010
9	0.1174	-0.023
10	0.1167	-0.023
11	0.0696	-0.441
12	0.0519	-0.0003

The 12 lowest mode shapes are plotted in Fig. 17. Modes 1 and 11 are breathing type modes in which all the column points are in phase. The other modes shown are floor vibration type modes. The character of the mode shapes is more clearly demonstrated by the building cross-section sketches shown in Fig. 18. The order of the floor vibration type modes is influenced by the general reduction in N-S girder stiff-

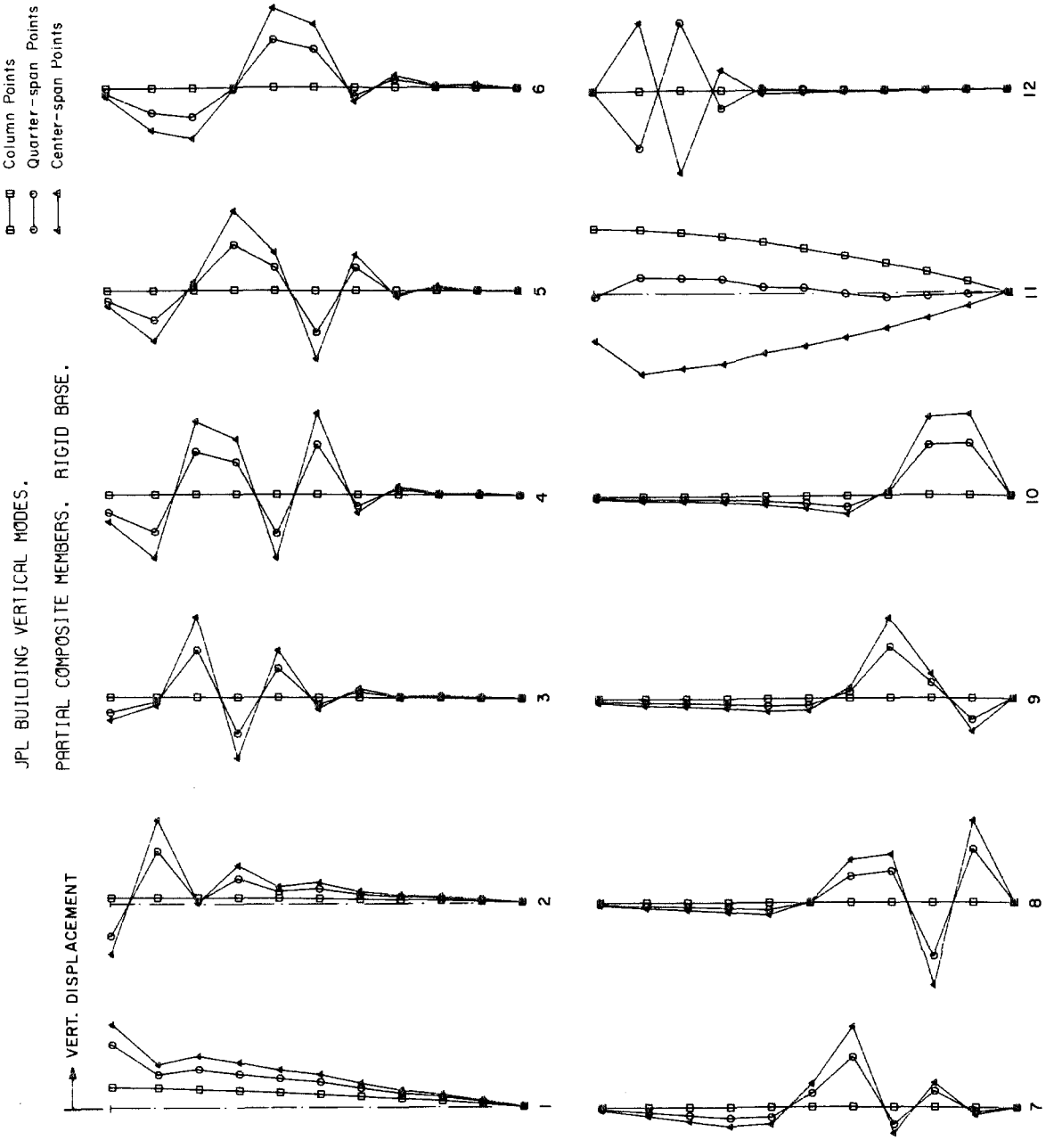

Figure 17. Computed mode shapes.

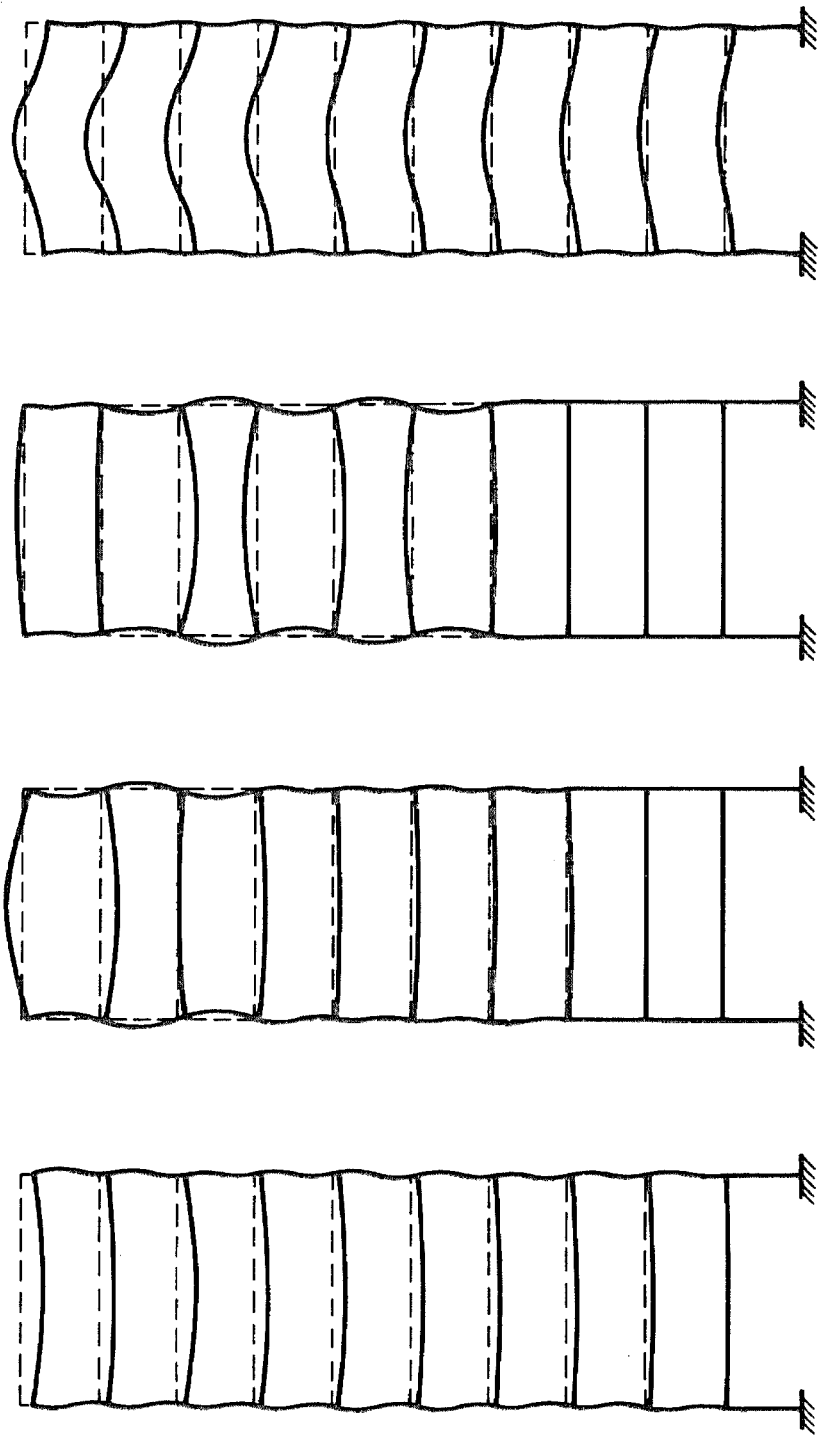

JPL BUILDING VERTICAL MODE SHAPES

Figure 18.

ness with height in the building. All these modes, with the exception of the second mode, have small roof participation factors which indicates that their contribution to the total roof response will be small.

6. NATURAL FREQUENCIES FROM EARTHQUAKE RECORDS

The natural frequencies of the lower modes of vibration of the building can be determined from the recorded earthquake accelerograms. A suitable method is to compute the Fourier amplitude spectra of both the corresponding base and roof records and plot the ratio obtained by dividing the roof spectra values point by point by the base spectra. Roof and base Fourier amplitude spectra were computed for the first 40 sec of each of the three components of motion using a standard Fast Fourier Transform computer program[4]. (A definition of the Fourier amplitude spectrum and its relationship to the undamped velocity spectrum is given by Hudson[9]). Plots of the spectra obtained after one cycle of the smoothing operation defined below are shown in Figures 19 to 21.

The smoothed amplitude spectrum is given by

$$|A(\omega)|_j^s = 0.5\,|A(\omega)|_j^u + 0.25\left\{|A(\omega)|_{j-1}^u + |A(\omega)|_{j+1}^u\right\} \quad (6.1)$$

where $|A(\omega)|_j^s$ = the smoothed value of the spectrum at point j.

$|A(\omega)|_j^u$ = the unsmoothed value of the spectrum at point j.

This smoothing operation has been suggested by Trifunac and Udwadia in Reference (11b) as a convenient way of minimizing the leakage error. (A complete account of the errors occurring in the Fourier spectrum computation is given in Reference (11b).

A horizontal line termed the 90% confidence level and defined by

$$Y_{90} = \frac{\sigma T}{2}\left\{2\, g_{P=0.10}\right\}^{\frac{1}{2}} \quad (6.2)$$

is plotted on the spectra.

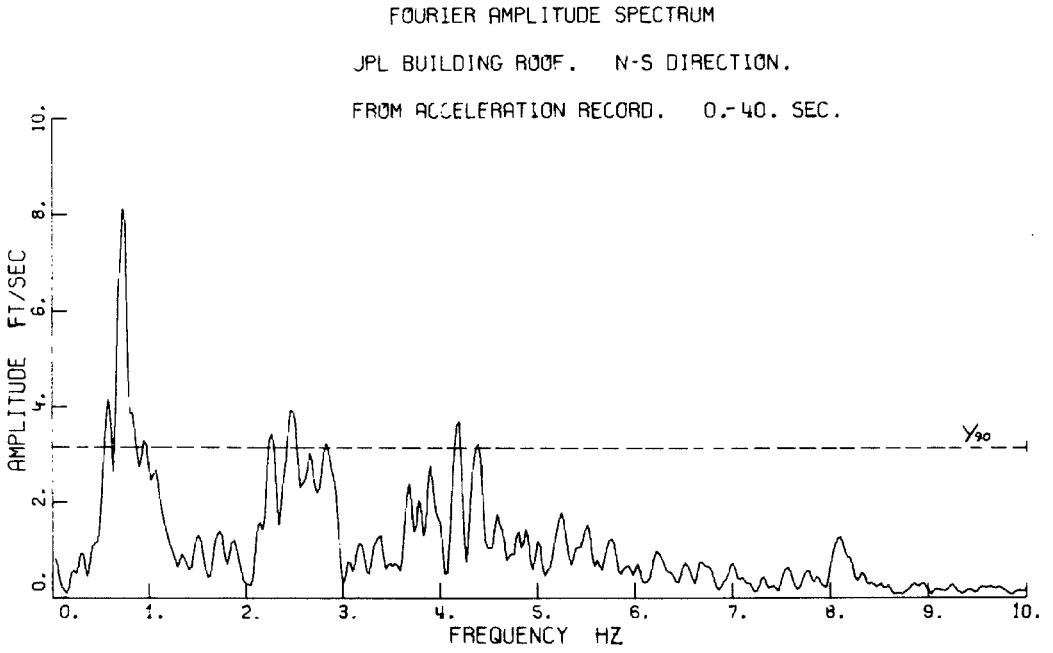
FOURIER AMPLITUDE SPECTRUM
JPL BUILDING ROOF. N-S DIRECTION.
FROM ACCELERATION RECORD. 0.-40. SEC.
AMPLITUDE FT/SEC
0.
2.
4.
6.
8.
10.
Y90
0.
1.
2.
3.
4.
5.
6.
7.
8.
9.
10.
FREQUENCY HZ

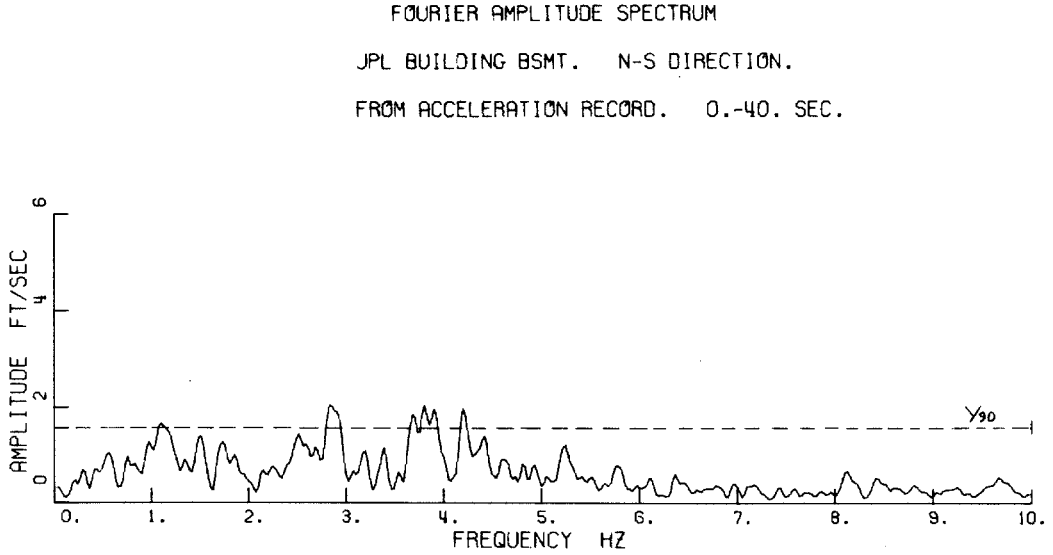
FOURIER AMPLITUDE SPECTRUM
JPL BUILDING BSMT. N-S DIRECTION.
FROM ACCELERATION RECORD. 0.-40. SEC.
AMPLITUDE FT/SEC
0
2
4
6
Y90
0.
1.
2.
3.
4.
5.
6.
7.
8.
9.
10.
FREQUENCY HZ

Figure 19.

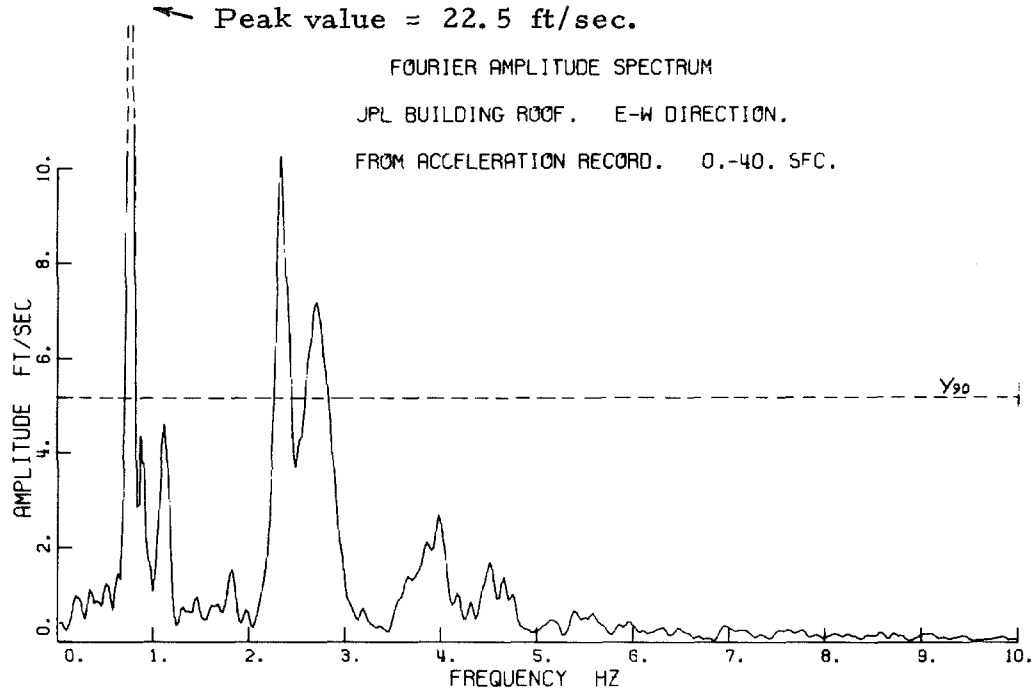
Peak value = 22.5 ft/sec.
FOURIER AMPLITUDE SPECTRUM
JPL BUILDING ROOF. E-W DIRECTION.
FROM ACCELERATION RECORD. 0.-40. SEC.
AMPLITUDE FT/SEC
0.
2.
4.
6.
8.
10.
Y90
0. 1. 2. 3. 4. 5. 6. 7. 8. 9. 10.
FREQUENCY HZ

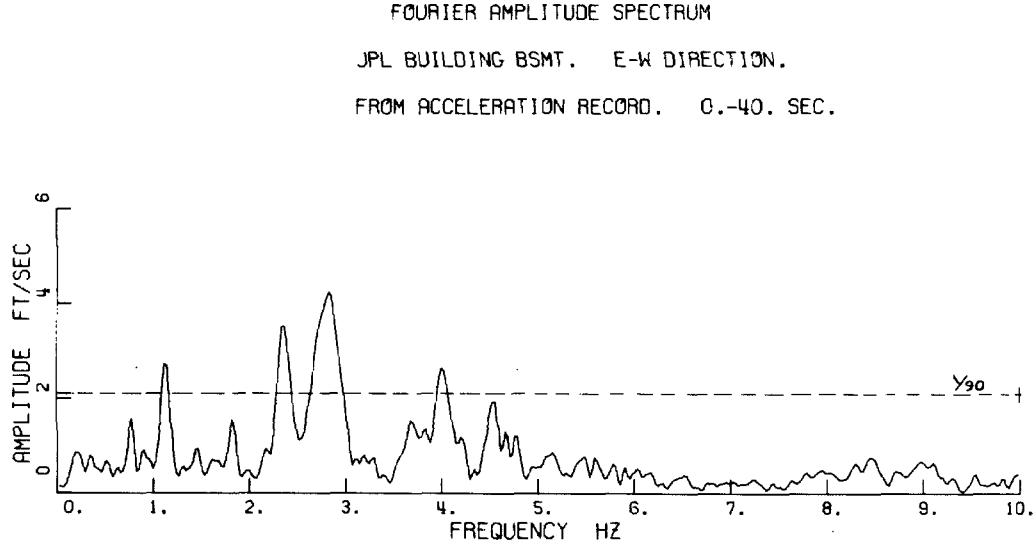
FOURIER AMPLITUDE SPECTRUM
JPL BUILDING BSMT. E-W DIRECTION.
FROM ACCELERATION RECORD. 0.-40. SEC.
AMPLITUDE FT/SEC
0
2
4
6
Y90
0. 1. 2. 3. 4. 5. 6. 7. 8. 9. 10.
FREQUENCY HZ

Figure 20.

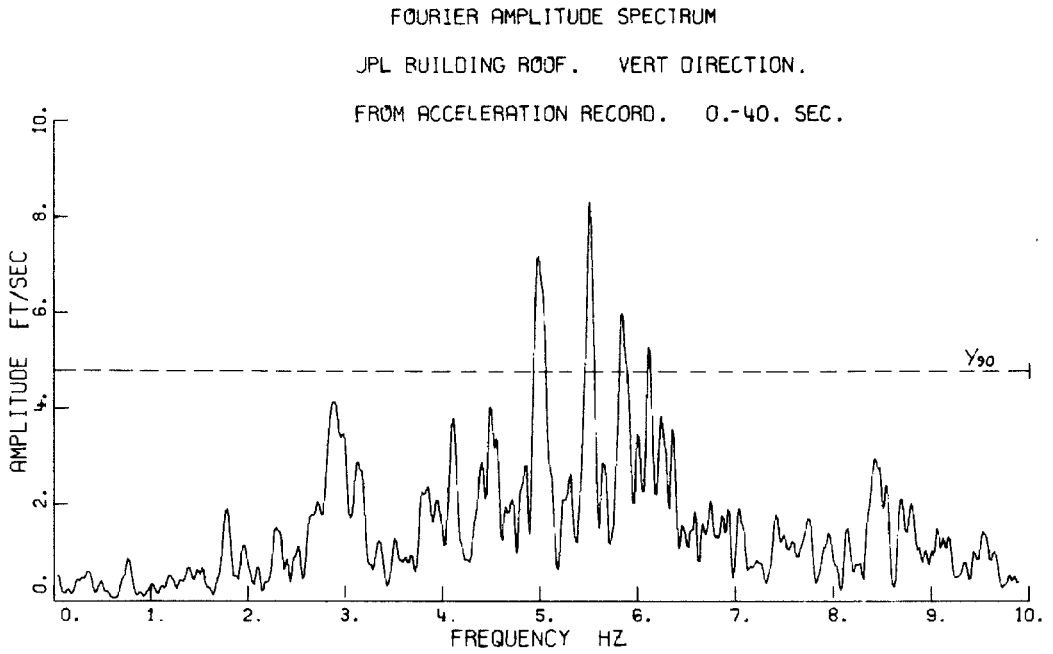
FOURIER AMPLITUDE SPECTRUM
JPL BUILDING ROOF. VERT DIRECTION.
FROM ACCELERATION RECORD. 0.-40. SEC.
AMPLITUDE FT/SEC
0.
2.
4.
6.
8.
10.
Y90
0.
1.
2.
3.
4.
5.
6.
7.
8.
9.
10.
FREQUENCY HZ

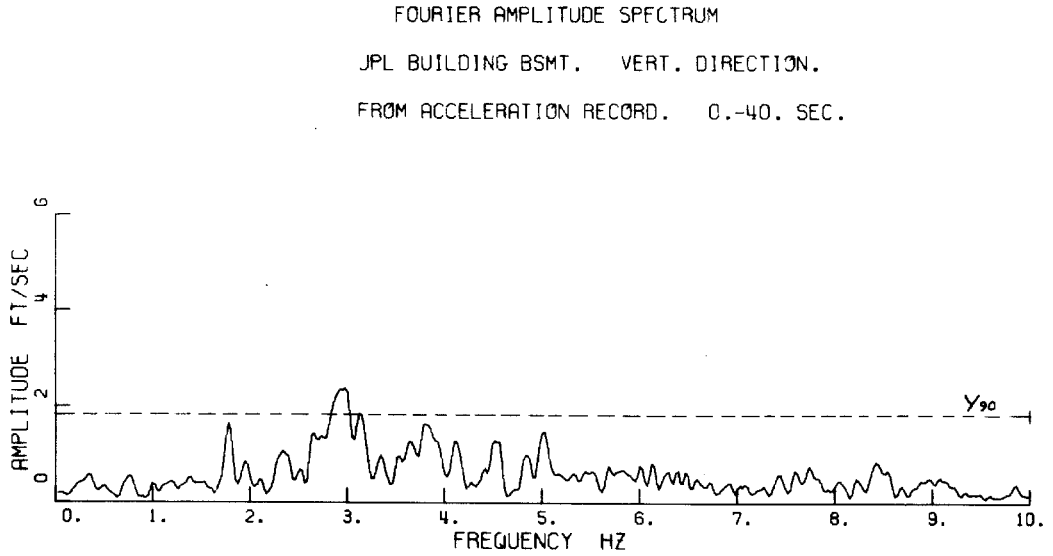
FOURIER AMPLITUDE SPECTRUM
JPL BUILDING BSMT. VERT. DIRECTION.
FROM ACCELERATION RECORD. 0.-40. SEC.
AMPLITUDE FT/SEC
0
2
4
6
Y90
0.
1.
2.
3.
4.
5.
6.
7.
8.
9.
10.
FREQUENCY HZ

Figure 21.

where,

σ = the standard deviation of the acceleration record data points.

T = the acceleration record length.

$g_{P=0.10}$ = a parameter for probability P = 0.10 and depends on the number of data points in the acceleration record. Values are given in Reference (11b). 2049 data points were used to compute the spectra from the horizontal records giving $g_{P=0.10} = 0.00899$.

Spectral peaks greater than Y_{90} can be taken as representing a harmonic component in the acceleration record at the 90% confidence level. In other words, peaks in a random record have a probability of 0.1 of exceeding the Y_{90} level.

Plots of the building transfer functions, or the ratio of roof amplitude spectra divided by the base amplitude spectra, are shown in Figures 22a, 23a and 24a. Both basic unsmoothed and smoothed ratio plots are shown. The unsmoothed ratios were computed directly from the single-cycle smoothed base and roof spectra and the smoothed ratios were computed by applying 10 cycles of the operation defined by equation (6.1) to the unsmoothed ratios. The frequency resolution of the Fourier spectra and transfer functions presented in this study is equal to the reciprocal of the acceleration record length. For a record length of 40 sec the points are spaced on the spectra at an interval of 0.025 hz.

Interpretation of the spectra ratio plots is aided by comparing them with the theoretical plots computed from the building model responses and shown in Figures 22b, 23b and 24b. Refined building models were obtained by the procedures discussed in Section 8 and their roof

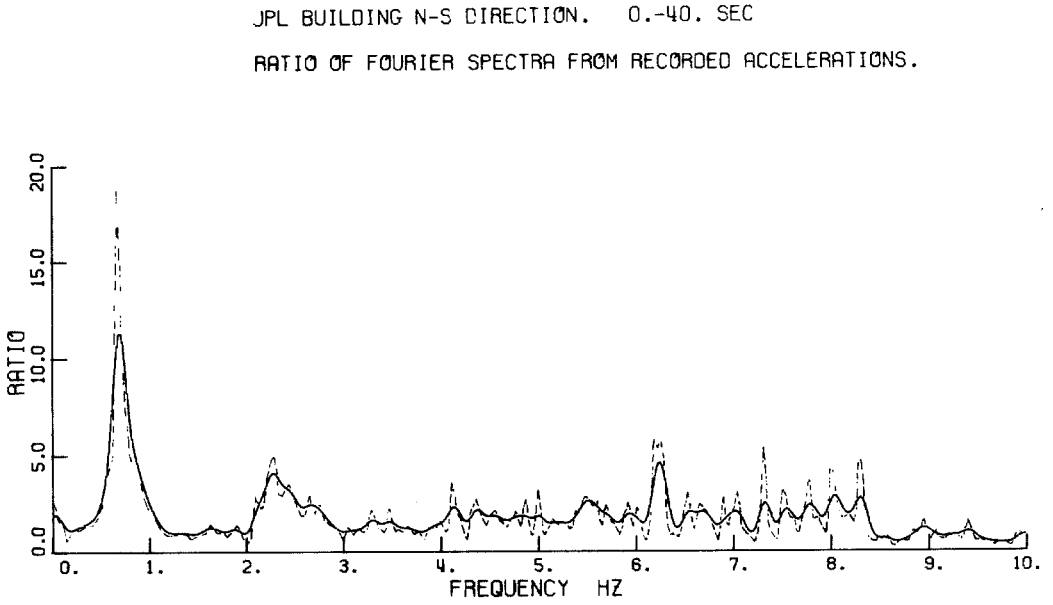

Figure 22a.

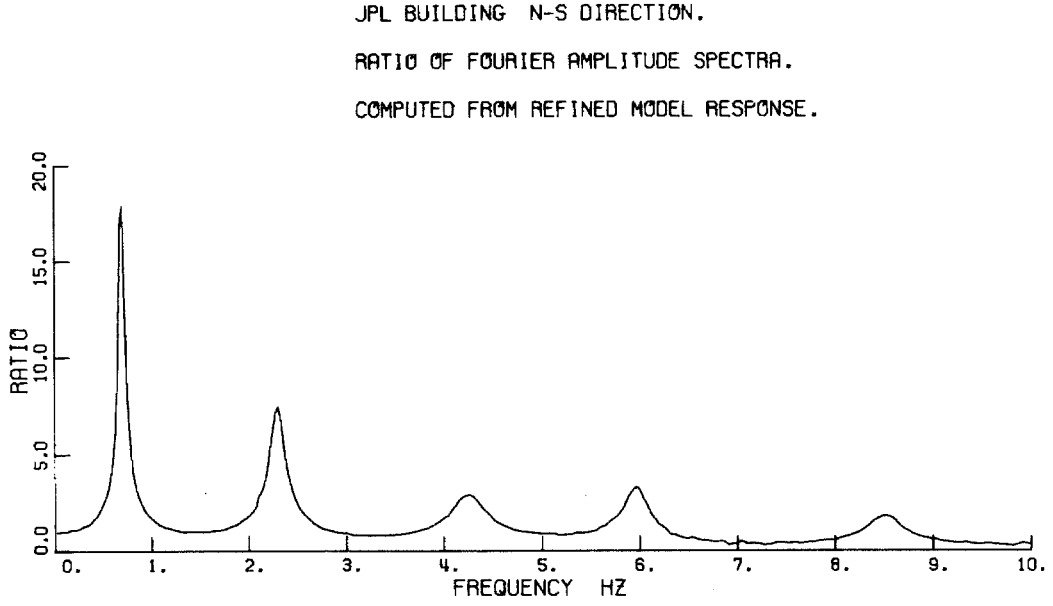

Figure 22b.

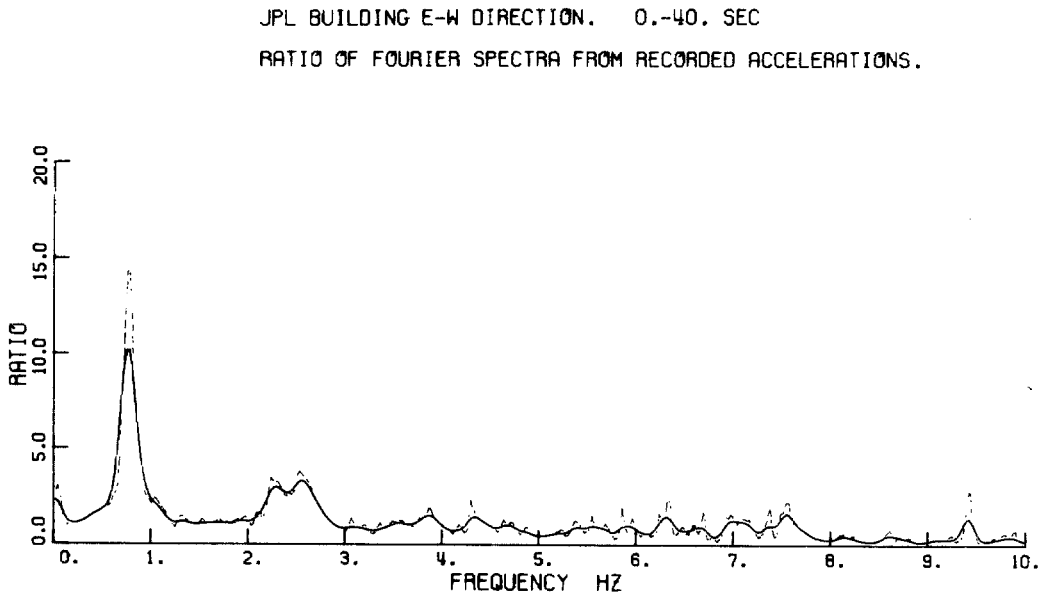

Figure 23a.

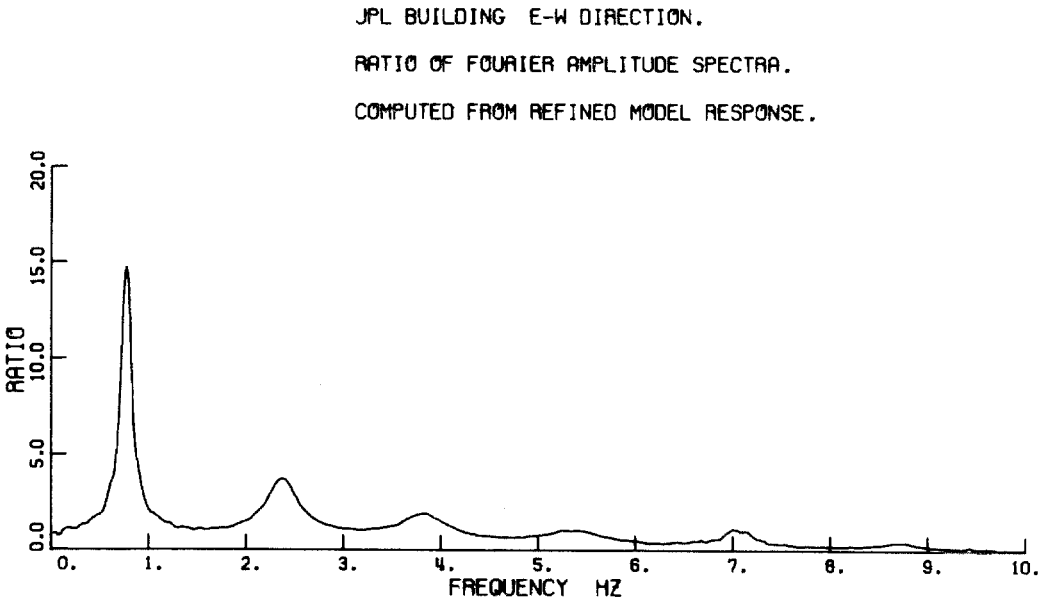

Figure 23b.

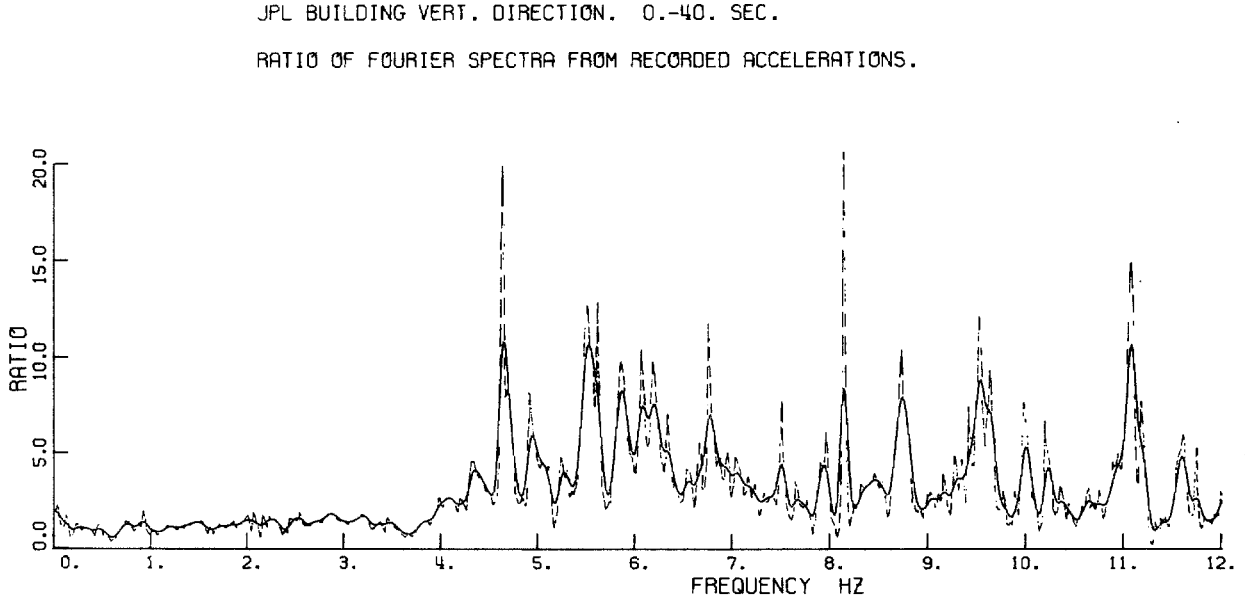

Figure 24a.

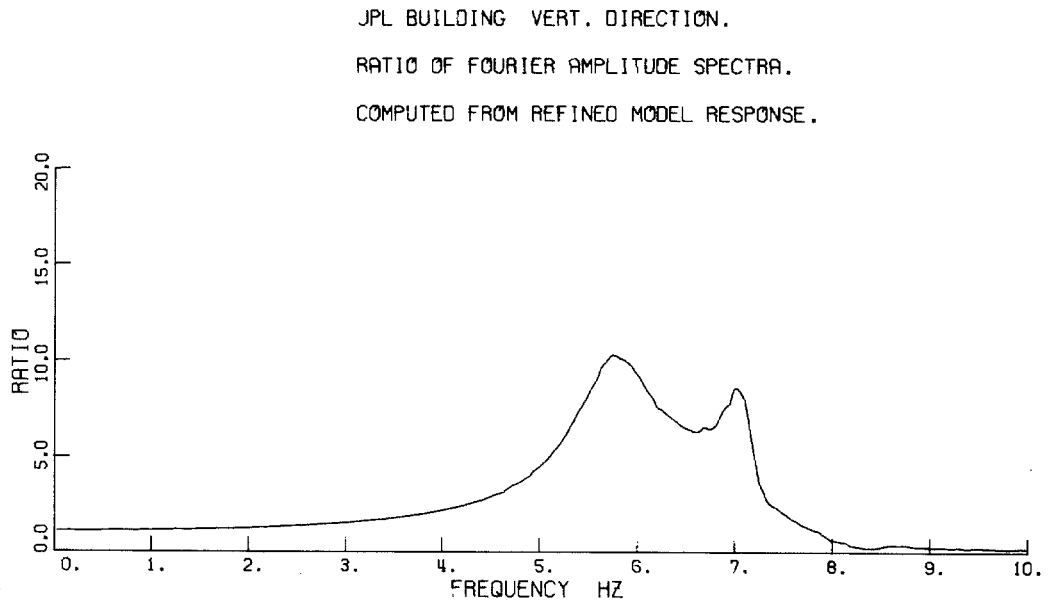

Figure 24b.

acceleration responses to the recorded base motions were computed. (The acceleration responses and the refined model periods and critical damping ratios are shown in Figures 27, 29 and 34). Fourier spectra ratios for the models were computed from the model roof response spectra and the spectra of the recorded base motions.

The building transfer functions can be evaluated more directly from the dynamic properties of the models. From the solution of the horizontal equations of motion (equation (5.3)) for the case of harmonic forcing, the base to roof transfer function for absolute roof response can be derived as,

$$|H_r(\omega)| = \left| 1 + \sum_{n=1}^{N} \frac{P_{n,r} \left(\frac{\omega}{\omega_n}\right)^2 \left\{1 - \left(\frac{\omega}{\omega_n}\right)^2 - 2i \frac{\omega}{\omega_n} \zeta_n\right\}}{\left\{1 - \left(\frac{\omega}{\omega_n}\right)^2\right\}^2 + \left(2 \frac{\omega}{\omega_n} \zeta_n\right)^2} \right| \quad (6.3)$$

where $|H_r(\omega)|$ is defined by,

$$|\ddot{\bar{u}}_r| = |H_r(\omega)| \; |\ddot{\bar{u}}_g + \ddot{\bar{u}}_b|$$

$|\ddot{\bar{u}}_r|$ = amplitude of absolute roof acceleration

$|\ddot{\bar{u}}_g + \ddot{\bar{u}}_b|$ = amplitude of absolute base acceleration

Equation (6.3) was evaluated for the refined partial composite models and was found to give almost identical results to the plots shown in Figures 22b, 23b and 24b, with the exception that the minor irregularities resulting from numerical errors in the previous method were eliminated. The results of the model response method of evaluating $|H_r(\omega)|$ are presented because they illustrate the accuracy of the numerical techniques used to compute the spectra ratios from the recorded motions.

This less direct method may provide for future research work a convenient way of studying the effects of assuming that the model periods and dampings change at various points during the earthquake.

The spectra ratio plots obtained from the recorded motions are considerably less smooth than the theoretical plots computed from the models. Although the smoothing procedure used helps interpretation it is still difficult to deduce more than the two lowest natural frequencies in each direction. Possible reasons for the lack of smoothness in the spectra ratios are:

(a) Additional response peaks produced by modes of vibration not possible in the simplified models.

(b) Shifts in the natural frequencies during the earthquake.

(c) Errors in the Fourier spectra resulting from random errors in the recording and reduction of the data.

Further research is required to determine the modifications resulting from (a) and (b). The influence of random errors is discussed below.

6.1 ERRORS IN SPECTRA RATIO PLOTS

A discussion of the errors occurring in the recording and data reduction of strong-motion accelerograms is given by Trifunac, Udwadia and Brady [26]. By digitizing a number of straight lines they evaluated the average Fourier spectrum resulting from human and discretization errors in the process of reducing an accelerogram to digital data. By applying their results to the Building 180 records it was found that the Fourier amplitude resulting from this type of error is of the order of 0.1 ft/sec over a frequency range 0 - 5hz. The error tends to decrease with increasing frequency and can be expected to be about 0.03 ft/sec at 10 hz. Recording instrument errors and systematic errors in the digitizing system are not included in this estimate and because the data used in this study was not corrected for these types of error the total error magnitudes will probably be rather larger than the above estimates.

An alternative method based on equation (6.2) may be used to estimate the likely error in the Fourier spectra resulting from random errors in the data points representing the accelerogram. The human and discretization errors from the process of digitizing a straight line were found to be nearly normally distributed with a standard deviation $\sigma \approx 1/300$ cm [26]. Assuming that a similar error would occur in the process of preparing the data from the building accelerograms and applying equation (6.2), it is found that with probability $P = 0.10$ the maximum Fourier amplitude of the error will exceed 0.15 ft/sec.

From the above error estimates it is apparent that peaks on

the spectra ratio plots corresponding to points on the base record spectra having amplitudes of less than 0.1 ft/sec may be significantly in error.

6.2 HORIZONTAL MODE PERIODS

The horizontal mode periods estimated from the spectra ratio plots are given in Tables 1 and 2.

The N-S spectra ratio plot shows well defined peaks at the first and second mode frequencies, $f_1 = 0.69$ hz, $f_2 = 2.3$ hz. The third mode frequency is poorly defined; however, the peak at $f_3 = 4.25$ hz was taken to represent the predominant frequency during the largest amplitude motions. Most of the peaks at frequencies greater than 6.0 hz correspond to amplitudes of less than 0.2 ft/sec in the base record spectra and consequently many contain significant random error. Some of the peaks near 6.0 hz and 8.0 hz may be associated with the fourth and fifth natural frequencies.

The E-W spectra ratio plot shows a well defined peak representing the first mode at $f_1 = 0.78$ hz. The second mode shows as a pair of peaks between 2 - 3 hz and the reason for this behavior is not clear. A frequency of $f_2 = 2.4$ hz was assumed to be the predominant frequency during the largest amplitude motions. The third mode frequency was assumed to be at the peak $f_3 = 3.85$ hz. A peak at 4.3 hz corresponds with a low value in the base record spectrum and may be in error. Generally the peaks occurring at frequencies greater than 5 hz correspond to points in the base spectra of amplitudes less than 0.2 ft/sec and so are probably not significant. The peak at approximately 7.0 hz corresponds to base record spectrum amplitudes of about 0.25 ft/sec and may represent the fifth mode.

The percentage variations between the periods determined by the ambient vibration test after the earthquake and the periods estimated from the spectra ratio plots are listed in Table 9.

TABLE 9

Percentage Change in Horizontal Mode Periods

Mode No.	% Increase in period between ambient test after earthquake and maximum periods during earthquake	
	N-S	E-W
1	30	23
2	26	27
3	47	30

6.3 VERTICAL MODE PERIODS

A relatively broad response peak between 4.0 and 7.0 hz can be detected on the vertical direction spectra-ratio plot shown in Figure 24a. The lack of smoothness of this peak, which represents the lowest vertical natural frequency, results mainly from several points of low amplitude in the base record spectrum. Presumably these low points contain significant random error. The peak ratio value appears to lie between 5.4 - 6.3 hz corresponding to a fundamental vertical period between 0.185 - 0.159 sec. The computed vertical model first mode period was 0.162 sec. This period is relatively sensitive to the assumption made concerning the column areas. Full composite action was assumed for the model column areas and consequently the computed period would be expected to be rather low.

The spectra ratio plot (Fig. 24a) shows significant amplification between 8 - 10 hz. Over this frequency range the base record spectrum has low amplitudes and some of the peaking may be attributable to random errors, but because amplification extends over a large number of points a resonance within the building seems likely. The lowest natural frequency of the floor slab and I-girders acting in the longitudinal direction of the building is expected to be in this range. A good estimate of the roof slab longitudinal natural frequencies can not be readily computed because mechanical equipment adds considerable complexity to the roof system.

7. CHANGES IN BUILDING PERIODS DURING EARTHQUAKE

The maximum roof accelerations occurring during the 40-100 sec section of the earthquake were less than 1.5% g and hence the building amplitudes were an order of magnitude less than excited during the first 40 sec. Fourier spectra ratios were computed from the 40-98 sec sections of the recorded accelerations and smoothed plots are shown in Figure 25. These plots were computed by the same method previously described for the 0 - 40 sec record sections. Points are plotted at a frequency interval of approximately 0.017 hz. The relative lack of smoothness in the ratios is probably the result of the greater significance of random errors occurring in the recording and data reduction of the low amplitude accelerations.

The predominant periods during the 40 - 98 sec interval were estimated from the ratio plots and are compared in Table 10 with the values obtained from the 0 - 40 sec sections of recorded acceleration and the values from the ambient tests after the earthquake.

TABLE 10

Periods from Earthquake Records

Mode	0 - 40 sec periods	40 - 98 sec periods	Ambient test periods after earthquake
1 N-S	1.44	1.46	1.11
2 N-S	0.44	0.39	0.35
3 N-S	0.24	0.22	0.16
1 E-W	1.29	1.11	1.05
2 E-W	0.42	0.38	0.33

JPL BUILDING N-S DIRECTION. 40.-98. SEC.

RATIO OF FOURIER SPECTRA FROM RECORDED ACCELERATIONS.

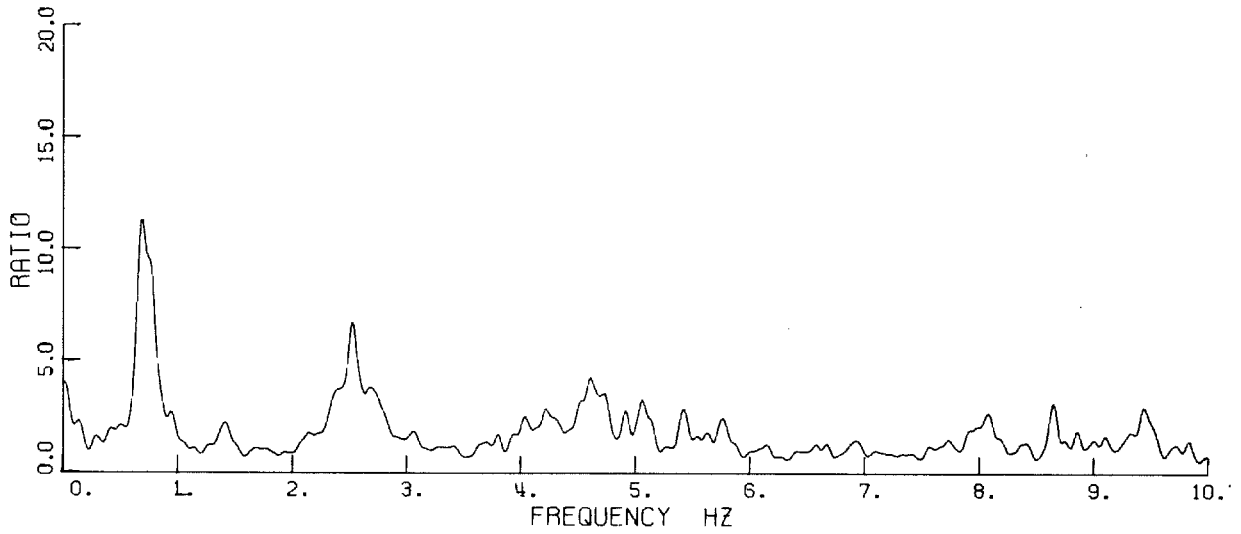

JPL BUILDING E-W DIRECTION. 40.-98. SEC.

RATIO OF FOURIER SPECTRA FROM RECORDED ACCELERATIONS.

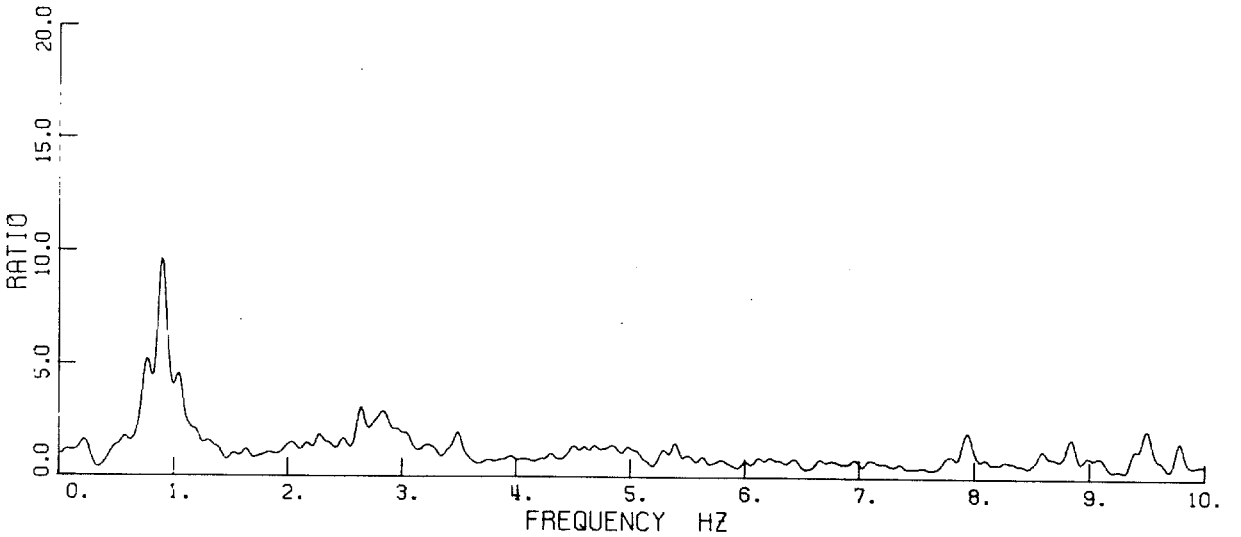

Figure 25.

With the exception of the first N-S mode the 40 - 98 sec periods lie between the 0 - 40 sec values and the ambient test results. The peak representing the first N-S mode is unsymmetrical and probably indicates that the period during the smaller vibrations may have been shorter than the listed value. A large decrease in building stiffness with increasing amplitude of motion is reflected by the change in period values and is presumably mainly a result of the non-linear behavior of the concrete encased columns.

8. COMPUTED ROOF RESPONSES

Roof absolute acceleration responses to the recorded base motions were computed for the partial composite models using a numerical technique similar to that used by Nigam and Jennings[19] for response spectra computations. Individual modal responses were computed and summed at each time increment to give the total response (See equation (5.6)).

The responses of the basic models, having dynamic properties computed from the frame stiffness matrix, were computed assuming an equivalent viscous damping ratio of 5% in each mode. It is considered that the basic models could have been developed by a reasonably exact analysis of the building without prior knowledge of the recorded earthquake behavior.

Refined models were derived from the basic models by changing the periods and dampings in the lowest modes. The lower mode periods used were obtained from the 0 - 40 sec spectra ratio plots and are considered to be good estimates of the periods during the largest amplitude motions. Damping values in the lower modes were selected by a trial and error process described below and the final values were found to give close agreement between recorded and computed accelerations for the largest amplitude motions. Participation factors for all modes, and the periods for modes higher than the third translational and first vertical were taken to be the computed basic model values. Assumed damping ratios were used for modes higher than the fourth translational mode

and the first vertical mode. The period and damping values used are listed in Figures 27, 29 and 34, which show the computed refined model responses.

Roof velocities and displacements are not presented in this report, but in general agreement between computed velocities and displacements and the values obtained by direct integration of the recorded acceleration is better than the agreement between computed and recorded accelerations. Since the dynamic forces acting on the building are directly related to the accelerations, good correspondence between the computed and recorded roof accelerations implies that the stresses computed in the model will be a good estimate of earthquake induced stresses in the building.

8.1 HORIZONTAL DIRECTION ROOF RESPONSES

Computed roof acceleration responses for both the basic and refined partial composite models are compared with the recorded acceleration histories in Figures 26 to 29.

The shape or appearance of the computed acceleration histories was generally found to be considerably more sensitive to small changes in the building periods than to changes in the damping values. For example, a change in the periods of a few per cent was found to make a larger change in the appearance of the acceleration history than a change in the damping ratios of 20%. Consequently a comparison of acceleration time histories is not a good method of evaluating the equivalent modal damping ratios. A convenient and reasonably sensitive method of evaluating the building damping ratios is to compute the Fourier amplitude spectrum of the computed acceleration history and compare it with the spectrum from the recorded acceleration history. The damping ratios can then be adjusted by trial and error until the peak values on the spectra are in close agreement at frequencies close to the natural frequencies. Fourier amplitude spectra computed from the refined model acceleration histories are compared in Figures 30 and 31 with the spectra from the recorded roof accelerations. (One cycle of smoothing has been applied to the spectra). A difficulty with this method is that, because of shifts in the building periods and perhaps because of the existence of building modes of vibration not possible in the simplified model, the resonant peaks on the spectra from the records are spread over a wider frequency range than the peaks on the spectra computed

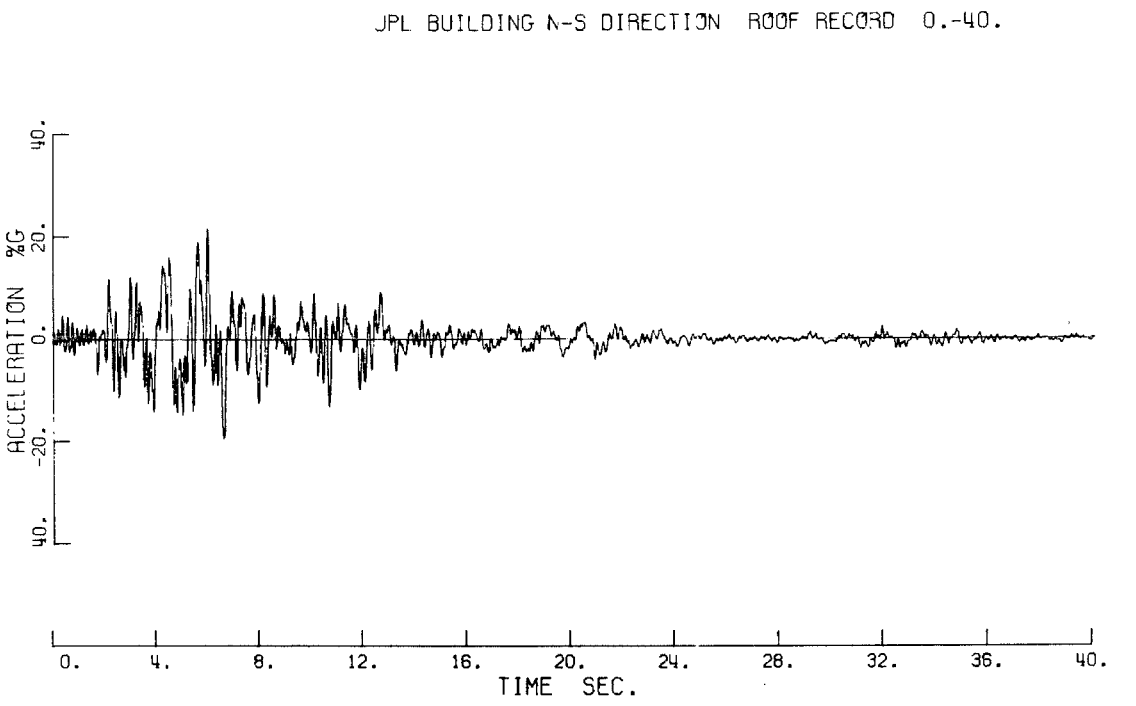

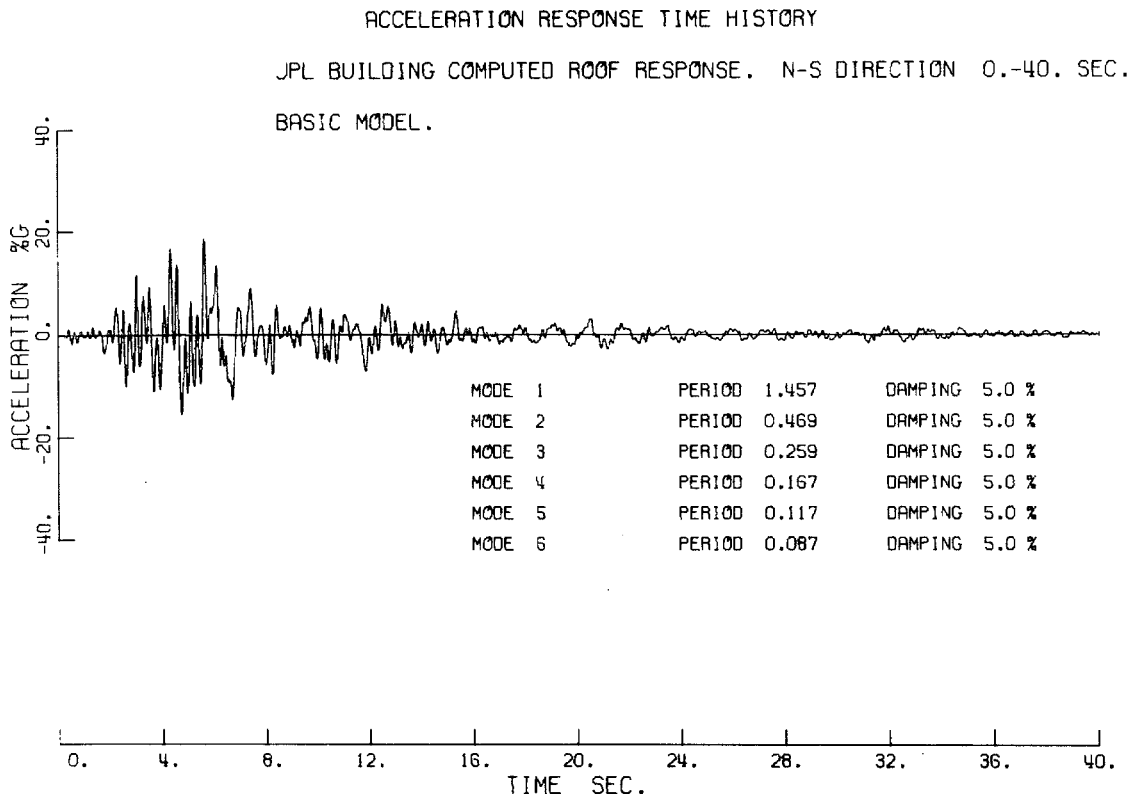

Figure 26. Comparison of recorded roof accelerations with computed basic model response.

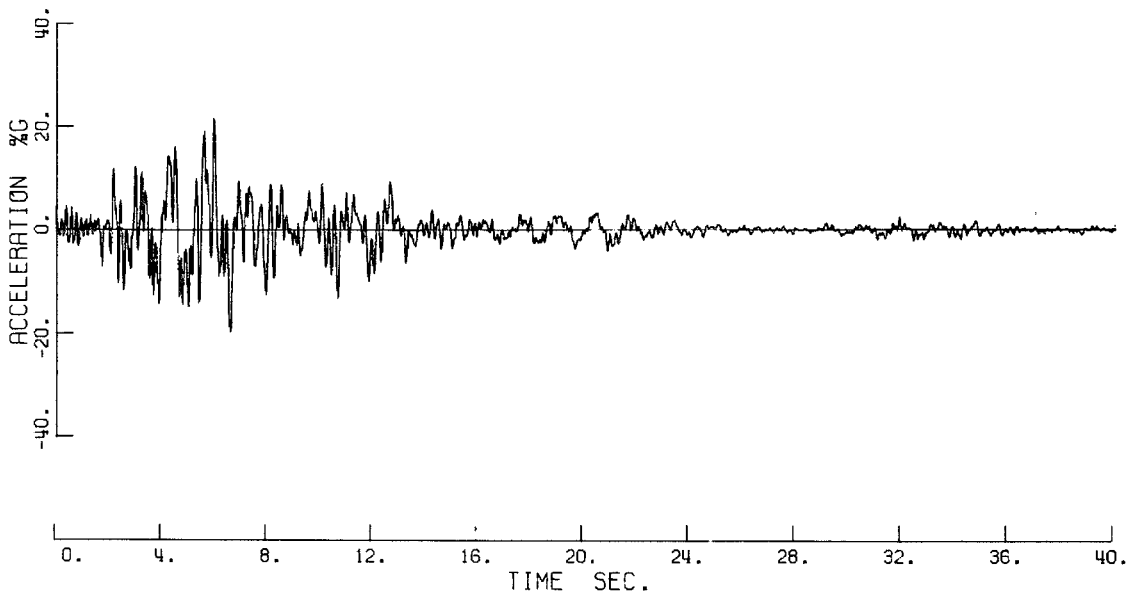

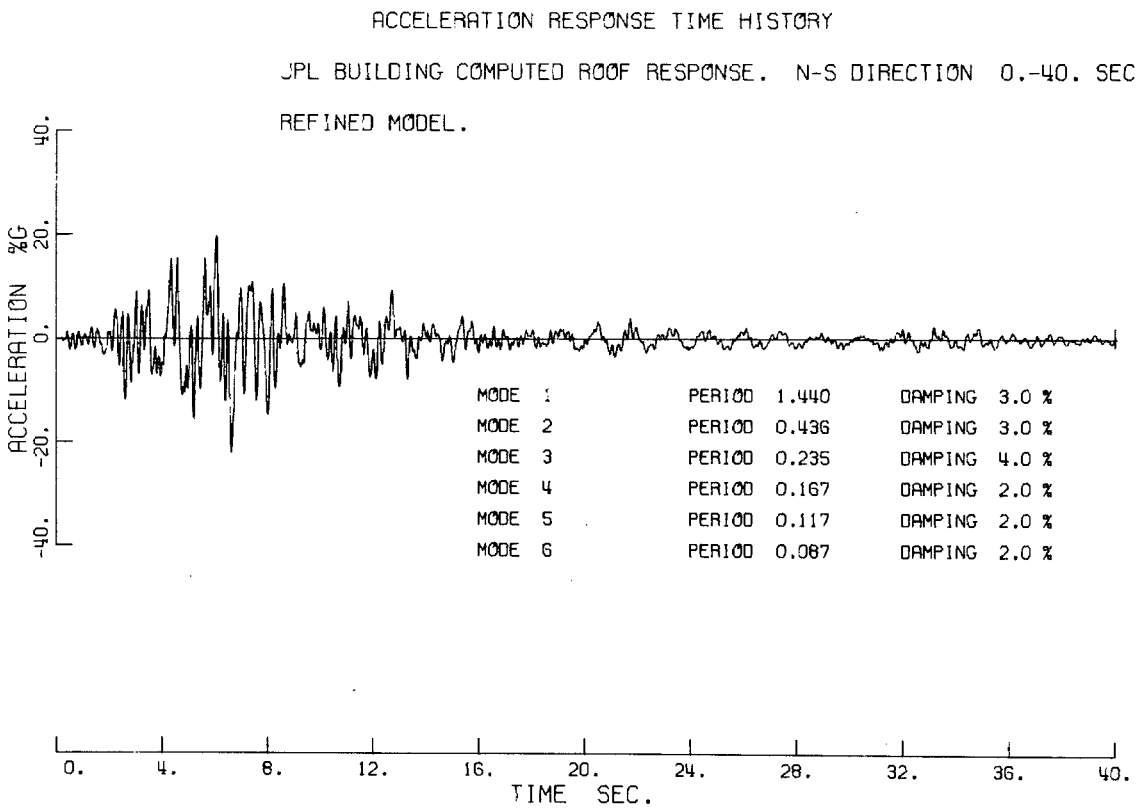

Figure 27. Comparison of recorded roof accelerations with computed refined model response.

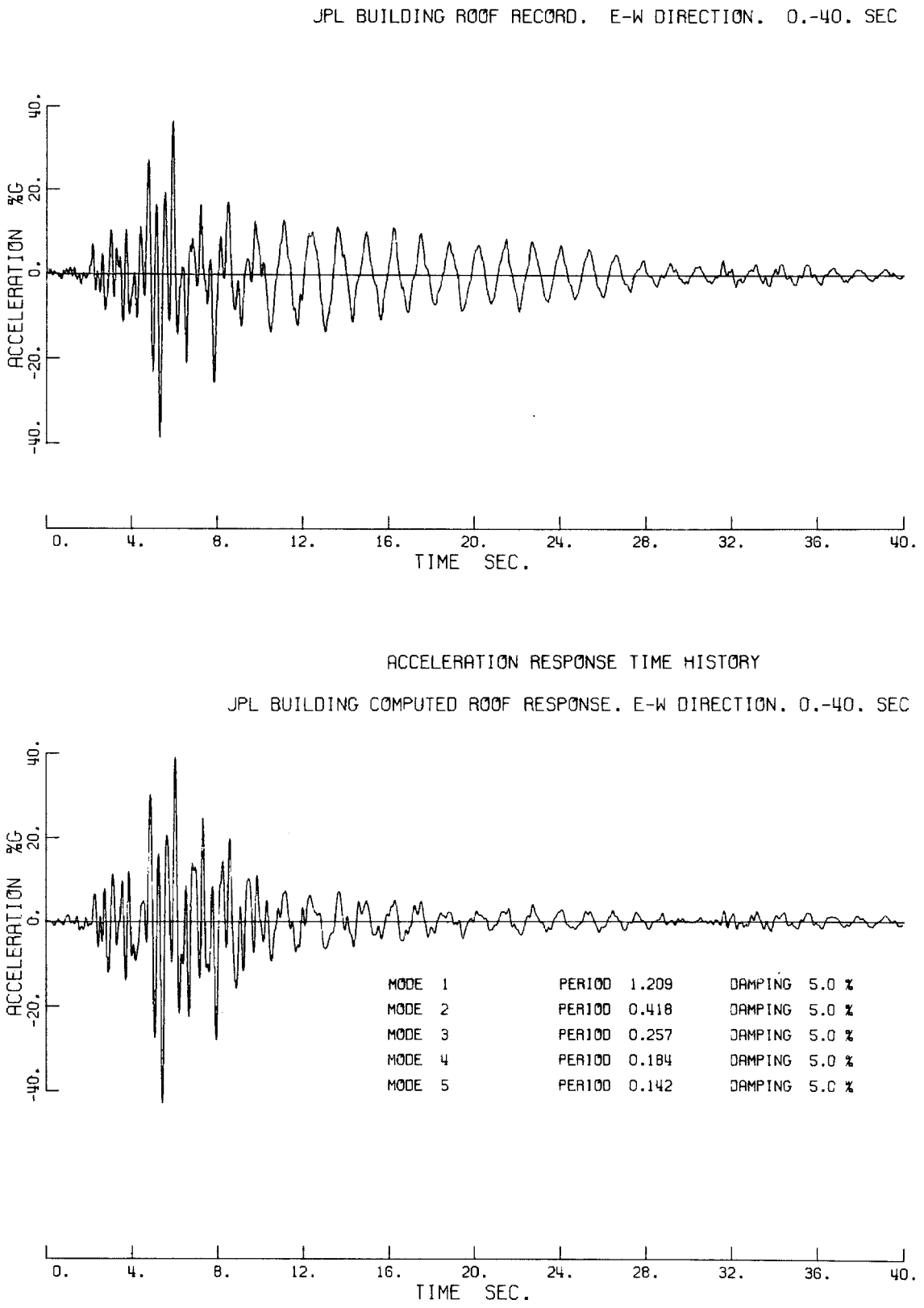

Figure 28. Comparison of recorded roof accelerations with computed basic model response.

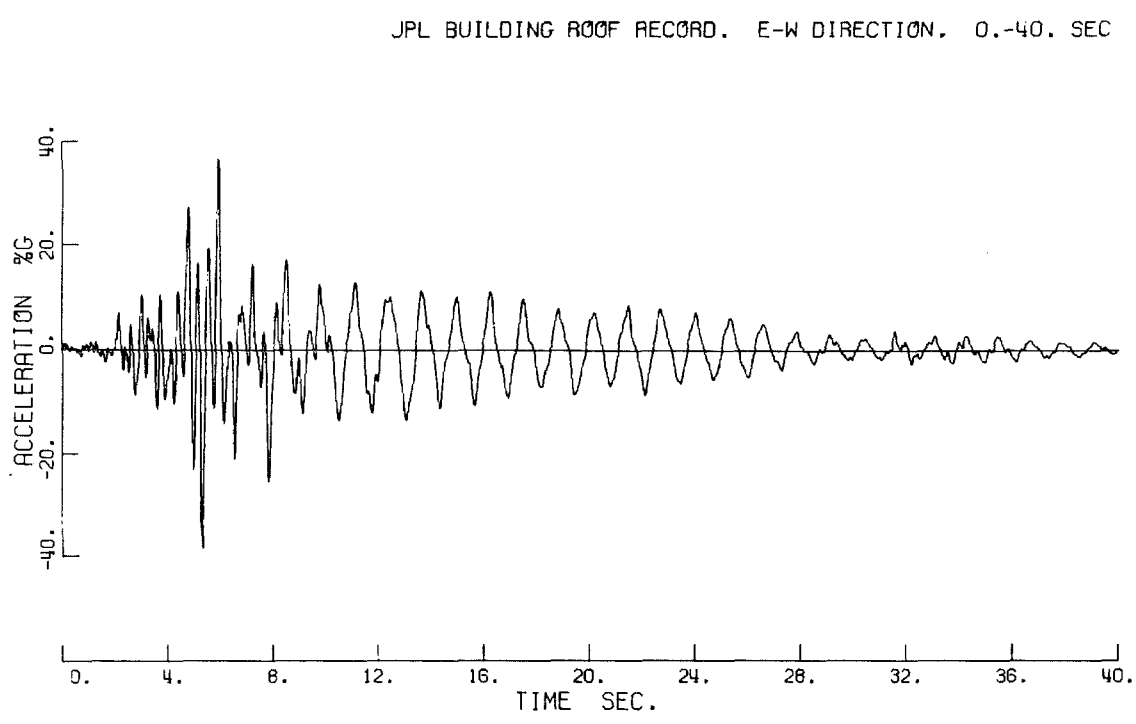

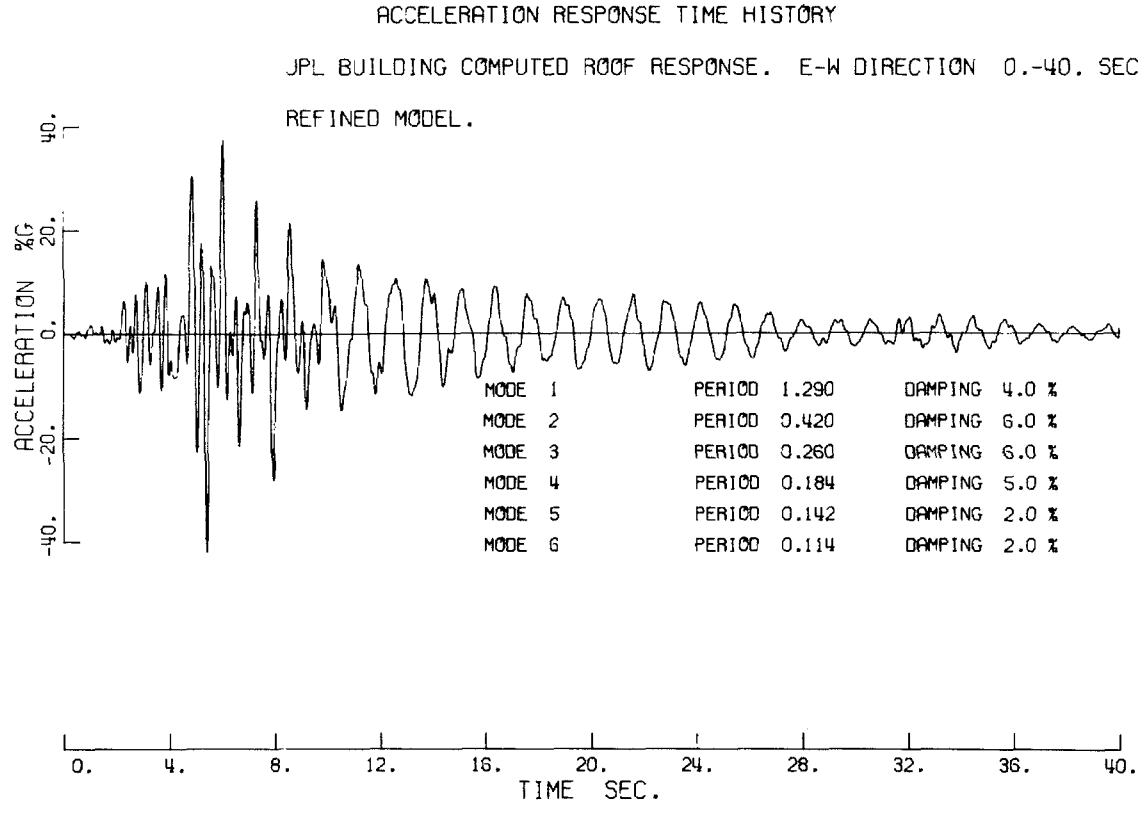

Figure 29. Comparison of recorded roof accelerations with computed refined model response.

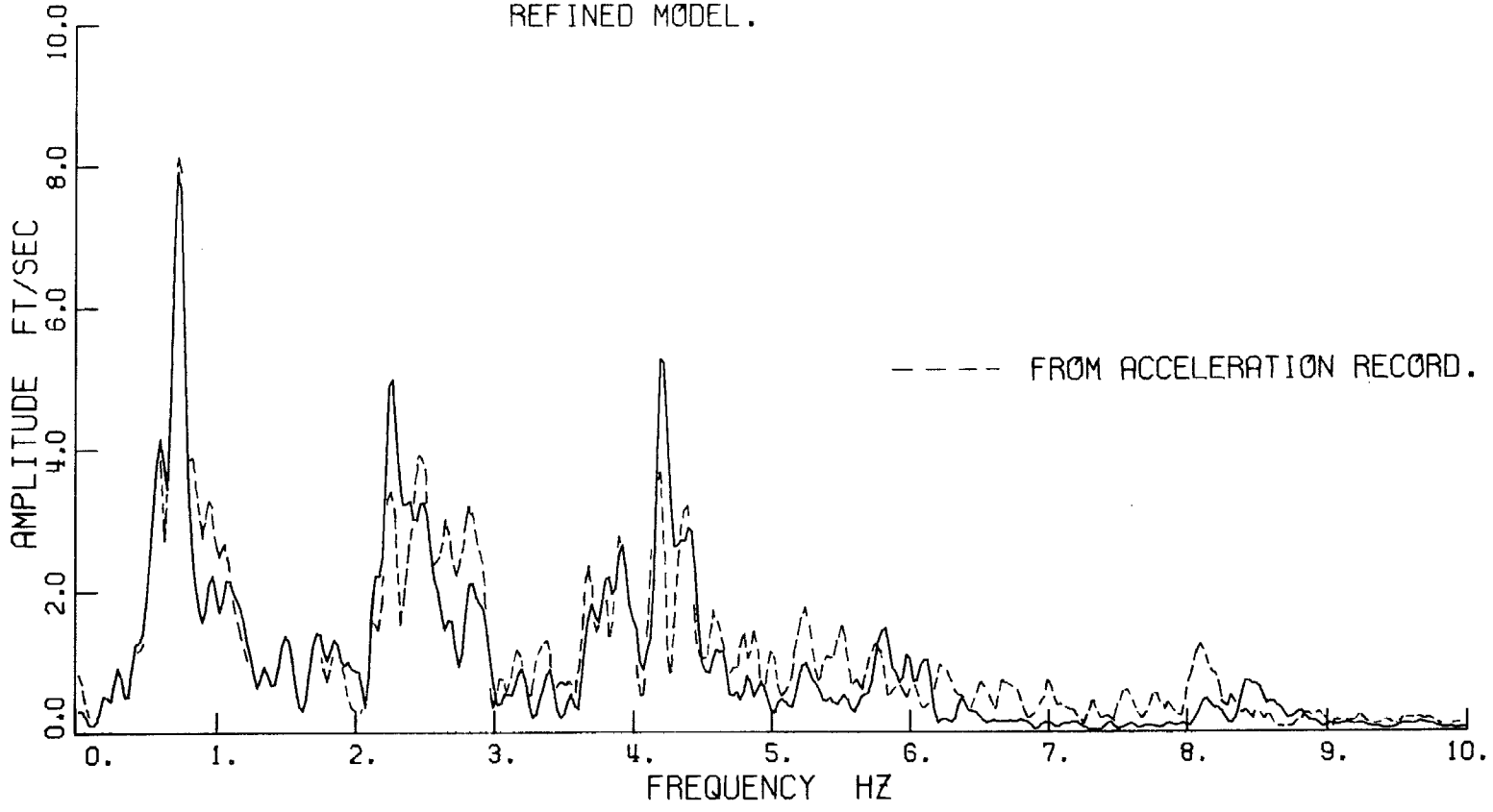

Figure 30. Comparison of Fourier amplitude spectra computed from acceleration record and refined model response.

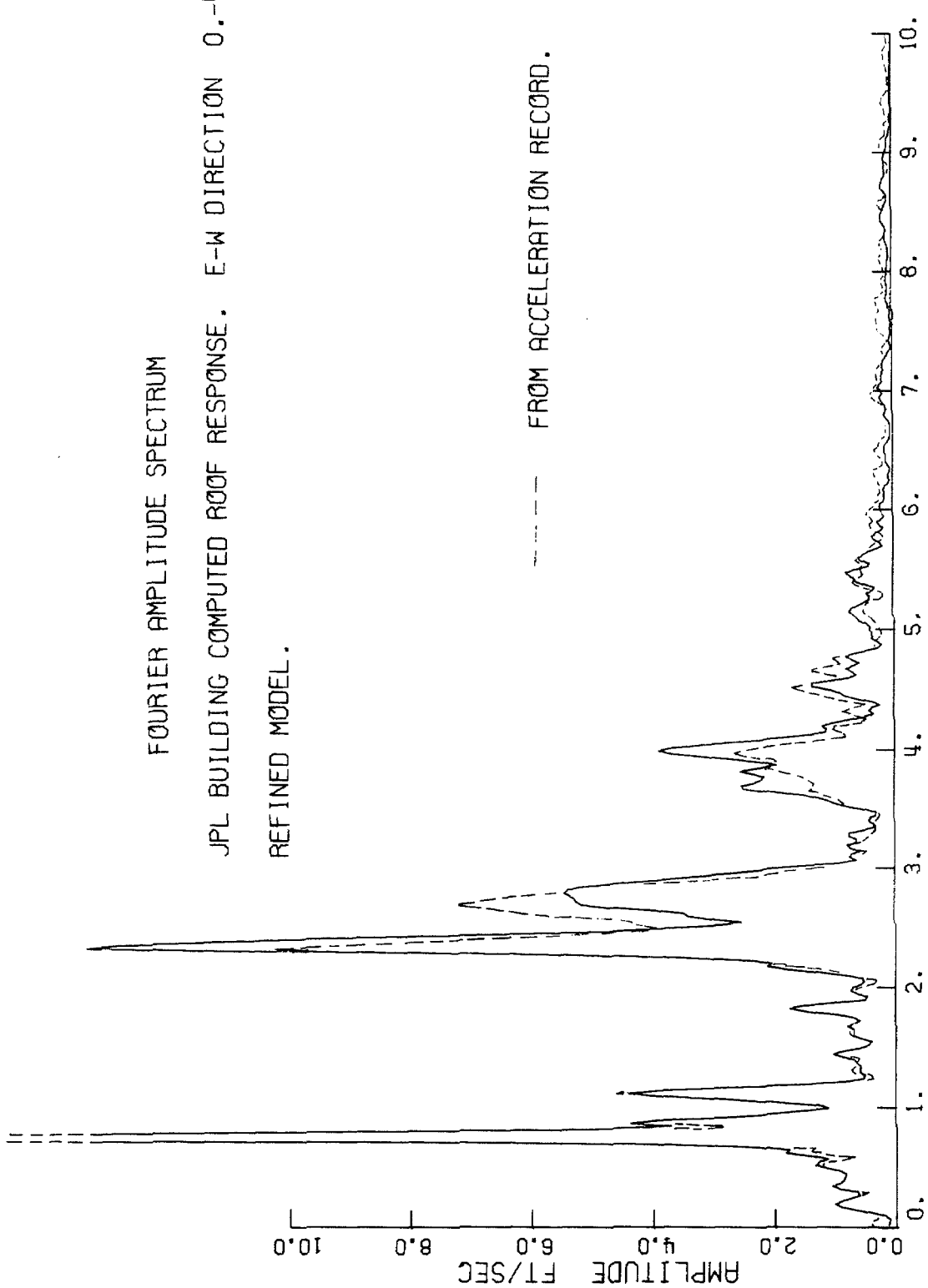

Figure 31. Comparison of Fourier amplitude spectra computed from acceleration record and refined model response.

from the model responses. Hence, if peaks are matched only at the model natural frequencies the building damping ratios are overestimated. In this study the damping ratios were adjusted until the peaks at the second and third natural frequencies were about 30% higher than the corresponding peaks in the recorded spectra. This technique would probably be improved by further smoothing of both spectra before making the comparison or alternatively incorporating a number of shifts in the model periods.

The damping values obtained from the earthquake records are compared with some of the values from Nielsen's[18] forced vibration tests in Table 11.

TABLE 11

Comparison of Damping Ratios

Mode	TEST A		TEST B		Earthquake records	
	Roof accn. amplitude % g	Damping % of critical	Roof accn. amplitude % g	Damping % of critical	Max. roof accn. %g	Damping % of critical
N-S 1	0.073	0.4	0.37	0.6	10	3.0
N-S 2	0.40	1.1	1.89	1.6	10	3.0
N-S 3	-	-	0.67	3.7	9	4.0
E-W 1	0.067	0.5	0.56	0.6	13	4.0
E-W 2	0.52	0.8	1.14	1.1	21	6.0
E-W 3	-	-	1.14	2.0	9	6.0

The earthquake damping ratios are significantly higher than the test values. Both the earthquake and test values tend to increase from mode 1 to mode 3 but the change is less pronounced for the earthquake values. Because of the non-linear behavior of the building, close agreement between the test and earthquake values is not expected.

One source of error in the method used to compute the damping ratios from the earthquake records arises from the fact that modal participation factors are not precisely known during the earthquake. Changes in member stiffnesses result in changes in the mode shapes and hence changes in the participation factors. An error in estimating the modal participation factors reflects itself as an error in the estimated building damping ratios. An estimate of how closely the model mode shapes resemble the building mode shapes during the earthquake can be obtained by comparing the frequency ratios given in Tables 1 and 2. The agreement for the E-W modes is rather better than for the N-S modes. By comparing the participation factors given in Tables 6 and 7 it is possible to estimate their sensitivity to different assumptions regarding the column flexural stiffnesses. The first mode participation factors are not very sensitive to changes in the building properties; however, the factors become more sensitive to changes with increasing mode number. In view of the above limitations in estimating the damping ratios the values given in Figures 27 and 29 represent average building values over the 0 - 40 sec section of record with accuracy of about $\pm$ 1.0 absolute error in the first mode and about $\pm$ 1.5 absolute error in the second and third modes.

The computed acceleration response histories shown in Figs. 27 and 29 are in good agreement with the recorded responses. The agreement could probably be improved by introducing a number of period shifts in the model related to the amplitude of the motions.

The roof acceleration components for the three lowest modes of the refined models are shown in Figs. 32 and 33. Of interest are the large second and third mode contributions over parts of the record.

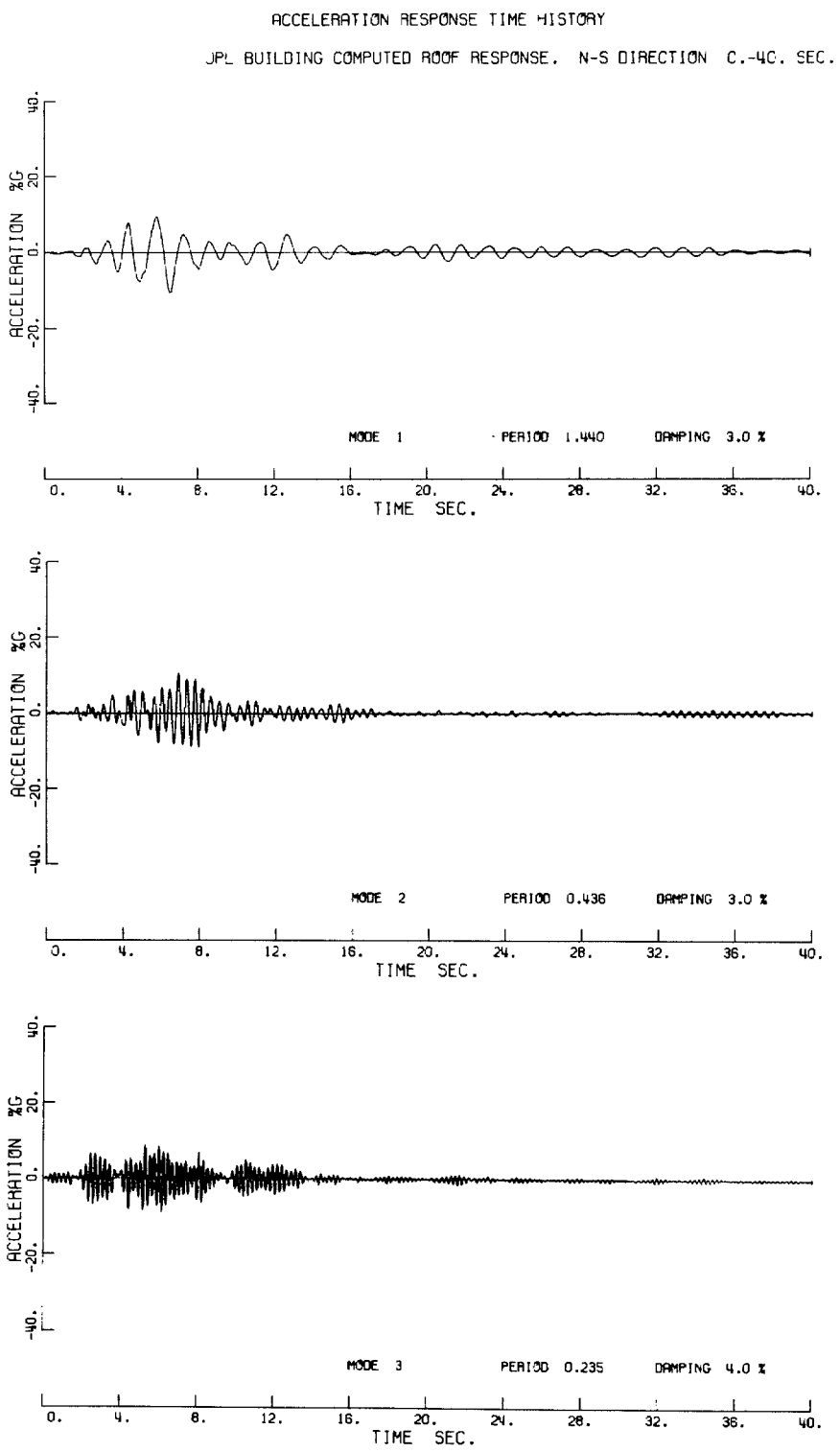

Figure 32. Components of refined model response.

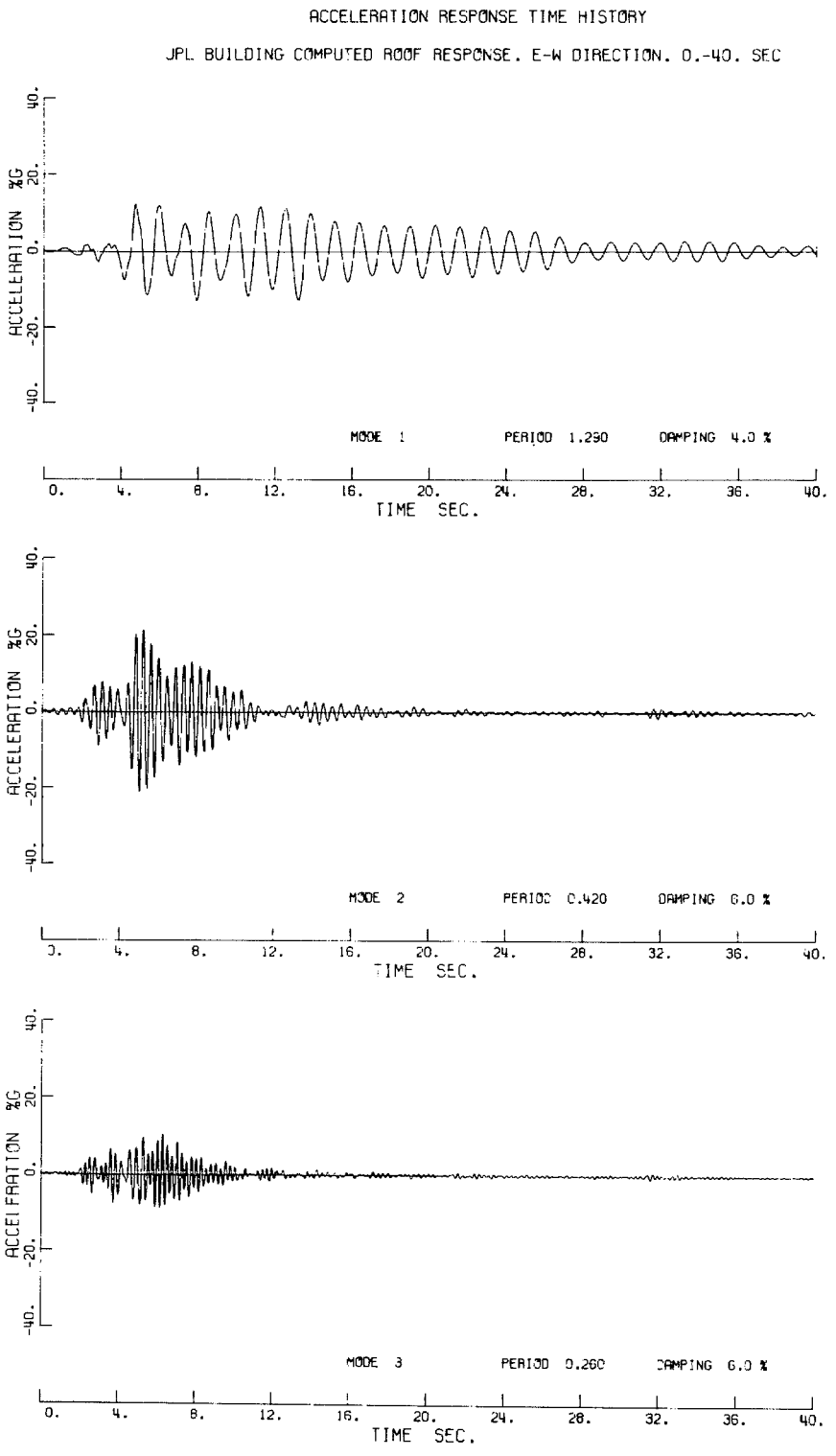

Figure 33. Components of refined model response.

8.2 VERTICAL DIRECTION ROOF RESPONSE

The vertical acceleration time history of the refined partial composite model is compared with the recorded accelerations in Fig. 34. The model periods and damping ratios used are listed on the figure. The first mode period was estimated from the spectra ratio plot (Fig. 24a) and the higher mode periods were taken as the basic model values. The damping ratio in the lowest mode was estimated from a comparison of the Fourier spectra from the computed and recorded vertical acceleration histories using the method described for the horizontal modes. The computed and recorded spectra are compared in Fig. 35. Damping ratios in the higher modes were taken as 2% on the assumption that because most of these modes were of the floor vibration type damping would be expected to be relatively low.

The damping ratio estimate of 7% for the first vertical mode is relatively high in comparison to the values of 3% and 4% obtained for the first N-S and the first E-W horizontal modes respectively. This high value may be to some extent a reflection of errors in the selection of the first mode period or in the computation of the first mode participation factor. The model is not sufficiently refined to enable a particularly good estimate to be made of the vertical response of the building. In particular, the roof weights have been assumed uniformly distributed along the length of the building and lumped at five points across the span in a uniform manner, whereas in fact the heavy mechanical equipment is distributed in a less regular manner. The first mode roof response at the accelerograph location has a contribution from the

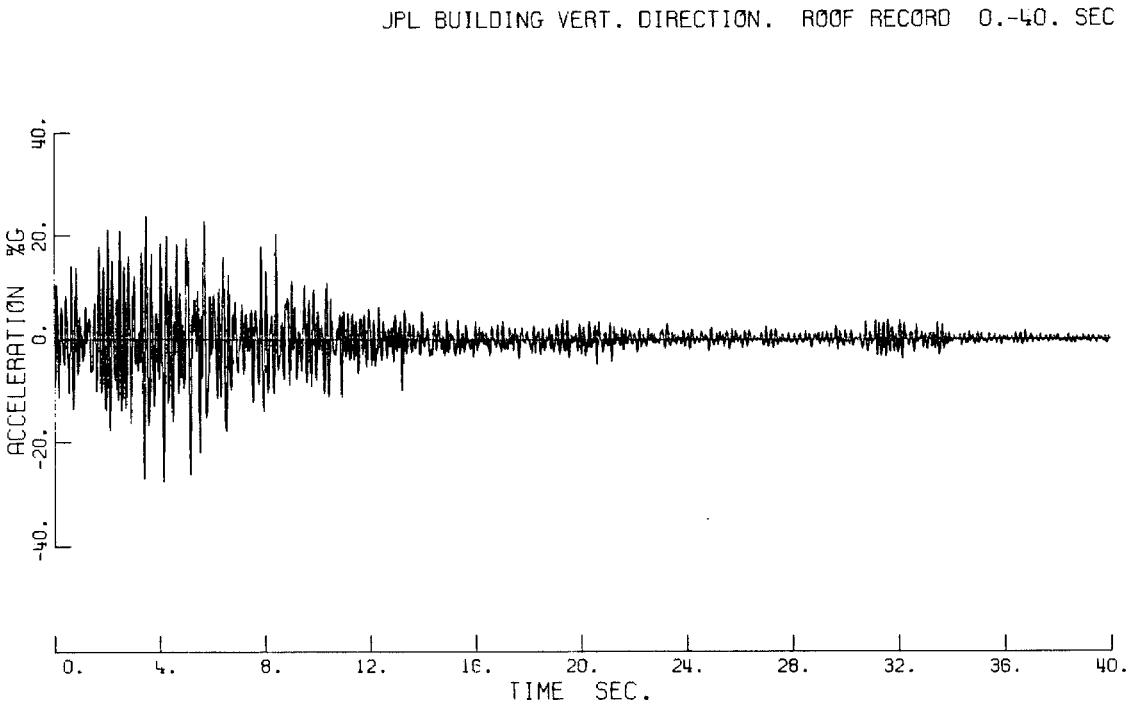

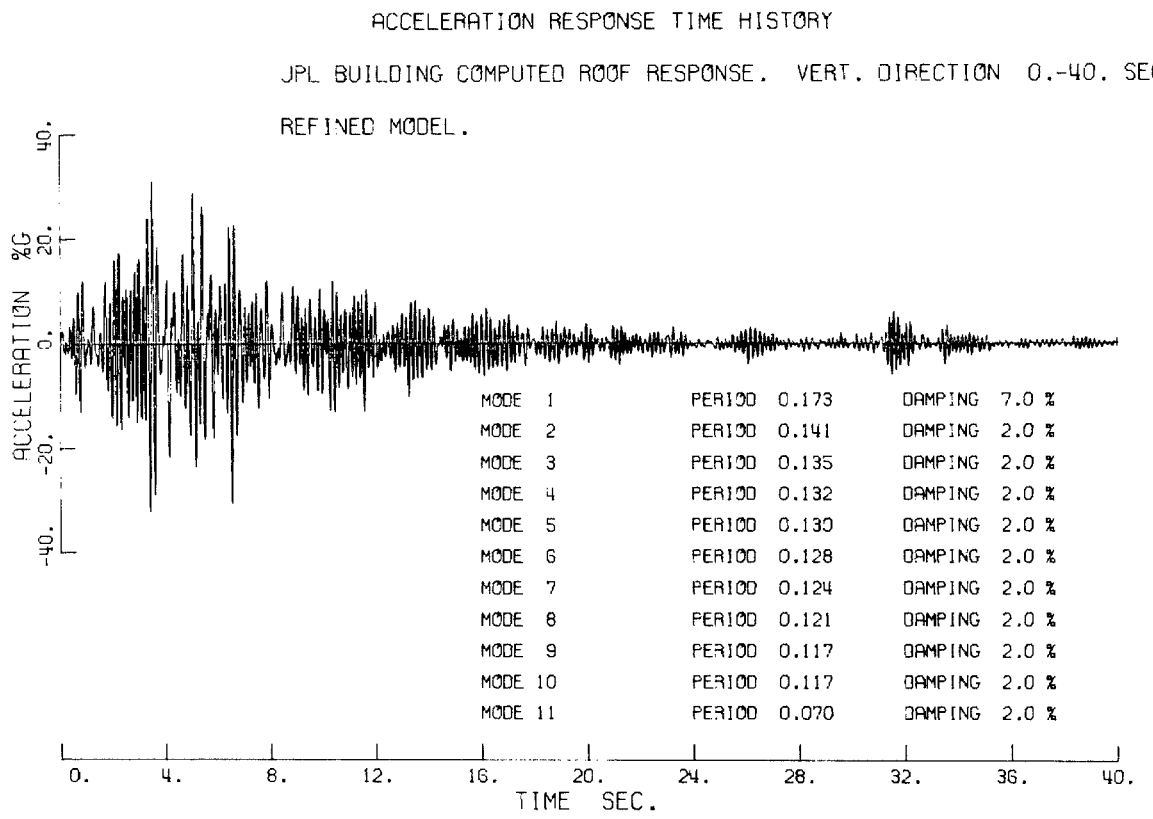

Figure 34. Comparison of recorded roof accelerations with computed refined model response.

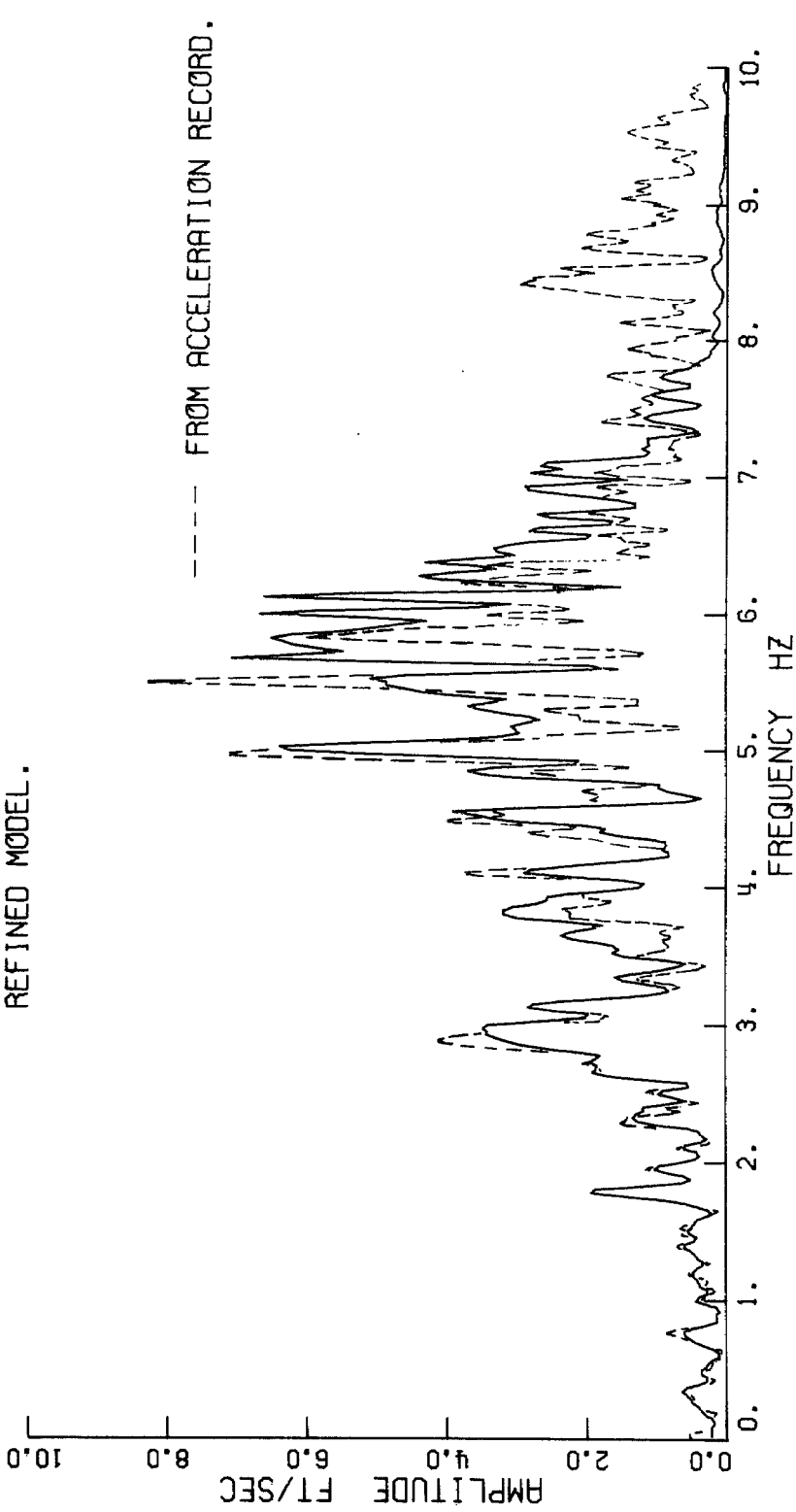

Figure 35. Comparison of Fourier amplitude spectra computed from acceleration record and refined model response.

floor girder deformation approximately twice the column axial deformation contribution and so assumptions made concerning mass and stiffness distributions in the roof system have a significant influence on the participation factor. The base accelerograph is located on the basement concrete floor slab approximately 3 ft above the top of the column foundation footings and about 3 ft horizontally from the footing edge (Fig. 7). In this location the instrument will not record the exact movement of the column base and this could also result in an error in the estimate of the vertical damping ratio.

In overall appearance the computed and recorded vertical response histories are reasonably similar although in detail the comparison is not particularly good. By comparing the Fourier spectra from the computed and recorded accelerations, it is evident that the model does not exhibit sufficient amplification in the 8 - 10 hz range and this is perhaps one explanation for lack of detailed agreement between the records.

Modes higher than the first contribute only a small amount to the total roof response as can be seen by the comparison in Figure 36 of the acceleration response of the 11 mode model and the response from the first mode only.

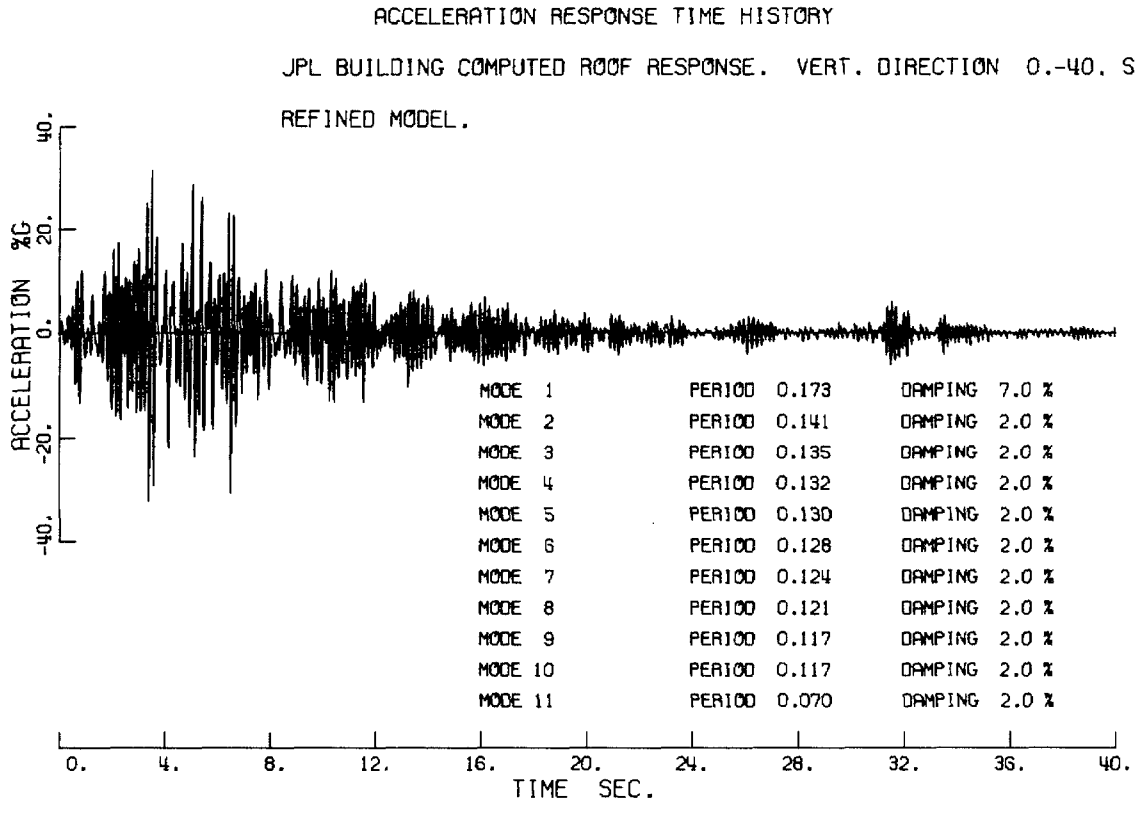

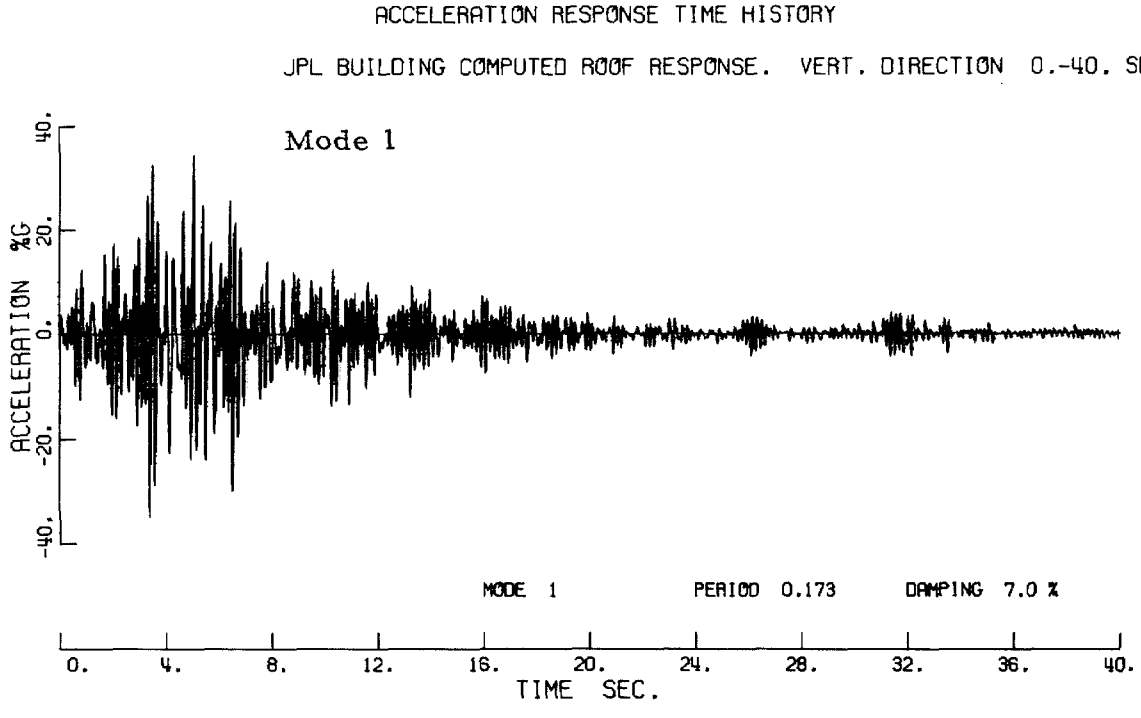

Figure 36. Comparison of response of 11 mode vertical model and response of first mode only.

9. MAXIMUM STRESSES

Approximate estimates of the maximum member stresses were computed from the refined model acceleration response histories. A complete time history of the member forces was not computed since, owing to the large number of members in the trussed girder models, this required excessive computing time. However, a time history of the story forces and shears can be conveniently computed from the acceleration history and this approach was used to determine the dynamic story forces producing the maximum lower story shears. The building models were then subjected to a number of static analyses using these sets of dynamic forces to obtain approximate estimates of the maximum member forces in the lower stories. Some of the member properties decrease with height in the building and so it is possible that some of the upper story stresses may have been higher than the computed lower story values.

Because the building models were derived by summing member properties over each story, the computed stresses are in effect average member stresses and stresses in some individual members may be slightly higher.

Maximum bending, axial and combined stresses in the steel sections are given in Table 12. Shear stresses were not computed.

TABLE 12

Maximum Steel Section Stresses

Stresses in kips/in^2 Compression +

Tension −

Direction	Member	Critical Stress & Location	DL + LL Axial	DL + LL bending	Hor. EQ Axial	Hor. EQ bending	Vert. EQ	Total stresses
N-S	Column Floor 1-2	Compression above floor 1 Inner fiber	10.5	- 3.5	- 2.3	18.6	1.6	24.9
N-S	Column Floor 2-3	Compression. Below bottom chord of floor 3 truss. Inner fiber	9.3	3.6	2.0	9.2	1.5	25.6
E-W	Column Floor 2-3	Compression. Above top chord of floor 2 truss	9.3	-	Low. Not com-puted	20.4	1.5	31.2
N-S	Floor 4 Truss diagonal	Compression. Top end of member.	9.8	1.1	8.0	4.6	1.2	24.7
N-S	Floor 3 Truss bottom chord	Compression. At column face	5.6	1.5	12.4	1.9	0.8	22.2
E-W	Floor 3 Truss bottom chord	Compression. At Column face	Low. Not computed		12.9	Low. Not com-puted		12.9

COMMENTS:

(1) The dead load plus live load stresses given are based on an assumed 20 lb/ft^2 live load plus partition load. Design dead load plus live load stresses would be about 25% higher.

(2) N-S direction stresses have been computed assuming the model to be held against translation at floor 1 only. Restraining the building at floor 2 as well as at the floor 1 level would change the location of the 2-3 column maximum stress but make only a small change in the total stress value given. The 1-2 column stresses would be reduced by additional restraint at floor 2.

(3) N-S column stresses have been computed on the assumption that the outer fiber stresses are not critical because of the concrete section. The inner fiber compressive stresses have been computed assuming complete cracking of the concrete area. If the concrete is neglected on the outer face then the maximum total outer fiber stresses become:

Column Floor 1 - 2	36.5 kips/in^2
Column Floor 2 - 3	26.0 kips/in^2

(4) E-W column stresses have been computed using the bare steel column section. Assuming partial composite action (concrete effective in compression) reduces the total stress given to 18.0 kips/in^2.

Maximum column stresses for combined N-S and E-W earthquake loading were computed assuming no composite action in the E-W direction and that the stresses on the inner fiber were critical. Both the absolute and root-mean-square sums of the horizontal direction earthquake stresses were added to the gravity stresses, giving the following total combined stresses:-

Absolute sum	40.9 kips/in^2
R-M-S sum	33.6 kips/in^2

Because of the simplifications made to compute the dynamic stresses it was not possible to find the exact maximum stresses from the combined earthquake loads. In general the RMS sum provides a satisfactory approximation to the true maximum. The absolute sum gives an upper bound to the maximum combined stress. The critical combined column stress is located just below the bottom chord of the third floor E-W truss.

Maximum story shears were computed for the refined models and are shown in Figure 37. In general the maximum shears in each story are reached at different times and this point is illustrated in Figure 37 by the plot of story shear-force distribution in the models at the time of occurrence of the maximum base shear.

The time history of the base shear for the E-W refined model is plotted in Figure 38. This plot gives an indication of the number of cycles of high stressing that occurred during the earthquake in the lower members of the building.

The building displacements were computed by a static analysis using only the dynamic load distributions which occurred at the time of each maximum story shear force. In order to obtain a good estimate of the maximum displacements in the earthquake, it would be necessary to compute displacements at each time step in the dynamic analysis. The limited analysis undertaken may underestimate the maximum values; however, the interstory displacements computed are expected

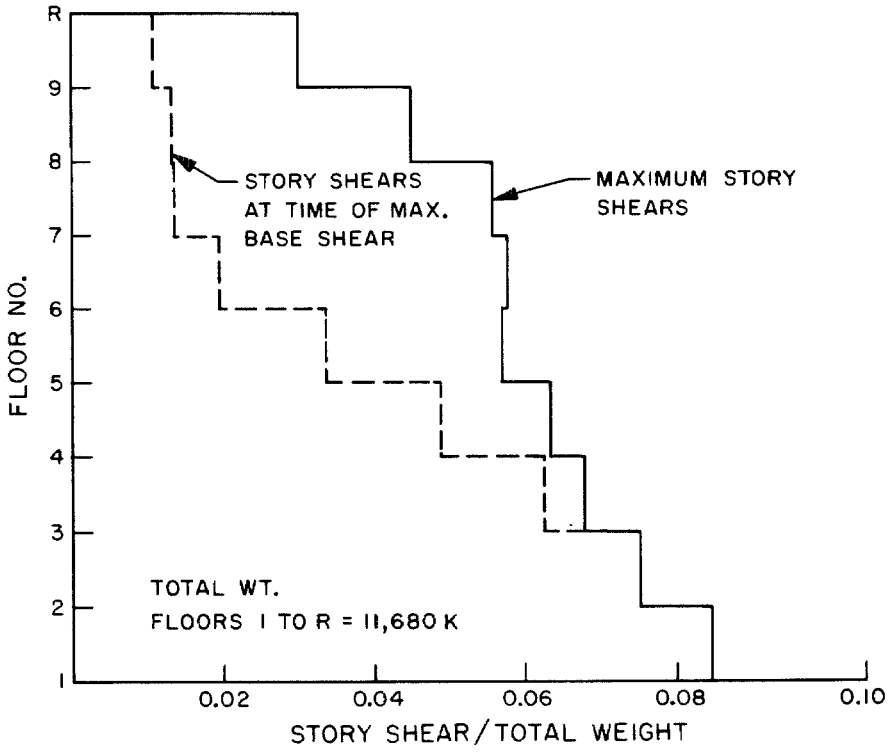

N-S DIRECTION

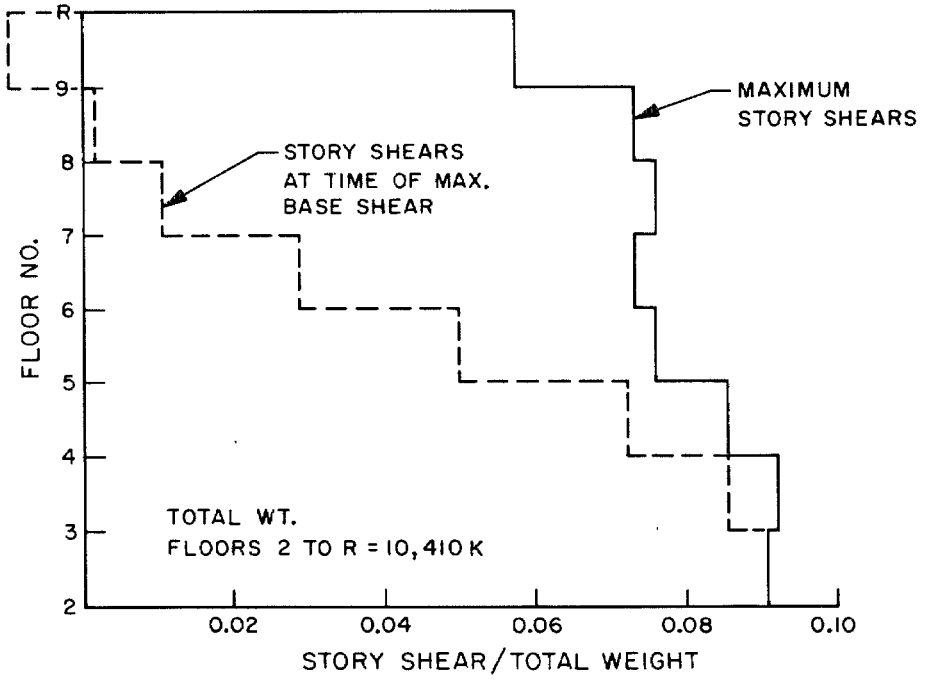

E-W DIRECTION

Figure 37. JPL Building 180. Maximum shears.

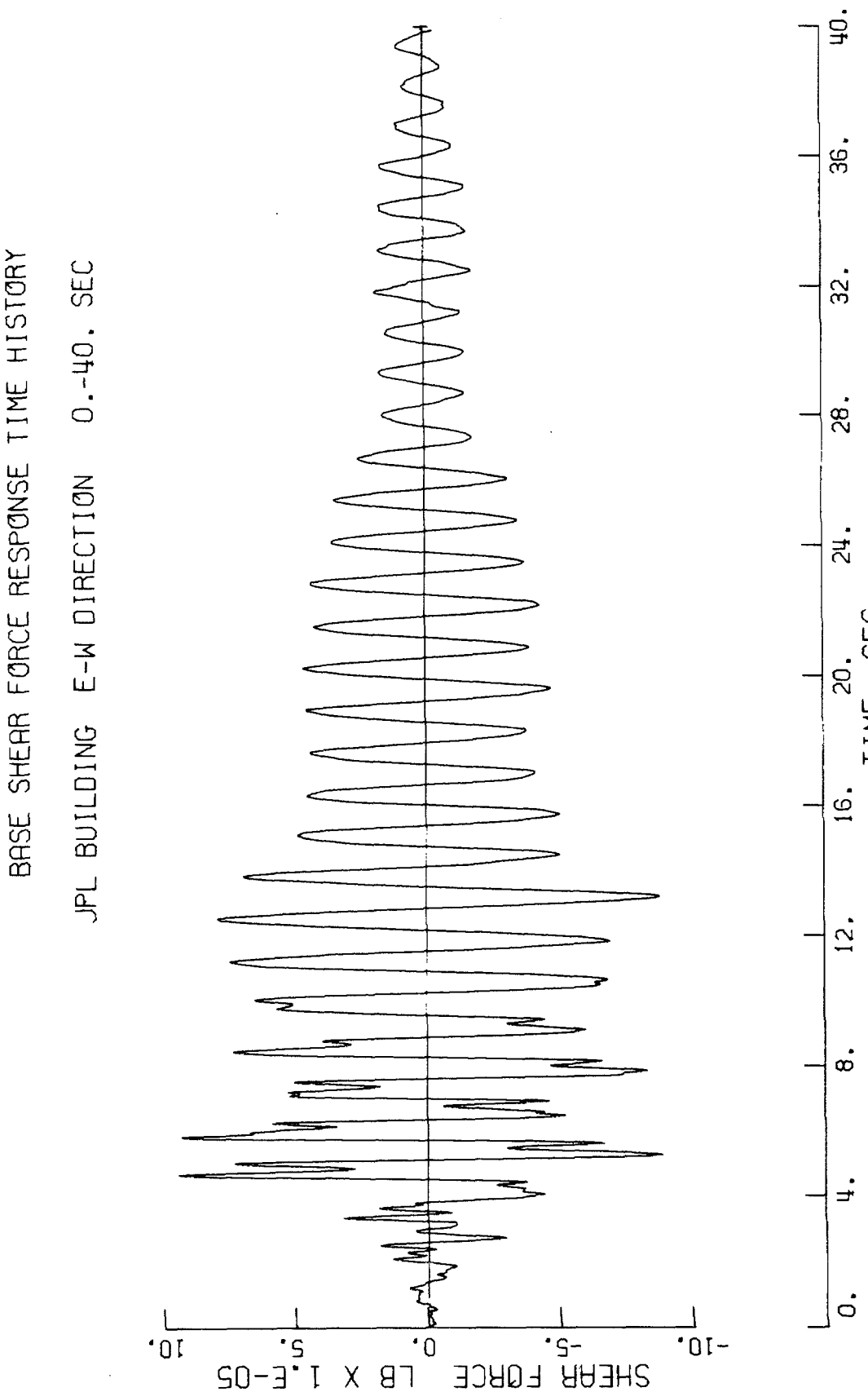
BASE SHEAR FORCE RESPONSE TIME HISTORY
JPL BUILDING E-W DIRECTION 0.-40. SEC
SHEAR FORCE LB X 1.E-05
10.
5.
0.
-5.
-10.
0.
4.
8.
12.
16.
20.
24.
28.
32.
36.
40.
TIME SEC.

Figure 38.

to be close to the true maximum values. In both the north-south and east-west directions a maximum total roof displacement of 2.5 ins was computed. The maximum computed interstory displacements are given in Table 13.

TABLE 13

Story	Max. Interstory Displacements ins	
	N-S	E-W
9	0.19	0.40
8	0.27	0.32
7	0.32	0.39
6	0.33	0.30
5	0.31	0.30
4	0.33	0.33
3	0.32	0.35
2	0.32	0.27
1	0.31	-

10. INFLUENCE OF SOIL - STRUCTURE INTERACTION ON RECORDED BASE ACCELERATIONS

If the Fourier amplitude spectra of the recorded horizontal base motions (Figs. 19 and 20) are compared with the Fourier spectra ratio plots (Figs. 22a, 23a) it is evident that relatively large peaks tend to occur in the base spectra at frequencies which correspond very closely to the predominant natural frequencies of the building. In the E-W direction, peaks in the base spectra at frequencies 0.78, 2.4 and 4.0 hz correspond closely with the natural frequencies of the building;

$f_1 = 0.78$ hz, ($T_1 = 1.29$ sec); $f_2 = 2.4$ hz, ($T_2 = 0.42$ sec);

$f_3 = 3.9$ hz, ($T_3 = 0.26$ sec). In the N-S direction peaks at frequencies 2.5 and 4.2 hz are reasonably close to the second and third natural frequencies; $f_2 = 2.3$ hz, ($T_2 = 0.44$ sec); $f_3 = 4.3$ hz, ($T_3 = 0.24$ sec). These corresponding peaks may suggest that either because of soil-structure interaction or for some other reason the vibrations of the building have modified the base record. An inspection of the building revealed that it was very unlikely that the building vibrations could be transmitted to the base instrument (located on the basement slab overlying the soil) other than by deformation of the soil foundation.

It is of interest to note that from the work presented in Section 10.2.3 it was found that the influence of soil-structure interaction on the spectra, particularly in the building modes higher than the first, may tend to show more as dips rather than peaks. Luco[15], and Meek and Veletsos[17] have presented soil-structure interaction solutions for shear buildings which also show this dipping modification.

10.1 COMPARISONS OF FOURIER AMPLITUDE SPECTRA

Comparisons between the Fourier amplitude spectra of the Building 180, Seismological Laboratory and Millikan Library base records are shown in Figures 39 and 40. In general a good degree of similarity exists between the Building 180 spectra and the Millikan Library spectra. (The predominant fundamental frequencies of the Library during the first 40 sec of the earthquake were N-S 1.65 hz, E-W 0.98 hz and peaks in the base record spectra can be seen at these frequencies). Relative to the Seismological Laboratory spectra both pairs of building spectra show amplifications at frequencies close to 1.0 hz and between the range 2.0 to 3.0 hz. In general at frequencies greater than 5.0 hz the peaks in the Seismological Laboratory spectra tend to be of greater magnitude than the peaks in the spectra from both buildings. It is of interest to note that the peak in the Building 180 E-W base spectra, which corresponds to the building fundamental frequency, can be seen in the Millikan Library spectra but does not appear in the Seismological Laboratory spectra.

Because of the irregular nature of the spectra and the influence of factors such as wave travel paths on their character, it is difficult to draw firm conclusions about the extent of soil-structure interaction modifications. However, from the comparison made there appears to be no particular reason to suspect that the Building 180 horizontal records were significantly modified by the presence of the building.

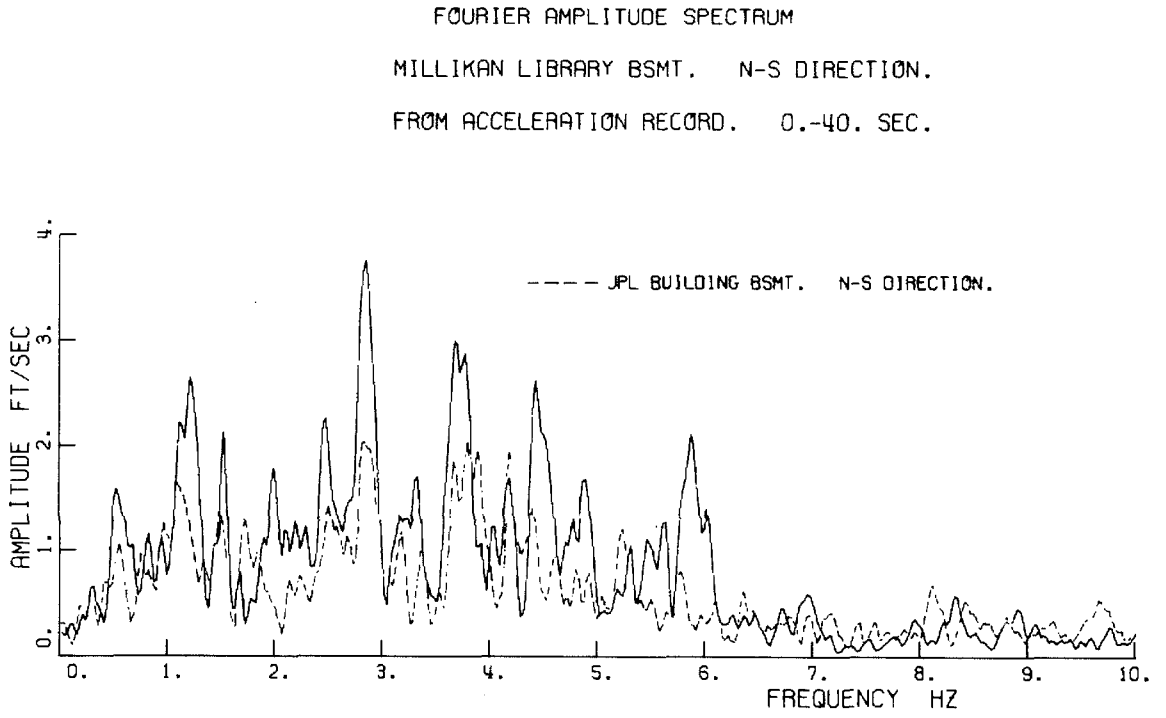

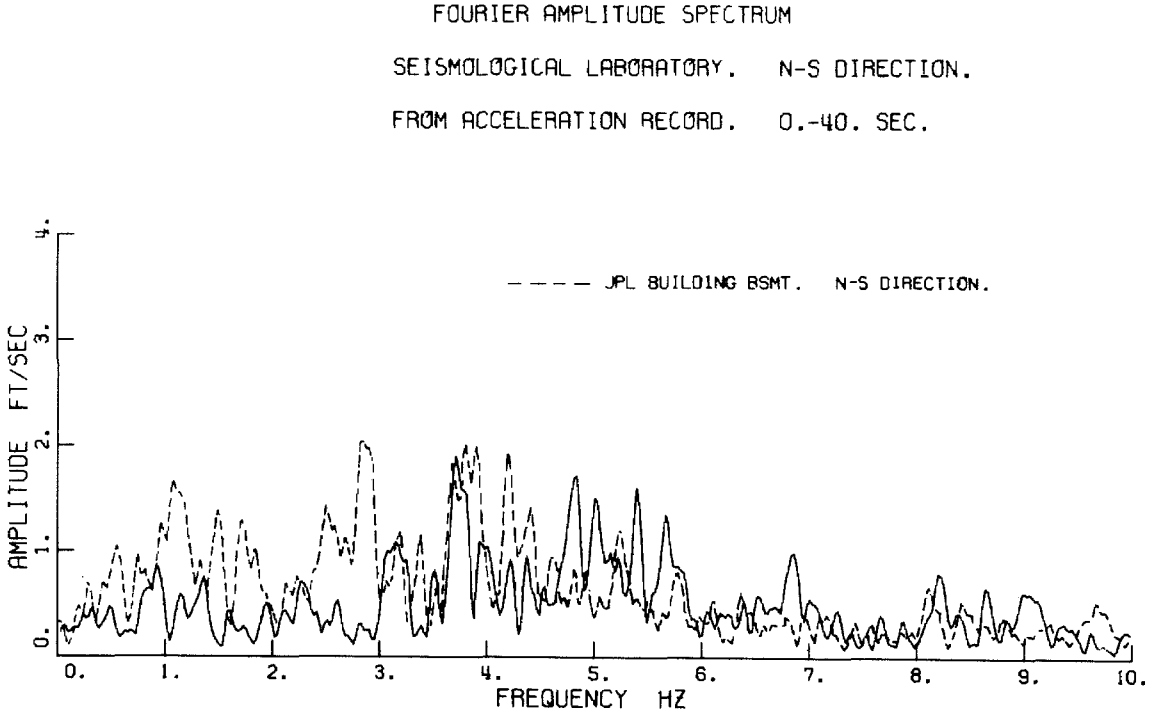

Figure 39. Comparison of Fourier amplitude spectra.

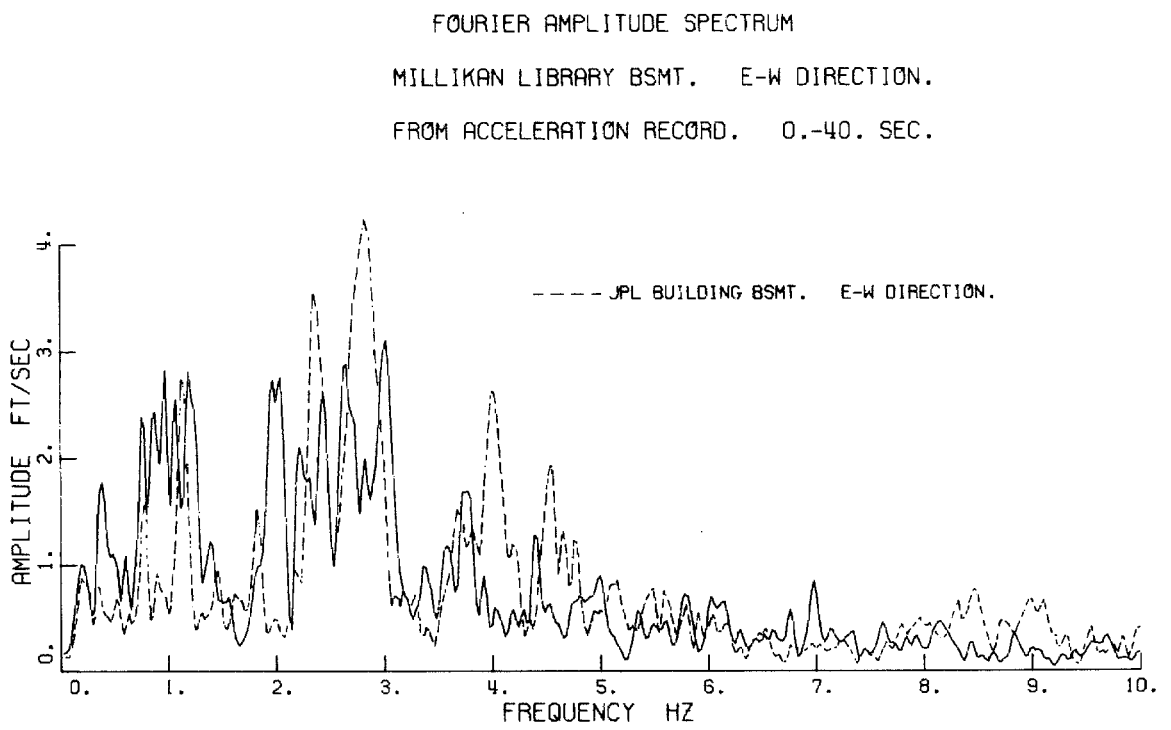

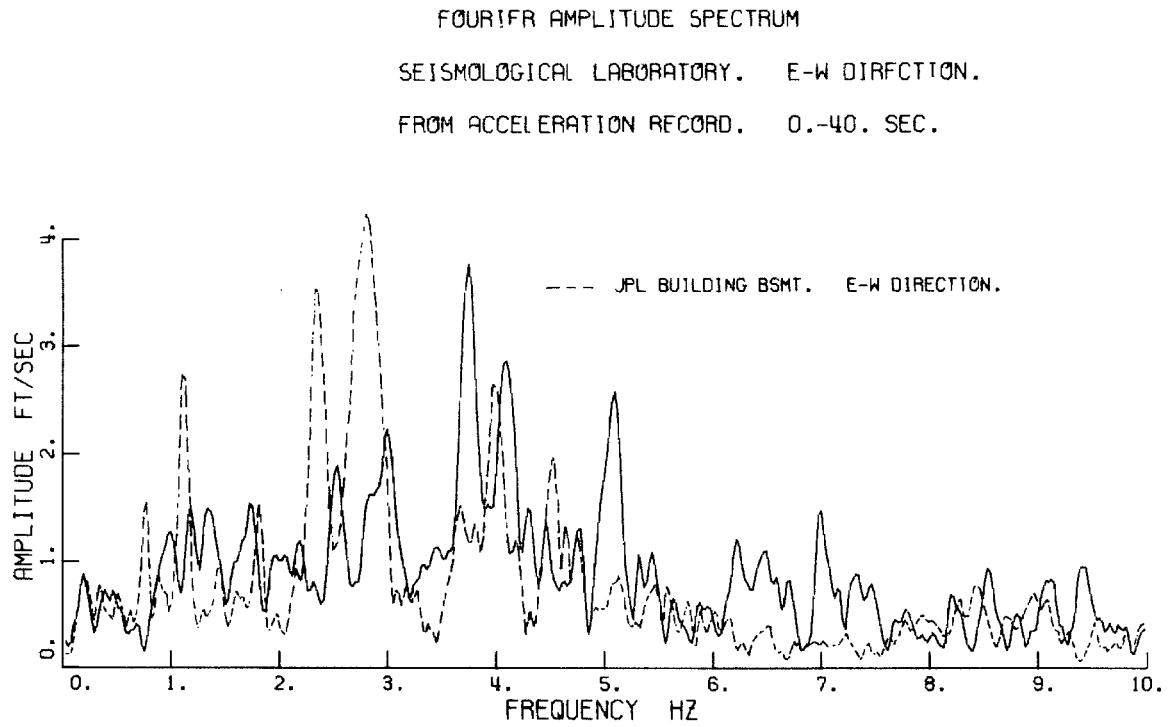

Figure 40. Comparison of Fourier amplitude spectra.

10.2 SOIL-STRUCTURE MODEL

The influence of soil-structure interaction may be studied by developing a simplified model that exhibits the basic dynamic characteristics of the building-soil system. In this section the influence of soil-structure interaction on the recorded Building 180 base records is studied by approximating the soil behavior with springs and dashpots.

In recent research (Bielak[1], Luco and Westmann[16], Veletsos and Wei[27]) the soil-structure interaction problem has been simplified by assuming that the soil can be represented by an elastic half-space. By making this assumption the problem is essentially reduced to the solution of the equations of three-dimensional elastic wave propagation for the prescribed boundary conditions. However, solution of the wave equations for all but the simplest of boundary configurations is difficult and at present only a limited number of relevant solutions have been presented in detail. Luco and Westmann[16] and Veletsos and Wei[27] have presented detailed solutions for the compliance functions of a rigid circular disc resting on an elastic half-space. Sarrazin[21] has presented a detailed summary of previous soil-structure interaction research and gives details of the solution of Kobori et al[14] for the rigid rectangular plate resting on the half-space. Dynamic compliances for a rigid strip footing have been computed by Karasudhi, Keer and Lee[13], and Oien[20].

Many building foundations have complex geometric details and may be rather poor approximations to a single rigid disc or rectangular plate resting on an elastic half-space. In particular foundations

are frequently embedded some distance below the surface and may consist of a number of individual footings or piles. Although the finite element method of analysis and full scale dynamic testing techniques are suitable for studying more complex foundation systems, only a very limited amount of information on application of these methods is available. In this study, because of the lack of more exact information, some of the results from the rigid disc and rectangle theory are applied to the complex Building 180 foundation system.

Veletsos and Wei[27] and other researchers have shown that for the case of the rigid disc, the elastic half-space may be conveniently approximated by pairs of springs and dashpots; one pair acting in the translational direction and one pair operating in the rotational direction. The spring constants and damping coefficients vary with the frequency of the disc oscillations. From the results of Veletsos and Wei it is apparent that the properties of the translational spring and dashpot are almost constant over a wide range of frequencies, but the rotational spring constant and damping factor vary significantly with frequency. The frequency range of interest for horizontal translation of Building 180 is 0 - 12 hz corresponding to a range of the dimensionless frequency $a_o = \frac{\omega r}{V_s}$ (r = disc radius; V_s = shear wave speed in the soil) from 0 - 5. Over this range the translation spring and dashpot parameters vary by less than 10% (at zero frequency the spring constant has the static value) and in view of the difficulty in estimating or measuring dynamic elastic constants for the soil and the generally poor approximation of the rigid disc to foundations systems these

parameters may be assumed to be frequency independent for many practical problems.

By defining an equivalent disc of equal area to the rectangular plate Sarrazin[21] has shown that the frequency dependence of its spring and dashpot parameters are approximately the same as the disc for an a_o range 0 - 1.5. Sarrazin has extended Kobori's solution for a rectangular plate having a width twice the length along the direction of translation from a_o = 2.0 to 5.5. At frequencies greater than a_o = 2.0 the behavior differs considerably from an equivalent disc. Solutions have not been evaluated for other geometries at frequencies greater than a_o = 2.0.

Translation spring constants are evaluated below for Building 180 using the static solution for the rectangular plate on the half-space and dynamic test results from the Millikan Library (Jennings and Kuroiwa[8]). Damping coefficients were estimated by using an equivalent radius and the solution for the rigid disc.

10.2.1 SOIL PARAMETERS FOR HORIZONTAL TRANSLATION

Apart from the seismic wave velocity measurements[3] made some distance from Building 180 no direct measurements were made to determine the soil elastic constants. Because basic similarities exist between the soils and the structural foundation systems of both Millikan Library and Building 180, it was assumed that the horizontal spring constant evaluated from the Library tests could be used to compute the Building 180 spring constant.

In a steady-state forced test of the Library building the N-S fundamental mode was excited at a period $T_1 = 0.53$ sec with an amplitude of roof acceleration of about 2% g. From the measured mode shape, the maximum base shear was computed, and by assuming this force to be statically applied and using the displacement measured on the basement slab a horizontal spring constant if $K_x = 2.4 \times 10^9$ lb/ft was computed. Strictly speaking, the value of K_x should be evaluated by solving the equation of motion for base translation given in Section 10.2.3. In this particular case the pseudo-static approach is a satisfactory approximation and introduces an error of less than 5% in K_x.

Whitman and Richart[29] present the following relationships for the static spring constants of a rigid rectangular plate resting on an elastic half-space. (The relationships were derived from Gorbunov-Possadov[6]).

$$\text{Horizontal } K_x = 2(1+\nu)\, G\, \beta_x \sqrt{BL} \qquad (10.1)$$

$$\text{Vertical } K_z = \frac{G}{(1-\nu)}\, \beta_z \sqrt{BL} \qquad (10.2)$$

where G = the shear modulus

ν = Poisson's ratio

β_x, β_z are dimensionless constants dependent on the plate geometry. B, L are the plate dimensions. L is in the direction of the horizontal force.

The relationships between β_x, β_z and the ratio L/B are plotted by Whitman and Richart[29] . β_x varies between 0.95 and 1.05 for a range of L/B 0.5 to 5.0, and so for most practical purposes may be assumed to be 1.0. β_z varies from 2.15 for L/B = 1.0 to 2.5 for L/B = 5.0

Substituting the value of K_x determined by the dynamic test into expression (10.1) and assuming a plate of 80 ft x 80 ft dimensions gives the Young's modulus for the library foundation soil as $E = 2.96 \times 10^7$ lb/ft^2. Assuming $\nu = 0.3$ and the unit weight of the soil to be 120 lb/ft^3 gives a shear wave speed of 1,750 ft/sec. This wave speed is significantly higher than given by direct wave speed measurements on similar soils (5) and presumably reflects to some extent the inadequacy of expression (10.1) for the relatively complex foundation system. To enable an approximate estimate to be made of the influence of foundation embedment on the translational spring constant a finite element analysis was made of the two horizontally loaded rigid strip foundations (plane strain) shown in Fig. 41. The analyses gave the following load displacement relationships.

Embedded foundation $\quad \frac{p}{uG} = 2.61$

Surface foundation $\quad \frac{p}{uG} = 1.76$

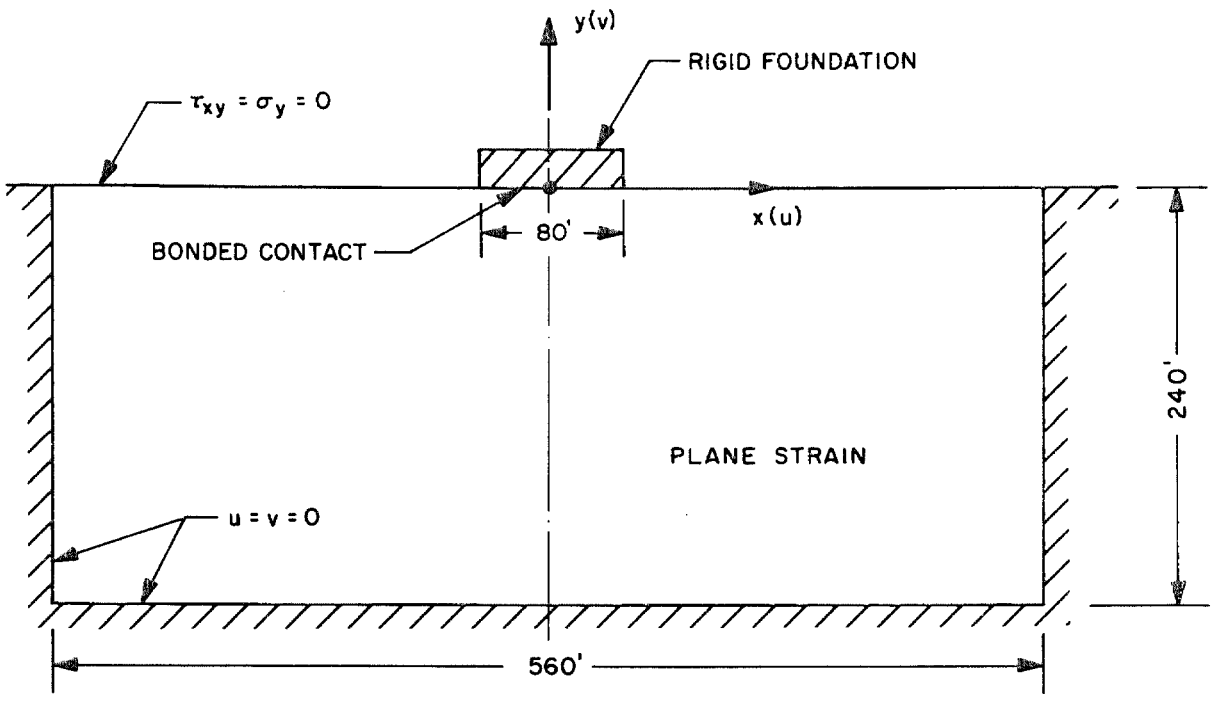

SURFACE FOUNDATION

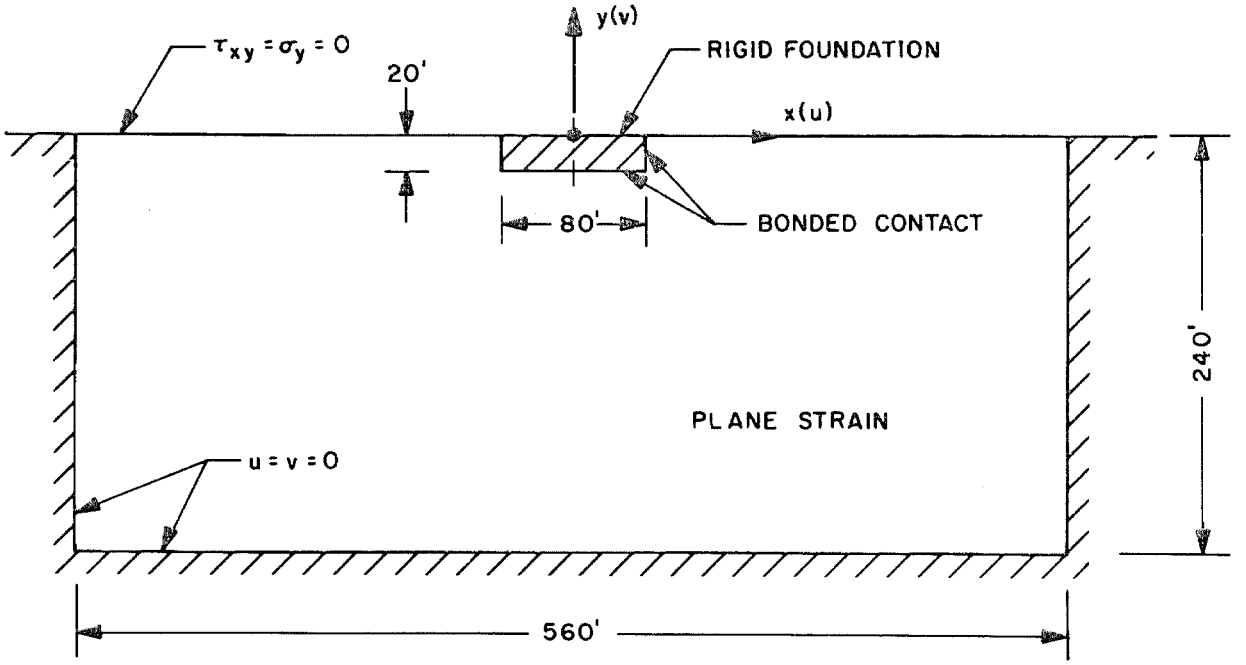

EMBEDDED FOUNDATION

Figure 41. Finite element foundation models.

where p = the horizontal load per unit length

u = the horizontal displacement of the contact surface

G = the soil shear modulus

(Poisson's ratio was taken as $\nu = 0.3$)

It is apparent that embedment produces an appreciable increase in the foundation horizontal translation stiffness for the plane strain problem. A larger increase would be expected for a rectangular three-dimensional problem.

A spring constant was calculated for E-W translation of Building 180 by using the elastic constants given above for the Library and the total base dimensions of Building 180 in expression (10.1). This value was reduced by a factor of 1.25 (obtained from the work of Seed[22] to allow for the greater soil strains occurring in the earthquake than in the building test. Of interest in this study was the determination of the maximum expected influence of base translation and so, in view of the possibility of relatively large errors from the assumptions made, a value of one-half the computed spring constant was used, giving $K_x = 1.13 \times 10^9$ lb/ft.

A damping coefficient was computed by assuming an equivalent radius for the total base and using the following relationship from Veletsos and Wei[27]:

$$C_x = C_1 \frac{K_x r}{V_s} \qquad (10.3)$$

where C_x = the base damping coefficient for horizontal translation

$C_1 \approx 0.6$, a parameter dependent on ν and the dimensionless frequency a_o. Values are plotted by Veletsos and Wei[27].

A value of V_s was used that was consistent with the elastic constants chosen to compute K_x. That is, V_s was computed from the value of E obtained by the Library test reduced by a factor of 2.5. (2.0 arbitrary factor x 1.25 strain factor). This gave the following value,

$C_x = 3.3 \times 10^7$ lb/ft/sec.

10.2.2 SOIL PARAMETERS FOR VERTICAL TRANSLATION

Vertical vibration tests conducted on the Millikan Library did not provide satisfactory details for computing a soil vertical spring constant.

In the vertical direction the Building 180 foundation can be approximated by two rigid parallel strips 7 ft x 230 ft under each row of columns. By assuming $\nu = 0.3$, a shear wave velocity of 910 ft/sec was computed from the measured compressional wave velocity of 1700 ft/sec (at 30 ft depth), which is consistent with measured shear wave velocity values for similar soils given by Duke et al[5]. By using this wave velocity and the solution of Karasudhi et al[13] for the dynamic compliances of an infinitely long rigid strip, values for the vertical spring constant and damping coefficient were obtained. The influence of the depth of foundation embedment was determined approximately by using the static finite element solutions given by Kaldjian[12]. Both the spring constant and the damping coefficient were increased by a factor of 1.6 to allow for embedment. A reduction by a factor of 1.1 was made to allow for the increase in soil strain during the earthquake. The corrected values used for each strip were,

$K_z = 1.2 \times 10^9$ lb/ft

$C_z = 2.0 \times 10^7$ lb/ft/sec.

10.2.3 BASE SPECTRA MODIFICATIONS FROM MODEL PARAMETERS

A building on an elastic foundation may be represented by the model shown in Figure 42 where the soil is replaced by two pairs of springs and dashpots.

The equations of motion for horizontal translation of the model may be written as,

$$M\ddot{\underline{u}} + C\dot{\underline{u}} + K\underline{u} + M(\ddot{u}_g + \ddot{u}_b) = 0 \qquad (10.5)$$

$$\sum_{j=1}^{N} m_j (\ddot{u}_j + \ddot{u}_g + \ddot{u}_b) + m_b(\ddot{u}_g + \ddot{u}_b) + C_x\dot{u}_b + K_x u_b = 0 \qquad (10.6)$$

where,

M = diagonal matrix of story masses

C = building damping matrix

K = building stiffness matrix

m_j = story mass at floor j

m_b = base mass

C_x = base translation damping coefficient

K_x = base translation spring constant

$\underline{u}$ = floor horizontal displacement vector. The displacements do not include the base translation component

u_j = floor horizontal displacement at floor j

u_b = relative horizontal displacement of the base

u_g = free field horizontal ground displacement, and is defined to be the motion that would have been recorded had the building not been present.

The dots above the symbols denote differentiation with respect to time.

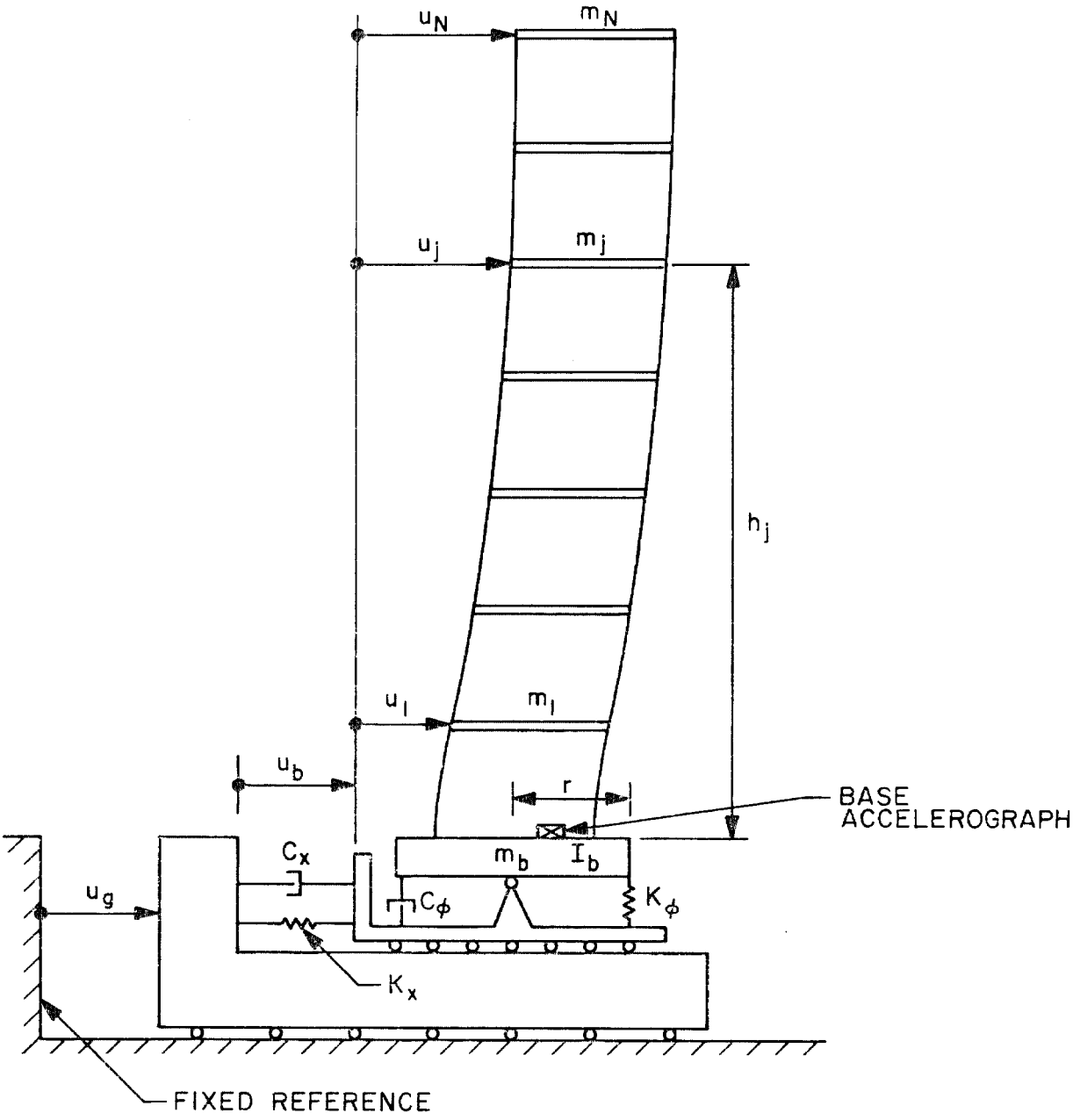

SOIL-STRUCTURE INTERACTION MODEL

Figure 42.

Since $(\ddot{u}_g + \ddot{u}_b)$ is recorded by the basement accelerometer equations (10.5) may be solved for $\underline{u}$ using the recorded motion as the forcing function. If the component in $\underline{u}$ due to base rotation is small, then the assumption of classical normal modes can be made and the previously described method of solution used. The influence of rocking can be considered in an approximate manner by employing in the solution the lower mode periods and damping evaluated from the study of the recorded roof and base motions.

Equations (10.6) may be written as

$$C_x \dot{u}_b + K_x u_b = -m_b(\ddot{u}_g + \ddot{u}_b) - S_b(t) \qquad (10.7)$$

where $S_b(t) = \sum_{j=1}^{N} m_j(\ddot{u}_j + \ddot{u}_g + \ddot{u}_b)$, and may be evaluated from the solution of equations (10.5).

Equation (10.7) may be solved for u_b by numerical integration; alternatively letting

$F_b(t) = m_b(\ddot{u}_g + \ddot{u}_b) + S_b(t)$ the solution of (10.7) may be written as,

$$\bar{u}_b(\omega) = \frac{-\bar{F}_b(\omega)}{K_x + i\omega C_x}$$

where $\bar{u}_b(\omega) = \int_0^T u_b(t)\, e^{-i\omega t} dt$, the Fourier transform of the truncated function $u_b(t)$ which differs from zero for $0 < t < T$

$$\bar{F}_b(\omega) = \int_0^T F_b(t)\, e^{-i\omega t} dt$$

The bar above the symbols is used to denote the transformed function.

Hence,

$$|\overline{\ddot{u}}_b(\omega)| = \frac{\omega^2 |\overline{F_b}(\omega)|}{\sqrt{K_x^2 + \omega^2 C_x^2}} \qquad (10.8)$$

where $|\overline{\ddot{u}}_b(\omega)|$ = the Fourier amplitude of the base relative acceleration response

$|\overline{F_b}(\omega)|$ = the Fourier amplitude of the base forcing function, $m_b(\ddot{u}_g + \ddot{u}_b) + S_b$.

The Fourier amplitude spectrum of the relative base accelerations can be evaluated from equation (10.8) by using the Fast Fourier Transform computer program to compute $|\overline{F_b}(\omega)|$ from $F_b(t)$.

It is easily shown that

$$|\overline{\ddot{u}}_g + \overline{\ddot{u}}_b| - |\overline{\ddot{u}}_b| \leq |\overline{\ddot{u}}_g| \leq |\overline{\ddot{u}}_g + \overline{\ddot{u}}_b| + |\overline{\ddot{u}}_b| \qquad (10.9)$$

where $|\overline{\ddot{u}}_g + \overline{\ddot{u}}_b|$ = the Fourier amplitude of the combined free-field and relative base accelerations.

$|\overline{\ddot{u}}_g|$ = the Fourier amplitude of the free-field acceleration.

Thus evaluating $|\overline{\ddot{u}}_b|$ enables an upper and lower bound to be established for the free-field spectrum $|\overline{\ddot{u}}_g(\omega)|$.

By using the values of K_x, K_z, C_x and C_z given in sections 10.2.1 and 10.2.2 in equation (10.8) relative base motion spectra were computed for the E-W and vertical base translation of the refined models and are shown in Fig. 43. To compute $|\overline{F_b}(\omega)|$ it is necessary to assume a value for the base mass m_b. In the application of elastic

FOURIER AMPLITUDE SPECTRUM

JPL BUILDING E-W DIRECTION. RELATIVE BASE ACCELERATION.

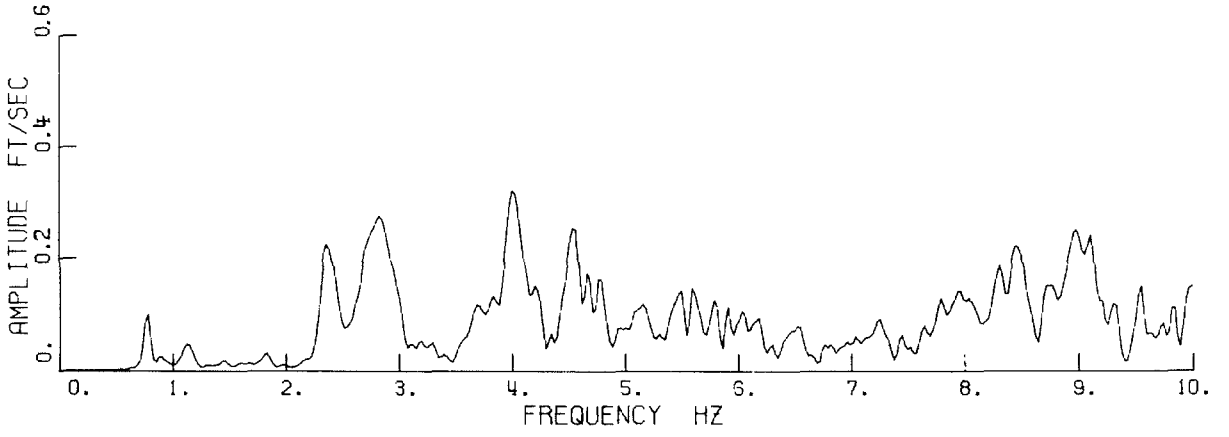

FOURIER AMPLITUDE SPECTRUM

JPL BUILDING VERT. DIRECTION RELATIVE BASE ACCELERATION

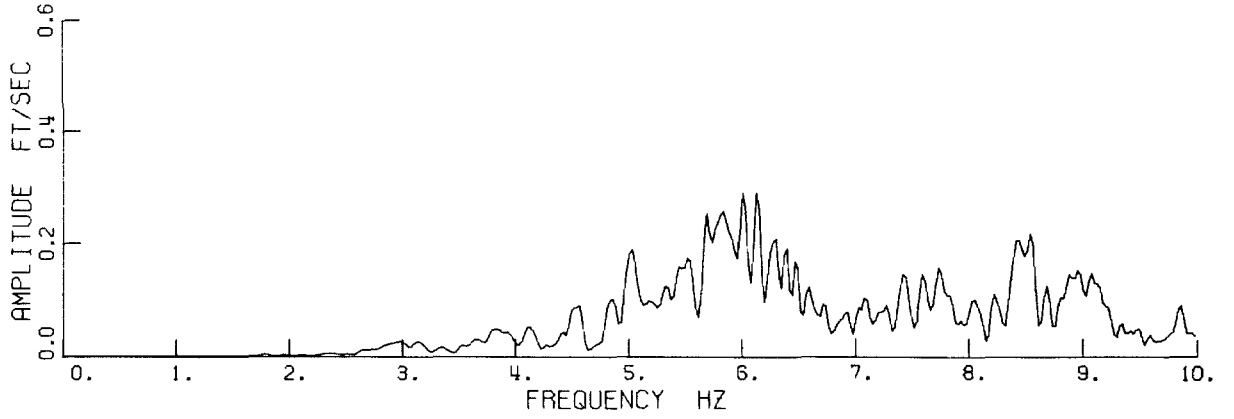

Figure 43.

half-space theory to foundation dynamics it is usual to take the base mass as the mass of the rigid foundation structure; however, for the case of an embedded foundation the present theory gives no indication of how the soil mass displaced by the foundation or surrounding the foundation should be treated. In this study the base mass was taken to be the mass of the basement and the first story (including the foundation strips and walls) assumed in the evaluation of the natural frequencies to have no relative displacement. The base weights used were,

E-W horizontal direction = 7,190 kips

vertical direction = 4,650 kips

Over the 0 - 10 hz frequency range shown in Figure 43 the E-W relative base acceleration spectrum has peak values less than 30% of the peak values of the spectrum of the recorded base motion. In the range 0 - 5 hz, which includes the three lowest natural frequencies of the building, the relative base motion spectrum has peak values less than 10% of the recorded spectrum values.

At frequencies close to the fundamental vertical frequency, $f_1 = 5.8$ hz, the spectrum of relative base vertical acceleration (Figure 43) has peak values of approximately 35% of the peak values in the spectrum of the recorded vertical acceleration. The other peaks over the frequency range 0 - 10 hz have amplitudes that are less significant in relation to the spectrum of the recorded motion.

Determining bounds for the free-field spectra by the above method is informative because the influence of the assumptions regarding the soil-base parameters K_x, C_x and m_b is clearly demonstrated

by equation (10.8). If the soil-base parameters are known and if the assumption is made that the building model with a rigid base (in the translation sense) exhibits classical normal modes, then it is possible to derive a direct relationship between the free-field Fourier amplitude spectra and the recorded base motion spectra. The following method was found convenient for this study.

Equation (10.7) may be written as

$$m_b \ddot{u}_b + C_x \dot{u}_b + K_x u_b = - m_b \ddot{u}_g - S_b(t) \qquad (10.10)$$

Taking the Fourier transform of equation (10.10) gives

$$\bar{u}_b(\omega) \{ - \omega^2 m_b + i\omega C_x + K_x \} = - m_b \bar{\ddot{u}}_g(\omega) - \bar{S}_b(\omega)$$

$\bar{S}_b(\omega)$ may be written as

$$\bar{S}_b(\omega) = H_{11}(\omega) \{ \bar{\ddot{u}}_b(\omega) + \bar{\ddot{u}}_g(\omega) \}$$

where,

$H_{11}(\omega)$ = a transfer function relating the base shear to the base acceleration.

Hence,

$$\bar{u}_b(\omega) = \frac{- \{ m_b + H_{11}(\omega) \} \bar{\ddot{u}}_g(\omega)}{\{ -\omega^2 [m_b + H_{11}(\omega)] + i\omega C_x + K_x \}} \qquad (10.11)$$

Defining,

RH = the real part of $H_{11}(\omega)$

IH = the imaginary part of $H_{11}(\omega)$

and arranging (10.11) gives,

$$(\bar{\ddot{u}}_g + \bar{\ddot{u}}_b) = \frac{(K_x + i\omega C_x) \bar{\ddot{u}}_g}{\{ K_x - \omega^2 (m_b + RH) \} + i \{ \omega C_x - \omega^2 IH \}} \qquad (10.12)$$

Hence,

$$\frac{|\ddot{\bar{u}}_g + \ddot{\bar{u}}_b|}{|\ddot{\bar{u}}_g|} = \frac{\sqrt{K_x^2 + \omega^2 C_x^2}}{\sqrt{\{K_x - \omega^2(m_b + RH)\}^2 + \{\omega C_x - \omega^2 IH\}^2}} \qquad (10.13)$$

From the normal mode solution of equations (10.5) for the case of harmonic forcing, $H_{11}(\omega)$ may be derived to be,

$$H_{11}(\omega) = m_s + \sum_{n=1}^{N} \frac{Q_n P_{n,r} \frac{\omega^2}{\omega_n^2} \left\{\left(1 - \frac{\omega^2}{\omega_n^2}\right) - 2i\zeta_n \frac{\omega}{\omega_n}\right\}}{\left(1 - \frac{\omega^2}{\omega_n^2}\right)^2 + \left(2\zeta_n \frac{\omega}{\omega_n}\right)^2} \qquad (10.14)$$

where $m_s = \sum_{j=1}^{N} m_j$, the sum of the story masses.

$$Q_n = \frac{\underline{\Phi}_n^T \underline{M}}{\Phi_{n,r}}$$

N, $P_{n,r}$, ω_n, ζ_n, $\Phi_{n,r}$, $\underline{\Phi}_n^T$ and $\underline{M}$ are as defined for equations (5.6) and (5.7).

It should be noted that if the rocking of the base produces a significant contribution in the total displacement of the building then it is necessary to separate the component of rocking from the vector of displacements, $\underline{u}$, so that it may be assumed that the building system above the base satisfies the condition for the existence of classical normal modes. When the rocking component is excluded from $\underline{u}$ the steady state solution for the model may be derived in a manner similar to the above method and details of the solution are given in Appendix II. The solution presented above is convenient for this study because the base

rotation contribution to the displacements is small, and periods and damping ratios, which include the influence of rocking, were estimated from the acceleration records of the earthquake.

The ratio of the recorded base motion Fourier amplitude spectrum to the free-field spectrum, $\frac{|\ddot{\bar{u}}_g + \ddot{\bar{u}}_b|}{|\ddot{\bar{u}}_g|}$, can be evaluated by using the previously determined refined model dynamic properties and the soil parameters in equations (10.13) and (10.14). The ratio was computed for the E-W and vertical directions and plotted values are shown in Figure 44. Over the frequency range computed the maximum modification to the E-W free-field spectra is less than 12% and it is of interest to note that the modifications may tend to show as dips in the recorded base spectra. (The transfer function for the N-S direction is expected to be similar). To show the influence of reducing the soil stiffness the spectra ratio for the E-W direction was computed using one-quarter and one-half of the previously estimated, respective values of K_x and C_x and is shown in Figure 44. This reduction in the K_x and C_x values is equivalent to reducing the soil shear wave velocity by one-half.

The rather pronounced influence of soil-structure interaction in the vertical direction is shown by the broad rise and dip in the spectra ratio at frequencies close to the fundamental frequency $f_1 = 5.8$ hz. The spectrum from the base vertical acceleration record shows low amplitudes at frequencies greater than 5.5 hz. However, the Millikan Library, which has a fundamental vertical frequency of approximately

JPL BUILDING E-W DIRECTION.

RATIO OF FOURIER AMPLITUDE SPECTRA. BASE MOTION/FREE FIELD MOTION.

COMPUTED USING REFINED MODEL PROPERTIES.

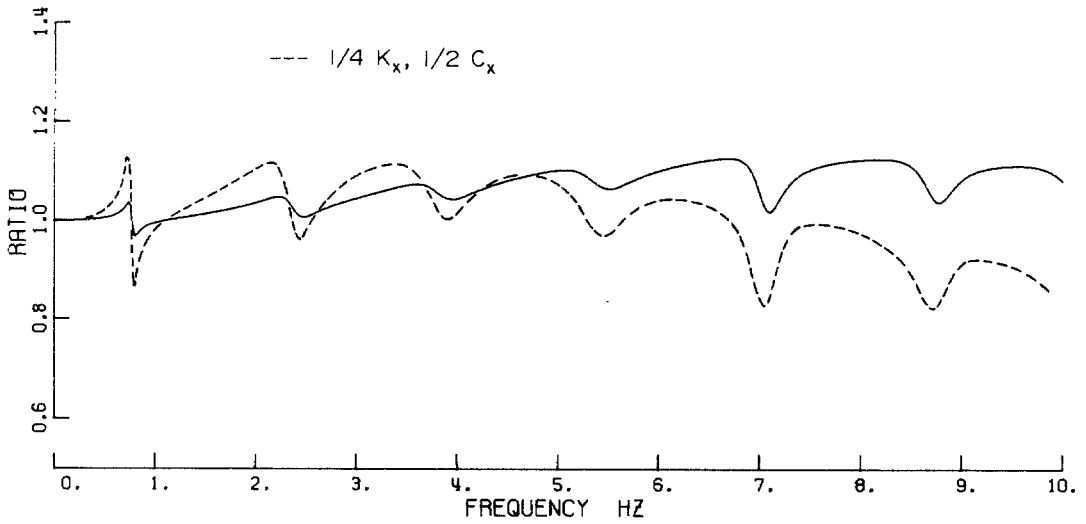

JPL BUILDING VERTICAL DIRECTION.

RATIO OF FOURIER AMPLITUDE SPECTRA. BASE MOTION/FREE FIELD MOTION.

COMPUTED USING REFINED MODEL PROPERTIES.

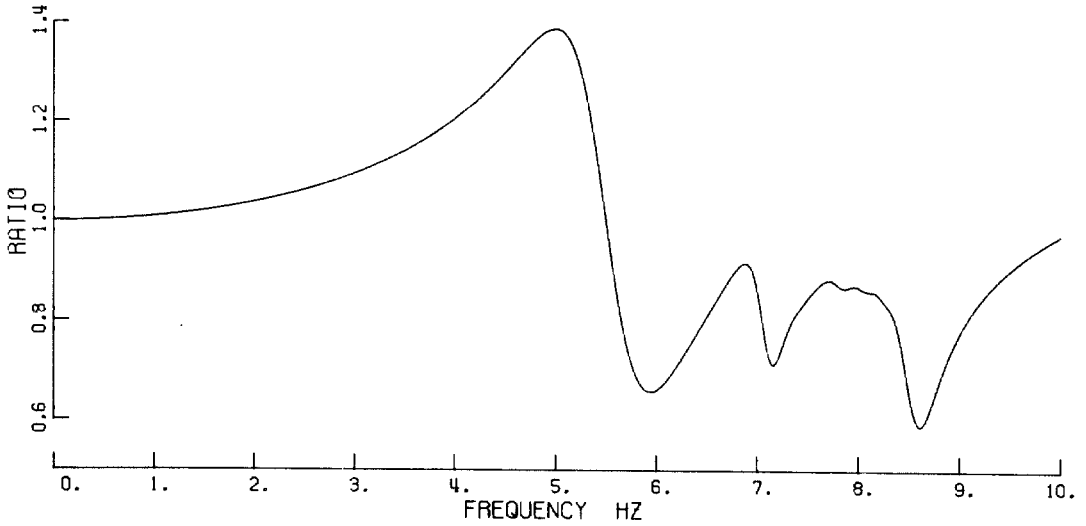

Figure 44.

9.0 hz, also had low amplitudes in the vertical spectrum at frequencies greater than 5.0 hz and so it is difficult to reconcile the predicted with the observed behavior without a free-field record.

The E-W free-field acceleration time history was computed by taking the inverse Fourier transform of the free-field Fourier spectrum which was evaluated from equation (10.12) and the recorded motion spectrum. The free-field acceleration time history was found to be almost identical in detail to the recorded motion and peak accelerations agree within 4%.

11. MILLIKAN LIBRARY BASE RECORDS

The ratio of the roof and base Fourier spectra for the N-S direction Millikan Library records is shown in Fig. 45a. The first and second mode natural frequencies during the strongest shaking are represented by peaks at f_1 = 1.65 hz, (T_1 = 0.61 sec) and f_2 = 7.8 hz, (T_2 = 0.128 sec). A narrow peak in the N-S base motion spectra, shown in Fig. 45b, can be seen at a frequency of 1.53 hz, which is very close to the first N-S frequency.

It is possible to make a preliminary estimate of the effect of soil-structure interaction on the lower frequency components of the recorded Library base motion spectra by estimating the maximum amplitude of the relative base motion produced by the maximum earthquake base shear in the fundamental mode and comparing this value with a similar estimate for Building 180. From the recorded earthquake roof acceleration history and the test measurements (Jennings and Kuroiwa[8]), the maximum amplitude of the relative base displacement in the Library N-S fundamental mode was calculated to be 0.013 in. The maximum amplitude of relative base displacement of the Building 180 E-W fundamental mode was computed from the refined model properties and the previously given soil parameters and found to be 0.011 in. During the earthquake the N-S fundamental frequency of the Library was about twice the E-W fundamental frequency of Building 180 and so it follows that the maximum relative base acceleration of the Library would be about five times greater than the maximum relative base acceleration of Building 180 at the respective fundamental frequencies of the buildings.

MILLIKAN LIBRARY N-S DIRECTION. 0.-40. SEC.

RATIO OF FOURIER SPECTRA FROM RECORDED ACCELERATIONS.

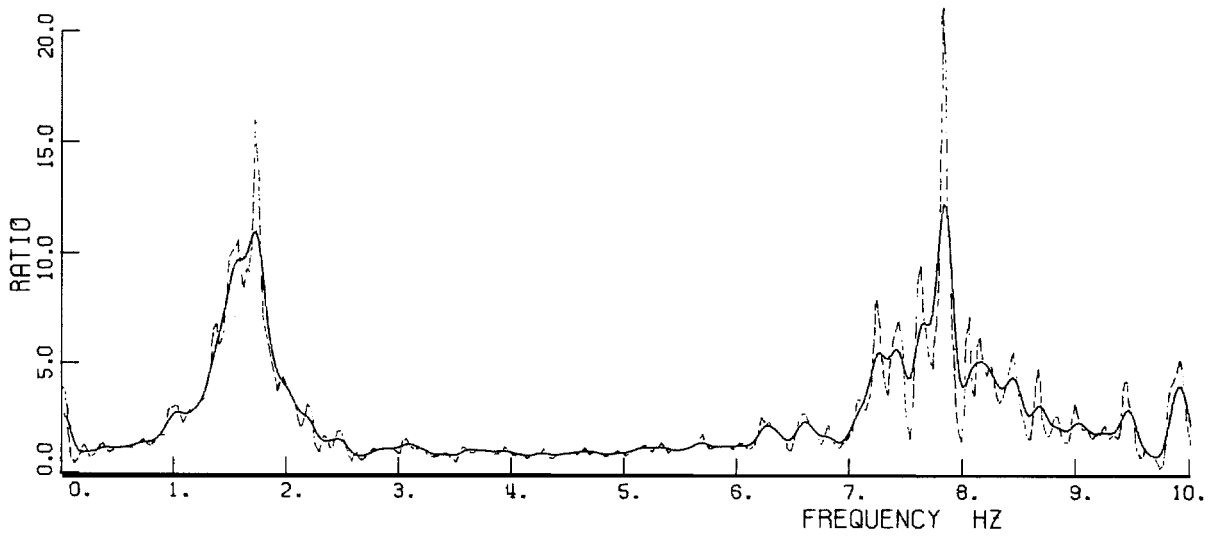

Figure 45a.

FOURIER AMPLITUDE SPECTRUM

MILLIKAN LIBRARY BSMT. N-S DIRECTION.

FROM ACCELERATION RECORD. 0.-40. SEC.

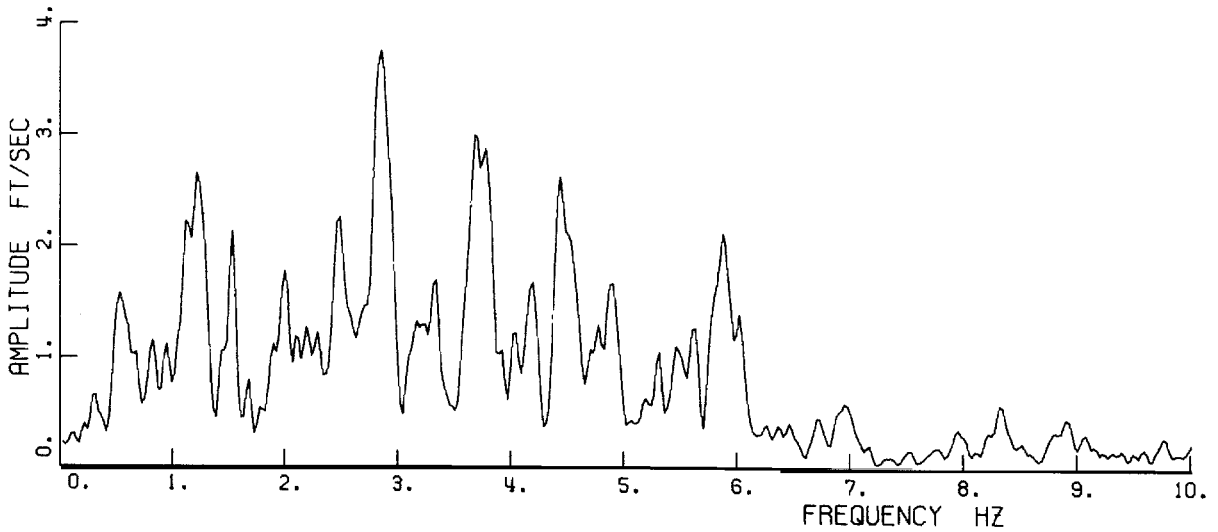

Figure 45 b.

The effect of soil-structure interaction on the Millikan Library base records is conveniently demonstrated by computing the base motion to free-field motion transfer function using the method described for Building 180. The transfer function for the N-S direction of the Library is shown in Figure 46 and was computed using the following building and soil parameters:

$T_1 = 0.61$
$T_2 = 0.128$ } From earthquake records.

$T_3 = 0.05$ Estimated.

$\zeta_1 = 4.0\%$
$\zeta_2 = 4.0\%$ } Approximate estimate from earthquake records.

$\zeta_3 = 4.0\%$ Estimated.

Mode 1 shape. From forced vibration test.

Mode 2 and 3 shapes. Estimated using the charts of dynamic characteristics of buildings given by Skinner[23].

Base weight = 5,200 kips. Estimated from the structural drawings.

$K_x = 1.9 \times 10^9$ lb/ft. From forced vibration test.

$C_x = 3.3 \times 10^7$ lb/ft/sec. From equation (10.3) and test data.

Significant peaks and dips can be seen in the transfer function at frequencies close to the first and second natural frequencies of the building. A comparison of the transfer function plot (Figure 46) with the spectrum from the N-S recorded base motions shown in Figure 45b reveals no strong evidence that would either support or discount the

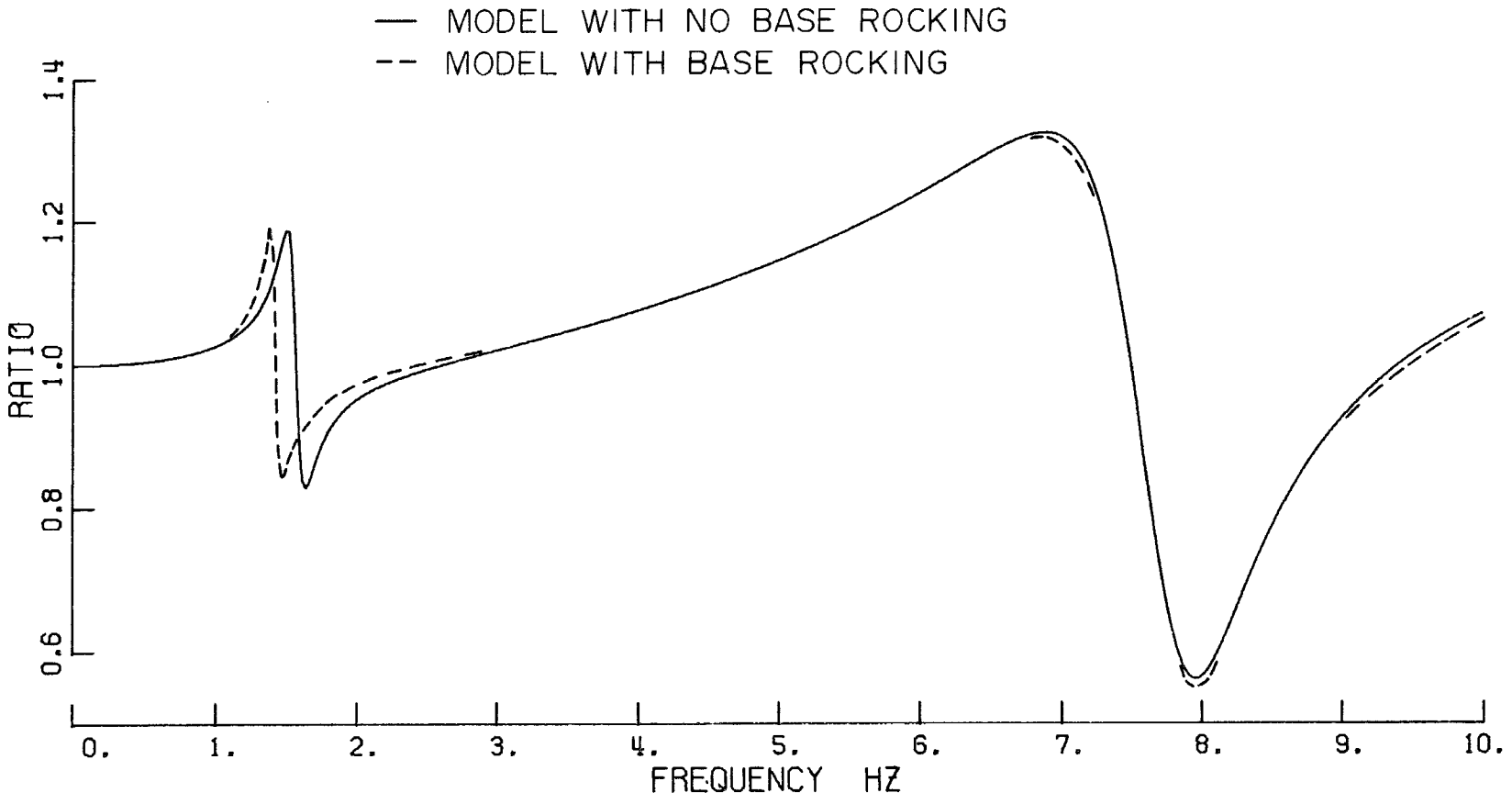
MILLIKAN LIBRARY N-S DIRECTION.
RATIO OF FOURIER AMPLITUDE SPECTRA. BASE MOTION/FREE FIELD MOTION.
— MODEL WITH NO BASE ROCKING
-- MODEL WITH BASE ROCKING
RATIO
0.6
0.8
1.0
1.2
1.4
0.
1.
2.
3.
4.
5.
6.
7.
8.
9.
10.
FREQUENCY HZ

Figure 46.

predicted behavior. A relatively sharp decrease in the base spectrum amplitudes occurs at about 6.0 hz but this behavior is apparent to some degree in all the records analyzed in this study.

To illustrate the relatively insignificant influence of rocking on the base to free-field transfer functions a solution for the Library transfer function was evaluated using equation (A.15) given in Appendix II and is shown in Figure 46. The rigid base building dynamic properties were assumed to have the same values as given above for the previous solution. Values of the soil rotational spring and damping coefficients were evaluated, using the same elastic constants previously used to compute the horizontal parameters and both the horizontal and rotational parameters were assumed to have the same variation with frequency as given by Veletsos and Wei[27] for the rigid circular disc with $\nu = 1/3$. The centroidal moments of inertia of the floors and the base mass were neglected.

It can be seen that the rocking of the building shifts the peak and dip representing the fundamental frequency of the system to a lower frequency but otherwise makes no significant change to the base to free-field motion transfer function.

A more detailed study of the Library records is required but it appears that soil-structure interaction could produce a detectable modification to the free-field spectra. It is unlikely that the modification represented by the transfer function shown in Figure 46 would result in a significant change in the character of the acceleration time history.

12. BUILDING 180 RESPONSE TO SEISMOLOGICAL LABORATORY RECORD

Fourier amplitude spectra ratios were computed by dividing the spectra of the Building 180 horizontal base components by the respective spectra computed from the Seismological Laboratory records and are shown in Figure 47. The ratios have been smoothed by applying 10 cycles of the operation defined by equation (6.1). Amplification can be seen over the frequency range 0.5 hz to 3.0 hz for both components and presumably results mainly from the influence of different wave travel paths to the two sites. Because of the complexity of the geology in the vicinity of the JPL site it would appear unlikely that the influence of the soil layers can be demonstrated by the use of a simple model. Because significant differences were observed (Hudson[10]) between the velocity response spectra from the records at the Millikan Library and the Athenæum, which are located in close proximity and on similar soils, it is not possible to conclude that the differences between the Building 180 and the Seismological Laboratory records are entirely a result of the influence of the soil layers.

It is of interest to note that the two lowest frequencies in both horizontal directions of Building 180 fall within the range of the amplification of the ground motion with respect to the Seismological Laboratory records. Figure 48 shows the roof acceleration response of the Building 180 refined E-W partial composite model to the E-W Seismological Laboratory record. The response, particularly in the first and second modes, is significantly less than observed during the earthquake.

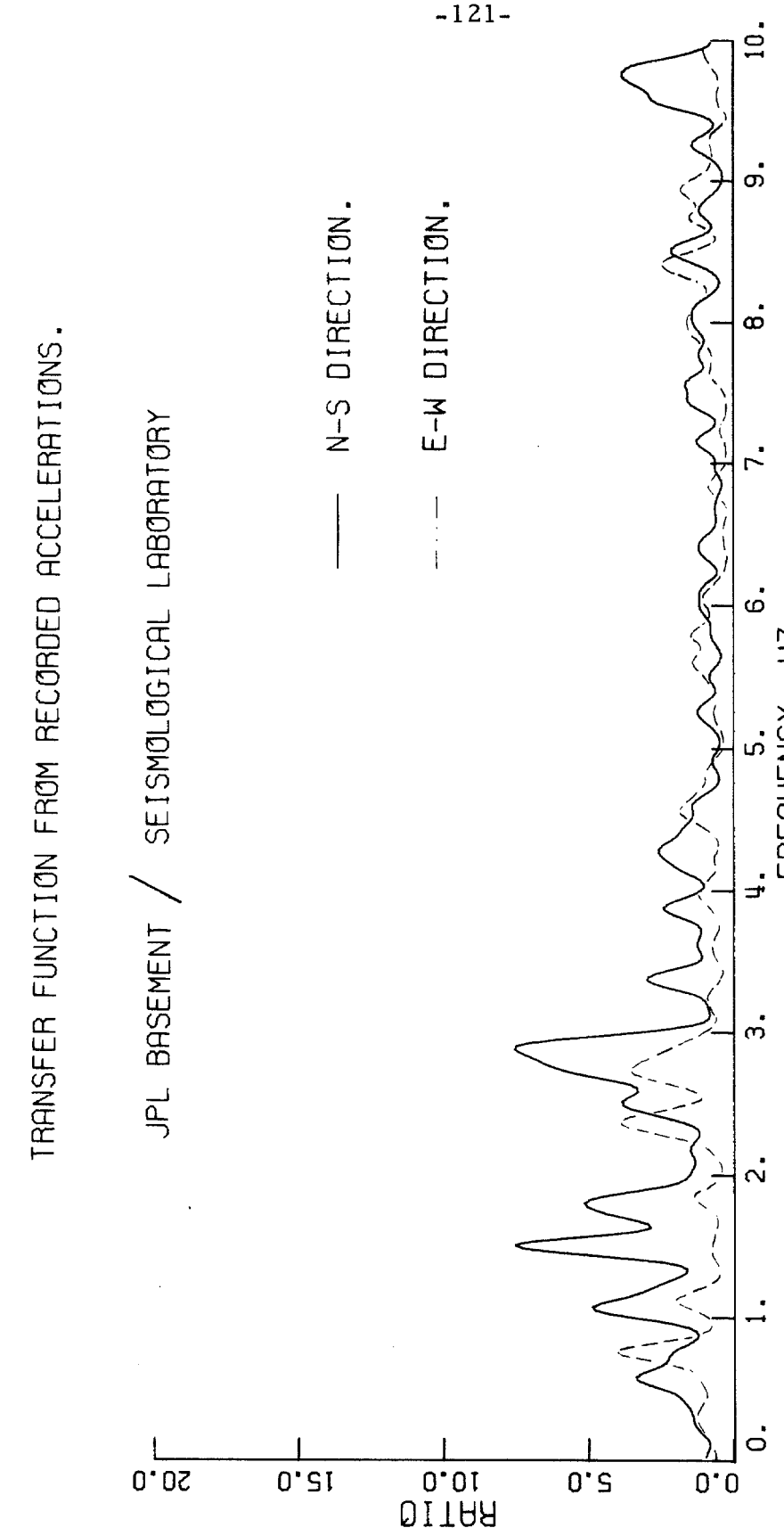
TRANSFER FUNCTION FROM RECORDED ACCELERATIONS.
JPL BASEMENT / SEISMOLOGICAL LABORATORY
N-S DIRECTION.
E-W DIRECTION.
RATIO
0.0
5.0
10.0
15.0
20.0
0.
1.
2.
3.
4.
5.
6.
7.
8.
9.
10.
FREQUENCY HZ

Figure 47.

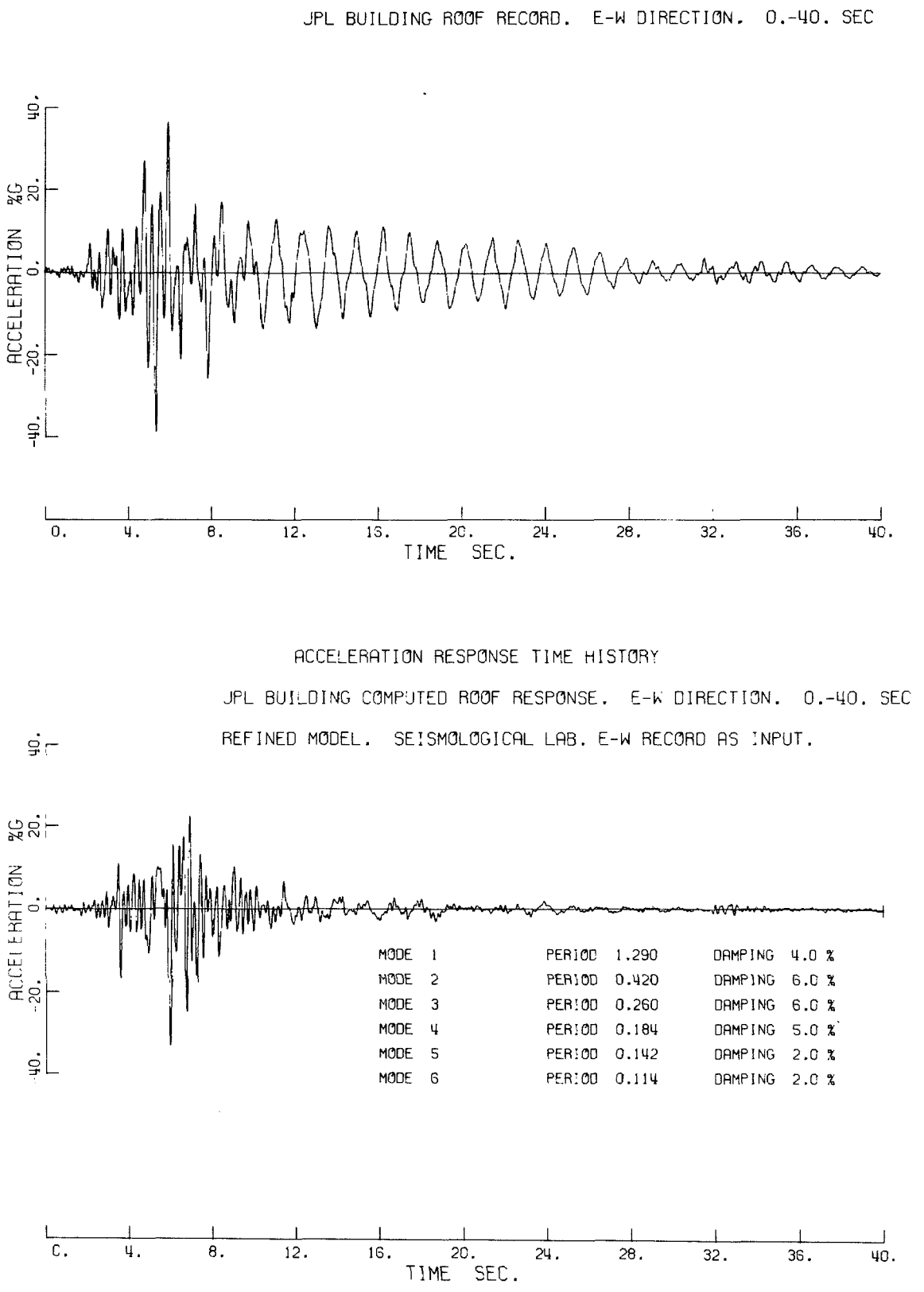

Figure 48. Comparison of recorded roof acceleration with refined model response to Seismological Laboratory record.

13. CONCLUSIONS

(1) Good agreement was found between the computed mode shapes and periods of the structural models and the values measured by the ambient test after the earthquake. In general the periods agreed within 5%, with the model values tending to be higher than the measured values. The ambient test periods measured after the earthquake were about 10% higher than values measured before the earthquake. This change in stiffness may have been due to loosening of the connections between the main structure and such non-structural components as facing panels, glass, partitions and elevator and stair wells. It is also possible that the earthquake may have caused minor changes to the structural frame and produced permanent deformations in the soil surrounding the basement walls, thus reducing the overall building stiffness.

(2) The building frequency ratios measured during the tests were in good agreement with the ratios computed from the structural models and the earthquake records. That is, the frequency ratios were found to be almost constant for quite large changes in building stiffness. Hence, although the dynamic tests may be unreliable for predicting the periods of the basic structural system, some of the important dynamic properties can be established. The building tests also provided useful information regarding base fixity conditions and the influence of higher order modes that cannot be studied with simplified structural models. The forced vibration test of the Millikan Library provided the relevant information to compute the horizontal spring constant for the soil, which is the most important parameter required in the study of soil-

structure interaction. This test also showed that the existing rigid-plate on the half-space theory is not entirely adequate for large building foundations.

(3) It was found that the predominant periods and damping ratios of the lowest two horizontal modes in each direction during the earthquake could be determined by a Fourier spectra study of the recorded roof and basement acceleration histories. A rather less precise estimate of the parameters for the third modes was also possible. The accuracy of the estimates of the periods and damping ratios was reduced by the appreciable non-linear behavior of the building.

(4) The lower horizontal mode periods were approdimately 30% higher in the earthquake than in the ambient test after the earthquake. Stresses in the steel sections during the earthquake were computed to be less than the yield stress and so presumably most of this large reduction in stiffness resulted from the non-linear behavior of the concrete encased columns and the composite N-S trusses. Cracking of the concrete sections would probably account for most of the non-linear behavior of these members.

(5) The acceleration response computations made using the basic structural models showed that the behavior of the building during the earthquake could have been closely predicted by a reasonably careful study of the building structural system. Although in detail the agreement between the computed and recorded roof acceleration histories was not exact, the magnitude and number of peak responses was in close agreement, indicating that stresses computed in the models would

have been in reasonable agreement with the earthquake induced stresses. Detailed agreement between the computed and recorded roof response was obtained by adjusting the model periods to the values observed during the earthquake. It appears necessary to have quite precise estimates of the lowest mode periods to accurately predict the response to a particular earthquake; however, because of the relatively random nature of the incoming earthquake, model periods accurate to within 10% of the building periods during the earthquake should be satisfactory for most design purposes. The periods of the Building 180 partial composite models were within 10% of the observed earthquake values and if more exact force displacement relationships were known for the composite members, it is likely that more exact values could have been computed.

(6) The computed acceleration histories were found to be significantly more sensitive to changes in the model periods than to similar percentage changes in the damping ratios. The reason for the sensitivity of the response to period changes can be seen by observing the irregular nature of the 5% damped velocity response spectra over the frequency range of the lower building periods. (Velocity response spectra for the JPL records are given in Appendix III). This sensitivity has important implications if building designs are to be based on earthquake response computations. Clearly it is important to subject the model of the design building to a number of different earthquake ground records or to establish the relationship of the building periods to any dips in the response spectrum of the earthquake used.

(7) The vertical response of the building did not add a significant contribution to the total member stresses. It was found that most of the roof vertical response resulted from the participation of the fundamental vertical mode and that the period of this mode was closely predicted by the simplified two-dimensional vertical model.

(8) Building 180 can be regarded as a moderately flexible building on a firm soil. It was found that soil-structure interaction was unlikely to have made significant changes to either the horizontal free-field motions or their Fourier spectra. In the vertical direction the lowest frequency is approximately seven times higher than the lowest horizontal frequencies and so the vertical behavior is characteristic of a very stiff structure. Vertical soil-structure interaction was found to produce a broad peak and dip in the free-field Fourier amplitude spectra at frequencies close to the fundamental vertical frequency.

It was apparent from the studies made that soil-structure interaction did not appreciably modify the horizontal earthquake response of this building.

(9) The transfer function relating the Fourier amplitude spectrum of the free-field motion to the recorded motion for a simplified multi-degree of freedom building-soil system can be evaluated from the steady-state solution. The form of the transfer function is essentially that of the single-degree of freedom response curve for the base system with superimposed peaks and dips at the natural frequencies of the flexible base building. The basic response curve is determined by the base mass m_b and the soil parameters K_x and C_x (or K_z and C_z), whilst the

peaks and dips are functions of the building periods, damping ratios, mode shapes and masses. The peaks and dips can be conveniently thought of as the modification of the simple base system response produced by the shear force of the building system above the base mass.

For buildings more flexible than Building 180 and with similar damping ratios the dips and peaks will in general be less significant. For foundations systems with larger spring constant values or smaller base masses the basic response curve will more closely approximate a horizontal line. Buildings of similar structural stiffness to Building 180 would require a foundation system about four times more flexible to produce a significant departure of the transfer function from unity.

(10) Embedment of the building into the soil was found to have an appreciable stiffening effect on the horizontal spring constant computed for a point at the base of the building. The influence of embedment on the damping coefficient and base mass assumption requires further study.

It is evident that existing theories for rigid discs and rectangles resting on an elastic half-space cannot be applied directly to many building foundations. Further research employing numerical methods and forced dynamic testing is required to extend the limited range of applicability of the theoretical solutions.

(11) The maximum computed total column stress in the second story, assuming a root-mean-square sum of the two horizontal earthquake contributions, was 34 kips/in^2. The contribution from dead and live loads in this total is 13 kips/in^2. In view of the fact that no structural damage

was observed and the computed member stresses were below the specified steel yield stress of 36 kips/in^2 the performance of the building during the San Fernando earthquake was satisfactory.

Without undertaking a more detailed study, it is not possible to predict the performance of the building under significantly more intense ground shaking. In particular, it would be necessary to investigate the adequacy of the frame member connections under repetitions of loading at yield stress levels, and to check the resistance to local buckling of the members in the critically stressed areas. One difficulty arises from the lack of information on the earthquake performance of the trussed girders and the connections used to fasten them to the columns. If the building were subjected to an earthquake with similar frequency components to the San Fernando earthquake but with twice the peak accelerations, the critical column sections would respond in the fully plastic range, and the maximum displacement of the structure would be approximately 50% greater than yield point displacement. Current earthquake engineering research has demonstrated that many adequately detailed structures perform satisfactorily beyond the yield stress level and that safety against collapse for relatively flexible structures can be expected in earthquakes producing response spectrum values significantly greater than produced by the earthquake giving yield stress force levels.

ACKNOWLEDGEMENTS

The author sincerely thanks Professor G. W. Housner for his guidance and assistance in the course of this study and the preparation of the manuscript. Mr. F. E. Springate of the Jet Propulsion Laboratory also assisted the study by providing information about Building 180.

The research was supported in part by grants from the National Science Foundation and the Earthquake Research Affiliates Program at the California Institute of Technology. The author is on graduate study leave from the New Zealand Ministry of Works and also wishes to acknowledge their financial support as well as the tuition Fellowship support from the California Institute of Technology.

REFERENCES

1.* Bielak, Jacobo, "Earthquake Response of Building-Foundation Systems." Report No. EERL 71-04. Earthquake Engineering Research Laboratory, California Institute of Technology, Pasadena, California, 1971.

2. Brandow and Johnston Associates, "Lateral Load Analysis of Building # 180, Jet Propulsion Laboratory, Pasadena, California." October, 1971.

3. Converse, Davis and Associates, "Geological Investigation of the Jet Propulsion Laboratory, Pasadena, California." Conducted for Jet Propulsion Laboratory, July, 1971.

4. DFT Program (Discrete Fourier Transform). California Institute of Technology Computing Center. System/360 Scientific Subroutine Package (360 A-CM-03X) Version III.

5. Duke, C.M., Johnson, J.A., Kharraz, Y., Campbell, K.W., and Malpiede, N.A., "Subsurface Site Conditions and Geology in the San Fernando Earthquake Area." Report No. UCLA-ENG 7206, School of Engineering and Applied Science, University of California, Los Angeles. December 1971.

6. Gorbunov-Possadov M. and Serebrjanyi, R.V., "Design of Structures on Elastic Foundations." Proceedings of 5th International Conference on Soil Mechanics and Foundation Engineering. Paris, 1961.

7. Jennings, Paul C., Editor, "Engineering Features of the San Fernando Earthquake." Report No. EERL 71-02. Earthquake Engineering Research Laboratory, California Institute of Technology, Pasadena, California, June 1971.

8. Jennings, Paul C. and Kuroiwa, Julio H., "Vibration and Soil-Structure Interaction Tests of a Nine-Story Reinforced Concrete Building." Bulletin of the Seismological Society of America, Vol. 58, No. 3, June, 1968.

9. Hudson, D.E., "Some Problems in the Application of Spectrum Techniques to Strong-Motion Earthquake Analysis." Bulletin of the Seismological Society of America, Vol. 52, No. 2, April 1962.

10. Hudson, D.E., "Local Distribution of Strong Earthquake Ground Motions." To be published in Bulletin of the Seismological Society of America, December 1972.

* Part of the material in this reference is to be published in a paper, "Dynamics of Building-Soil Interaction," P. C. Jennings & J. Bielak; Bulletin of the Seismological Soc. of America, February 1973.

11a. Hudson, D.E., and Brady, A.G., "Analysis of Strong-Motion Earthquake Accelerograms," Vol. I Part G, Report No. EERL 72-20. Earthquake Engineering Research Laboratory, California Institute of Technology, Pasadena, California, June 1972.

11b. Hudson, D.E., Trifunac, M.D., Udwadia, F.E., Vijayaraghavan, A., and Brady, A.G., "Analysis of Strong-Motion Earthquake Accelerograms," Vol. IV, Part A. Report No. EERL 72-100. Earthquake Engineering Research Laboratory, California Institute of Technology, Pasadena, California, August 1972.

12. Kaldjian, Movses J., Discussion on "Design Procedures for Dynamically Loaded Foundation." Whitman, R.V. and Richart, F.E. Jr., November, 1967. Journal of the Soil Mechanics and Foundation Division, ASCE, Vol. 95, SM 1, January 1969.

13. Karasudhi, P., Keer, L.M., and Lee, S.L., "Vibratory Motion of a Body on an Elastic Half Plane," Journal of Applied Mechanics, Vol. 35, Transactions of the ASME, Series E, December 1968.

14. Kobori, T., Minai, R., Suzuki, T., and Kusakabe, K., "Dynamical Ground Compliance of Rectangular Foundation." Proceedings of the Sixteenth Japan National Congress for Applied Mechanics, 1966.

15. Luco, J.Enrique, "Dynamic Interaction of a Shear Wall with the Soil." Journal of the Engineering Mechanics Division, ASCE, Vol. 95, No. EM2, April 1969.

16. Luco, Juan E., and Westmann, Russell A., "Dynamic Response of Circular Footings," Journal of the Engineering Mechanics Division, ASCE, Vol. 97, No. EM5, October, 1971.

17. Meek, J.W. and Veletsos, A.S., "Dynamic Analysis and Behavior of Structure Foundation Systems," Structural Research at Rice, Report No. 13. Department of Civil Engineering, Rice University, Houston, Texas, April 1972.

18. Nielsen, N. Norby, "Dynamic Response of Multistory Buildings." Earthquake Engineering Research Laboratory, California Institute of Technology, Pasadena, California, June 1964.

19. Nigam, Navin C. and Jennings, Paul C., "Digital Caclculation of Response Spectra from Strong-Motion Earthquake Records." Earthquake Engineering Research Laboratory, California Institute of Technology, Pasadena, California, June 1968.

20. Oien, M.A., "Steady Motion of a Rigid Strip Bonded to an Elastic Half-Space." Journal of Applied Mechanics, Vol. 38, Trans. ASME, Vol. 93, Series E, June, 1971.

21. Sarrazin, Mauricio A., "Soil Structure Interaction in Earthquake Resistant Design." Research Report R 70-59, School of Engineering, Massachusetts Institute of Technology, Cambridge, Massachusetts, September 1970.

22. Seed, H. Bolton, and Idriss, I.M., "Soil Moduli and Damping Factors for Dynamic Response Analyses." Report No. EERC 70-10. Earthquake Engineering Research Center, University of California, Berkeley, California. December 1970.

23. Skinner, R.I., "Earthquake-generated Forces and Movements in Tall Buildings." Bulletin 166. New Zealand Department of Scientific and Industrial Research, 1964.

24. Skinner, R.I., Skilton, D.W.C., and Laws, D.A., "Unbalanced Buildings and Buildings with Light Towers." Proceedings of the Third World Conference on Earthquake Engineering. Vol. II, New Zealand, 1965.

25. Teledyne Geotech West, "Ambient Vibration Survey of Building 180, Jet Propulsion Laboratory." For California Institute of Technology, Pasadena, California, November 1971.

26. Trifunac, M.D., Udwadia, F.E. and Brady, A.G., "High Frequency Errors and Instrument Corrections of Strong-Motion Accelerograms." Report No. EERL 71-05. Earthquake Engineering Research Laboratory, California Institute of Technology, Pasadena, California, July 1971.

27. Veletsos, Anestis S. and Wei Yau T., "Lateral and Rocking Vibration of Footings." Journal of the Soil Mechanics and Foundations Division, ASCE, Vol. 97, No. SM9, September, 1971.

28. Warren, Donald R. and Company, Los Angeles, California, "Foundation Investigation Proposed Central Engineering Building Jet Propulsion Laboratory Pasadena, California." For Jet Propulsion Laboratory, January 1961.

29. Whitman, R.V. and Richart, F.E. Jr., "Design Procedures for Dynamically Loaded Foundations." Journal of the Soil Mechanics and Foundation Division, ASCE, Vol. 93, No. SM6. November 1967.

APPENDIX I - NOTATION

$a_o = \frac{\omega r}{V_s}$, a dimensionless frequency.

$|A(\omega)|_j^s$ = Smoothed Fourier amplitude spectrum.

$|A(\omega)|_j^u$ = Unsmoothed Fourier amplitude spectrum.

B = Rectangular foundation dimension.

C = Building damping matrix.

C_1 = Parameter used to compute damping coefficient for rigid disc.

C_x = Horizontal damping coefficient for foundation.

C_z = Vertical damping coefficient for foundation.

C_φ = Rotational damping coefficient for foundation.

D = Relative displacement response of single degree of freedom oscillator.

E = Young's modulus.

f_n = Natural frequency of mode n.

F = Lateral flexibility matrix.

$F_b = m_b(\ddot{u}_g + \ddot{u}_b) + S_b$

g = Acceleration due to gravity.

g_P = Parameter for probability P, used to compute Fourier amplitude spectrum confidence level.

G = Soil shear modulus.

h_j = The height of floor j above the base.

$\underline{h}$ = A vector of floor heights above the base.

$H_{ij}(\omega)$ = Elements of building transfer matrix. i = 1, 2; j = 1, 2. Matrix relates base shear and moment to base displacement and rotation.

$H_r(\omega)$ = Transfer function relating building absolute roof response to base motion.

$i = \sqrt{-1}$

I = The unity matrix.

I_b = Centroidal moment of inertia of the base mass.

I_t = The sum of the centroidal moments of inertia of the floor and base masses.

IH = Imaginary part of H_{11}

K = Lateral stiffness matrix.

K* = Total frame stiffness matrix.

K_c = Sum of story column stiffnesses.

K_g = Sum of story girder stiffnesses.

K_x = Horizontal spring constant for foundation.

K_z = Vertical spring constant for foundation.

K_φ = Rotational spring constant for foundation.

L = Rectangular foundation dimension.

m_b = Building base mass.

m_j = Story mass at floor j.

m_s = Sum of story masses.

M = Diagonal mass matrix.

$\underline{M}$ = Vector of story masses.

M_b = The moment on the base from the superstructure.

n = Mode number.

N = Number of floor masses above the base.

p = Horizontal force per unit length.

$\underline{p}$ = A vector of horizontal forces at the floor levels.

$\underline{p}^*$ = A vector of nodal forces.

P = Probability.

$P_{n,r}$ = Roof participation factor in mode n.

$$Q_n = \frac{\underline{\Phi}_n^T \underline{M}}{\Phi_{n,r}}$$

r = Rigid disc radius or radius of equivalent disc for base.

$$R_{n,r} = \Phi_{n,r} \frac{\underline{\Phi}_n^T M \underline{h}}{\underline{\Phi}_n^T M \underline{\Phi}_n}$$

RH = Real part of H_{11}.

S_b = Shear force on the base from the superstructure.

$$S_n = \frac{\underline{\Phi}_n^T M \underline{h}}{\Phi_{n,r}}$$

t = Time.

T = Accelerogram record length.

T_n = Period of mode n.

u = Horizontal displacement.

u_b = Relative horizontal displacement of building base.

u_g = Free-field horizontal ground displacement.

u_j = Floor horizontal displacement at floor j.

u_j^s = Floor horizontal displacement at floor j relative to the base.

u_r = Roof horizontal displacement.

$\underline{u}$ = A vector of horizontal displacements of the floors.

$\underline{u}^s$ = A vector of horizontal displacements of the floors relative to the base.

$\underline{u}^*$ = A vector of nodal displacements.

V_s = Shear wave speed.

Y_{90} = 90% confidence level of Fourier amplitude spectrum.

β_x = Parameter used to compute horizontal static spring constant for rectangular plate.

β_z = Parameter used to compute vertical static spring constant for rectangular plate.

ζ_n = The fraction of critical damping in mode n.

λ = $\frac{1}{\omega^2}$ an eigenvalue.

ν = Poisson's ratio.

σ = Standard deviation.

φ = Rotation of building base.

$\underline{\Phi}$ = A mode shape.

$\Phi_{n,r}$ = Roof displacement in mode n.

$\underline{\Psi}$ = $M^{\frac{1}{2}}\underline{\Phi}$

ω = Angular frequency.

ω_n = Natural angular frequency for mode n.

Dots above symbols denote differentiation with respect to time.

A bar beneath a symbol denotes a vector quantity.

A bar above a symbol denotes the Fourier transform of the quantity.

APPENDIX II

Influence of Soil-Structure Interaction on Base Motion Spectrum Including the Effects of Rocking.

In Section 10.2.3 a simplified theory was developed to show the influence of soil-structure interaction on the base motion Fourier amplitude spectrum using the assumption that base rocking could be neglected. The more general case in which base rocking is included is discussed below.

The equations of motion for the soil-structure model shown in Figure 42 may be written as,

$$M\ddot{\underline{u}}^s + C\dot{\underline{u}}^s + K\underline{u}^s + M(\underline{h}\ddot{\varphi} + \ddot{u}_g + \ddot{u}_b) = 0 \qquad \text{(A. 1)}$$

$$\sum_{j=1}^{N} m_j(\ddot{u}_j^s + h_j\ddot{\varphi} + \ddot{u}_g + \ddot{u}_b) + m_b(\ddot{u}_g + \ddot{u}_b) + C_x\dot{u}_b + K_x u_b = 0 \qquad \text{(A. 2)}$$

$$\sum_{j=1}^{N} m_j h_j(\ddot{u}_j^s + h_j\ddot{\varphi} + \ddot{u}_g + \ddot{u}_b) + I_t\ddot{\varphi} + C_\varphi r^2\dot{\varphi} + K_\varphi r^2\varphi = 0 \qquad \text{(A. 3)}$$

where,

$\underline{u}^s$ = a vector of horizontal displacements of the floors relative to the base.

u_j^s = the horizontal displacement of floor j relative to the base.

$\underline{h}$ = a vector of floor heights above the base.

h_j = the height of floor j above the base.

φ = the rotation of the base.

I_t = the sum of the centroidal moments of inertia of the floor and base masses.

C_φ = the foundation rotational damping coefficient.

K_φ = the foundation rotational spring constant.

r = the equivalent radius of the base.

The other symbols are as previously defined.

Letting $$S_b = \sum_{j=1}^{N} m_j(\ddot{u}_j^s + h_j\ddot{\varphi} + \ddot{u}_g + \ddot{u}_b) \tag{A.4}$$

$$M_b = \sum_{j=1}^{N} m_j h_j(\ddot{u}_j^s + h_j\ddot{\varphi} + \ddot{u}_g + \ddot{u}_b) \tag{A.5}$$

and taking the Fourier transform of equations (A. 2) and (A. 3) gives,

$$\bar{S}_b(\omega) + m_b\{\bar{\ddot{u}}_g(\omega) + \bar{\ddot{u}}_b(\omega)\} + C_x\bar{\dot{u}}_b(\omega) + K_x\bar{u}_b(\omega) = 0 \tag{A.6}$$

$$\bar{M}_b(\omega) + I_t\bar{\ddot{\varphi}}(\omega) + C_\varphi r^2\bar{\dot{\varphi}}(\omega) + K_\varphi r^2\bar{\varphi}(\omega) = 0 \tag{A.7}$$

$\bar{S}_b$ and $\bar{M}_b$ may be related to the transformed absolute accelerations of the base $(\bar{\ddot{u}}_g + \bar{\ddot{u}}_b)$ and $\bar{\ddot{\varphi}}$ by a building transfer matrix $H(\omega)$

$$\begin{Bmatrix} \bar{S}_b \\ \bar{M}_b \end{Bmatrix} = \begin{bmatrix} H_{11}(\omega) & H_{12}(\omega) \\ H_{21}(\omega) & H_{22}(\omega) \end{bmatrix} \begin{Bmatrix} \bar{\ddot{u}}_g + \bar{\ddot{u}}_b \\ \bar{\ddot{\varphi}} \end{Bmatrix} \tag{A.8}$$

The coefficients $H_{ij}(\omega)$, i = 1, 2, j = 1, 2 can be derived from the solution of equations (A. 1), which can be obtained by assuming that the rigid base structure may be decomposed into classical normal modes and by considering the term $M(\underline{h}\,\ddot{\varphi} + \ddot{u}_g + \ddot{u}_b)$ to be the forcing function. The solution of the transformed version of equations (A. 1) may be written as,

$$\ddot{\underline{u}}^s(\omega) = \sum_{n=1}^{N} \frac{\underline{\Phi}_n P_{n,r}}{\Phi_{n,r}} \frac{\frac{\omega^2}{\omega_n^2}}{\left(1 - \frac{\omega^2}{\omega_n^2}\right) + 2i\zeta_n \frac{\omega}{\omega_n}} (\ddot{\bar{u}}_g + \ddot{\bar{u}}_b)$$

$$+ \sum_{n=1}^{N} \frac{\underline{\Phi}_n R_{n,r}}{\Phi_{n,r}} \frac{\frac{\omega^2}{\omega_n^2}}{\left(1 - \frac{\omega^2}{\omega_n^2}\right) + 2i\zeta_n \frac{\omega}{\omega_n}} \ddot{\bar{\varphi}} \qquad \text{(A. 9)}$$

where,

$$R_{n,r} = \Phi_{n,r} \frac{\underline{\Phi}_n^T M \underline{h}}{\underline{\Phi}_n^T M \underline{\Phi}_n}$$

From equation (A. 9) and equations (A. 4) and (A. 5),

$$H_{11} = \sum_{j=1}^{N} m_j + \sum_{n=1}^{N} \frac{Q_n P_{n,r} \frac{\omega^2}{\omega_n^2}}{\left(1 - \frac{\omega^2}{\omega_n^2}\right) + 2i\zeta_n \frac{\omega}{\omega_n}} \qquad \text{(A. 10)}$$

where,

$$Q_n = \frac{\underline{\Phi}_n^T \underline{M}}{\Phi_{n,r}}$$

$$H_{22} = \sum_{j=1}^{N} m_j h_j^2 + \sum_{n=1}^{N} \frac{S_n R_{n,r} \frac{\omega^2}{\omega_n^2}}{\left(1 - \frac{\omega^2}{\omega_n^2}\right) + 2i\zeta_n \frac{\omega}{\omega_n}} \qquad \text{(A. 11)}$$

where,

$$S_n = \frac{\underline{\Phi}_n^T M \underline{h}}{\Phi_{n,r}}$$

$$H_{12} = H_{21} = \sum_{j=1}^{N} m_j h_j + \sum_{n=1}^{N} \frac{S_n P_{n,r} \frac{\omega^2}{\omega_n^2}}{\left(1 - \frac{\omega^2}{\omega_n^2}\right) + 2i\zeta_n \frac{\omega}{\omega_n}} \qquad \text{(A. 12)}$$

$\bar{S}_b$ and $\bar{M}_b$ may be eliminated from equations (A. 6) and (A. 7) by substitution from equation (A. 8) to give,

$$(\bar{u}_b + \bar{u}_g) = \frac{(i\omega C_x + K_x)\ \bar{u}_g + \omega^2 H_{12}\ \bar{\varphi}}{\{-\omega^2(m_b + H_{11}) + i\omega C_x + K_x\}} \tag{A. 13}$$

$$\bar{\varphi} = \frac{\omega^2 H_{21}\ (\bar{u}_g + \bar{u}_b)}{\{-\omega^2 (I_t + H_{22}) + i\omega C_\varphi r^2 + K_\varphi r^2\}} \tag{A. 14}$$

Substituting (A. 14) into (A. 13) gives,

$$\frac{|\bar{u}_b + \bar{u}_g|}{|\bar{u}_g|} = \frac{|i\omega C_x + K_x|}{\left| -\omega^2(m_b + H_{11}) + i\omega C_x + K_x - \frac{\omega^4 H_{12} H_{21}}{\{-\omega^2(I_t + H_{22}) + i\omega C_\varphi r^2 + K_\varphi r^2\}} \right|} \tag{A. 15}$$

Evaluation of (A. 15) gives the ratio of the base motion Fourier amplitude spectrum to the free-field Fourier amplitude spectrum. The frequency dependence of the soil parameters K_x, C_x, K_φ, and C_φ may be included in the evaluation by using the tabulated values given by Veletsos and Wei[27] for the rigid disc on the half-space.

Bielak[1] has used the Laplace transform and a more rigorous mathematical formulation of the problem to derive expressions equivalent to (A. 15); however, the transfer functions evaluated from the above expressions and Bielak's work are identical for similar assumptions.

APPENDIX III

1. Relative Velocity Response Spectra from JPL Building Basement Records, San Fernando Earthquake, February 9, 1971.

2. Basement Velocities and Displacements Computed by Integration of Recorded Accelerations.

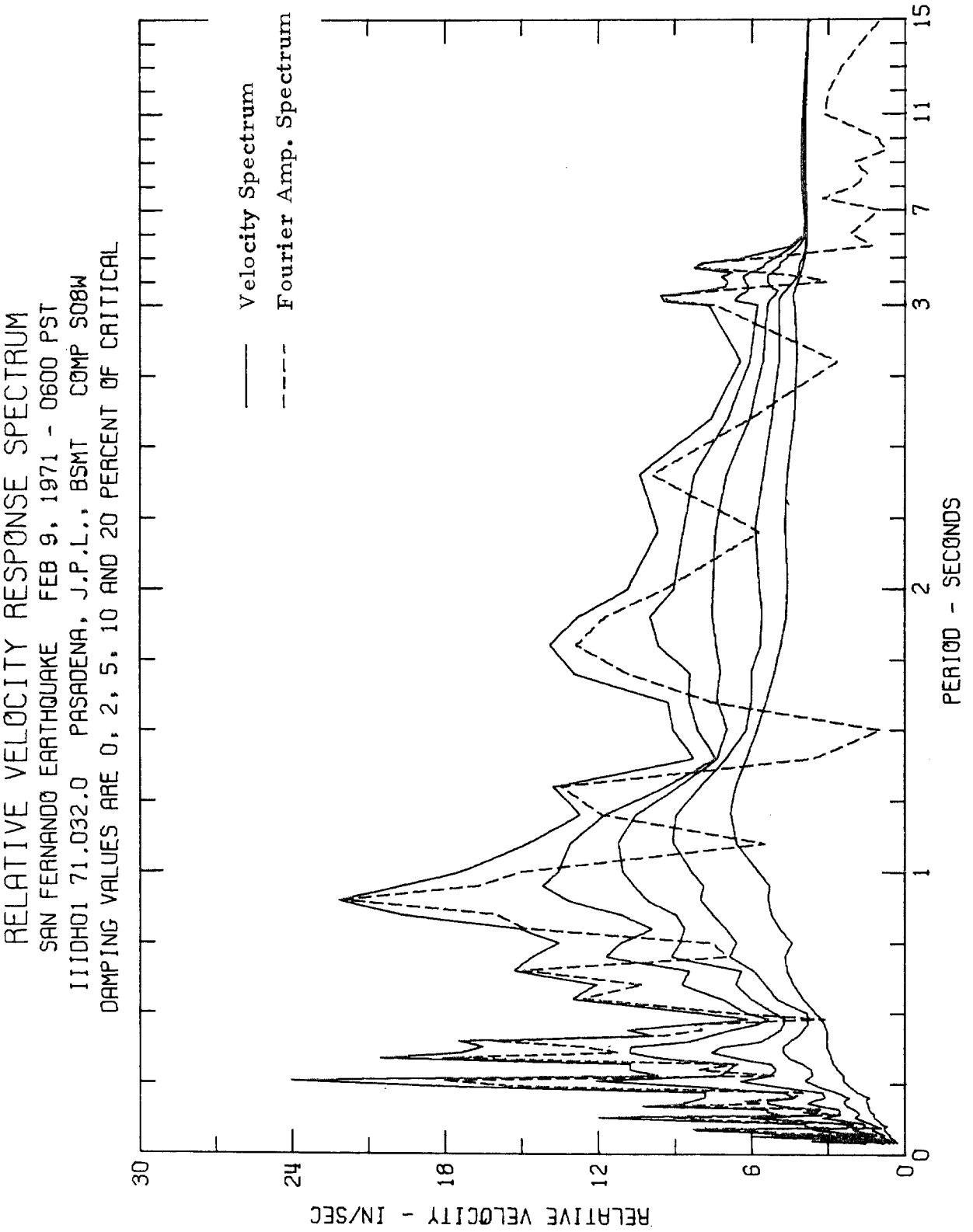
RELATIVE VELOCITY RESPONSE SPECTRUM
SAN FERNANDO EARTHQUAKE FEB 9, 1971 - 0600 PST
1110H01 71.032.0 PASADENA, J.P.L., BSMT COMP S08W
DAMPING VALUES ARE 0, 2, 5, 10 AND 20 PERCENT OF CRITICAL
Velocity Spectrum
Fourier Amp. Spectrum
RELATIVE VELOCITY - IN/SEC
PERIOD - SECONDS
0
6
12
18
24
30
1
2
3
7
11
15

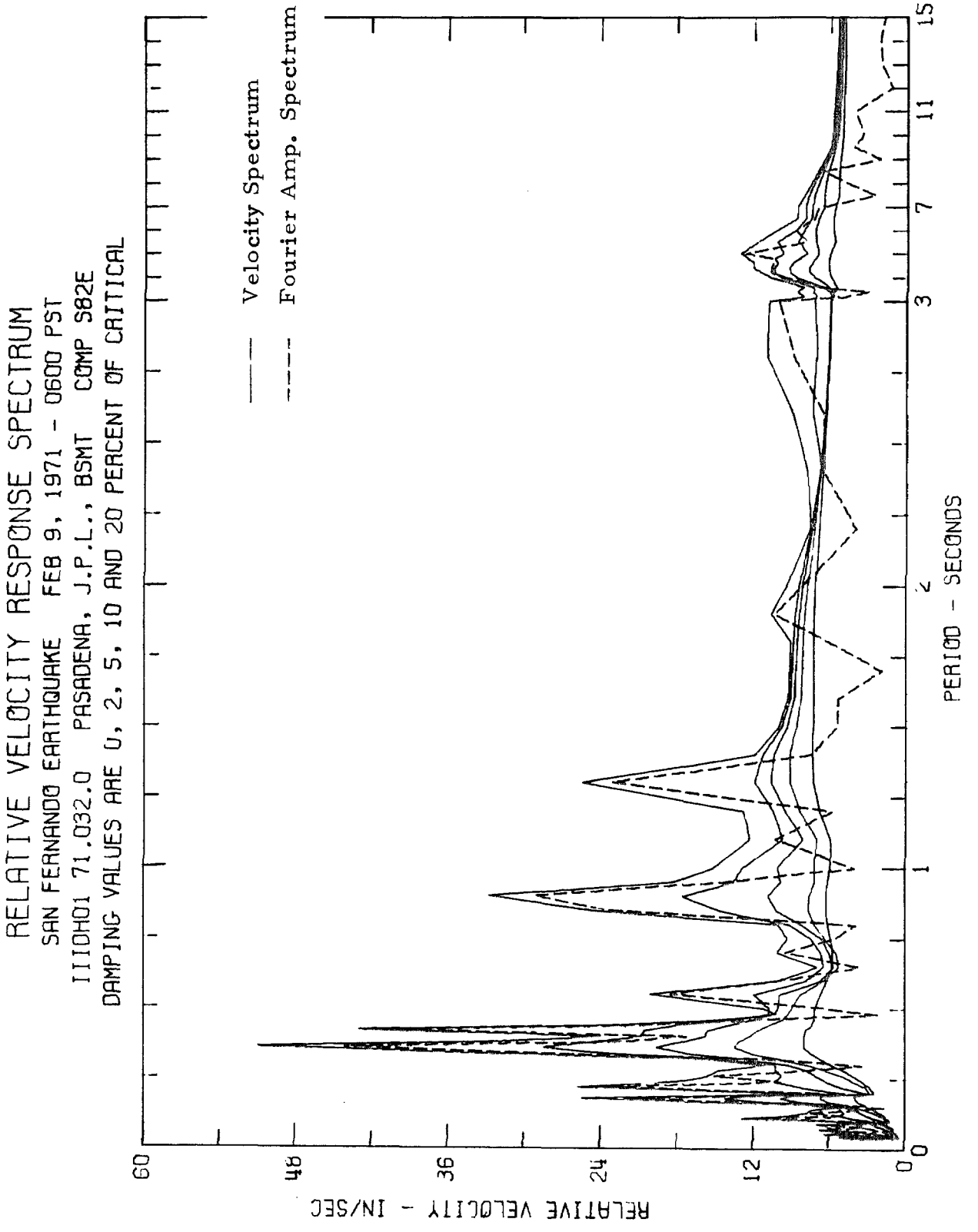
RELATIVE VELOCITY RESPONSE SPECTRUM
SAN FERNANDO EARTHQUAKE FEB 9, 1971 - 0600 PST
1110H01 71.032.0 PASADENA, J.P.L., BSMT COMP S82E
DAMPING VALUES ARE 0, 2, 5, 10 AND 20 PERCENT OF CRITICAL
Velocity Spectrum
Fourier Amp. Spectrum
RELATIVE VELOCITY - IN/SEC
PERIOD - SECONDS
0
12
24
36
48
60
1
3
7
11
15

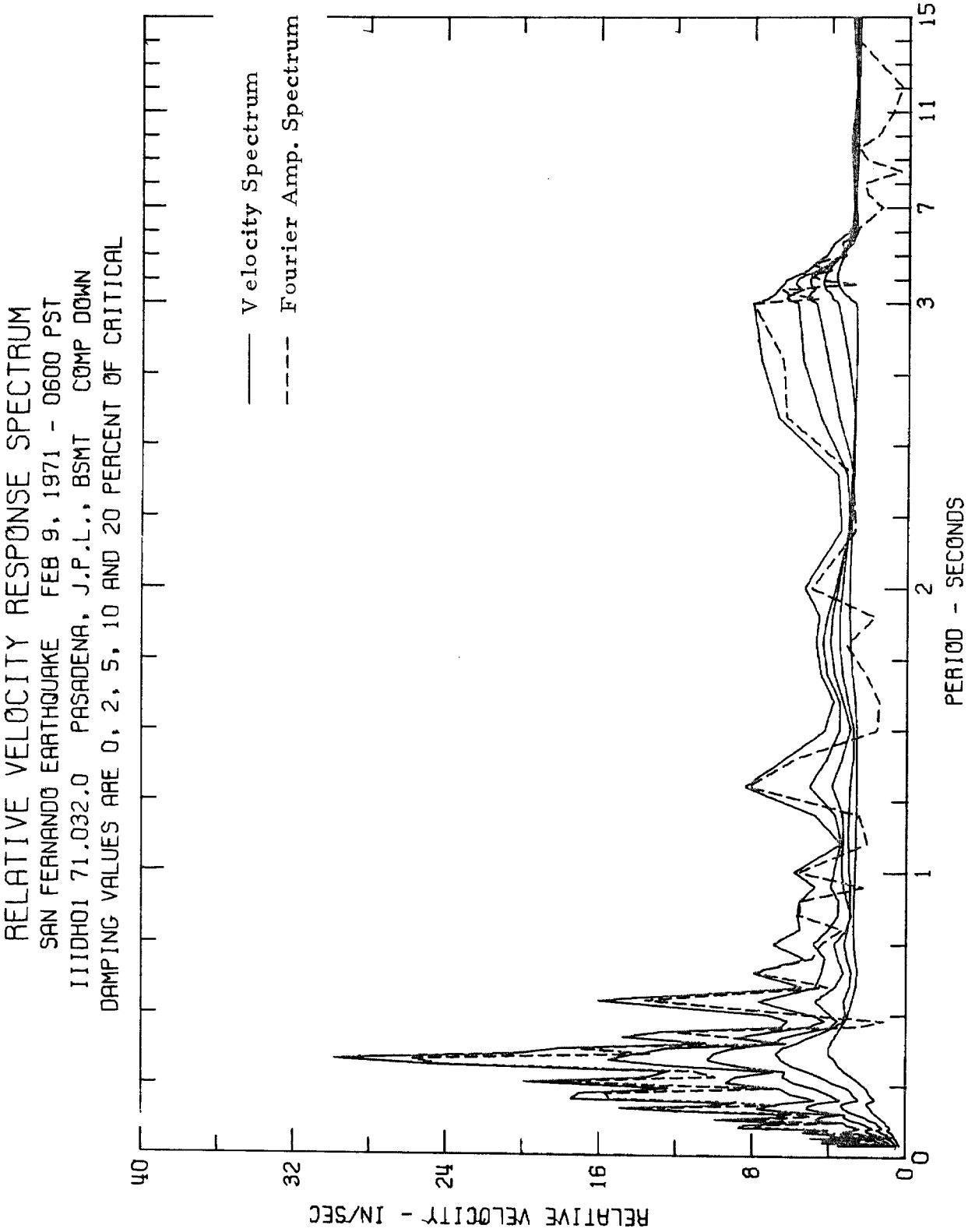
RELATIVE VELOCITY RESPONSE SPECTRUM
SAN FERNANDO EARTHQUAKE FEB 9, 1971 - 0600 PST
1111H01 71.032.0 PASADENA, J.P.L., BSMT COMP DOWN
DAMPING VALUES ARE 0, 2, 5, 10 AND 20 PERCENT OF CRITICAL
Velocity Spectrum
Fourier Amp. Spectrum
RELATIVE VELOCITY - IN/SEC
0
8
16
24
32
40
0
1
2
3
7
11
15
PERIOD - SECONDS

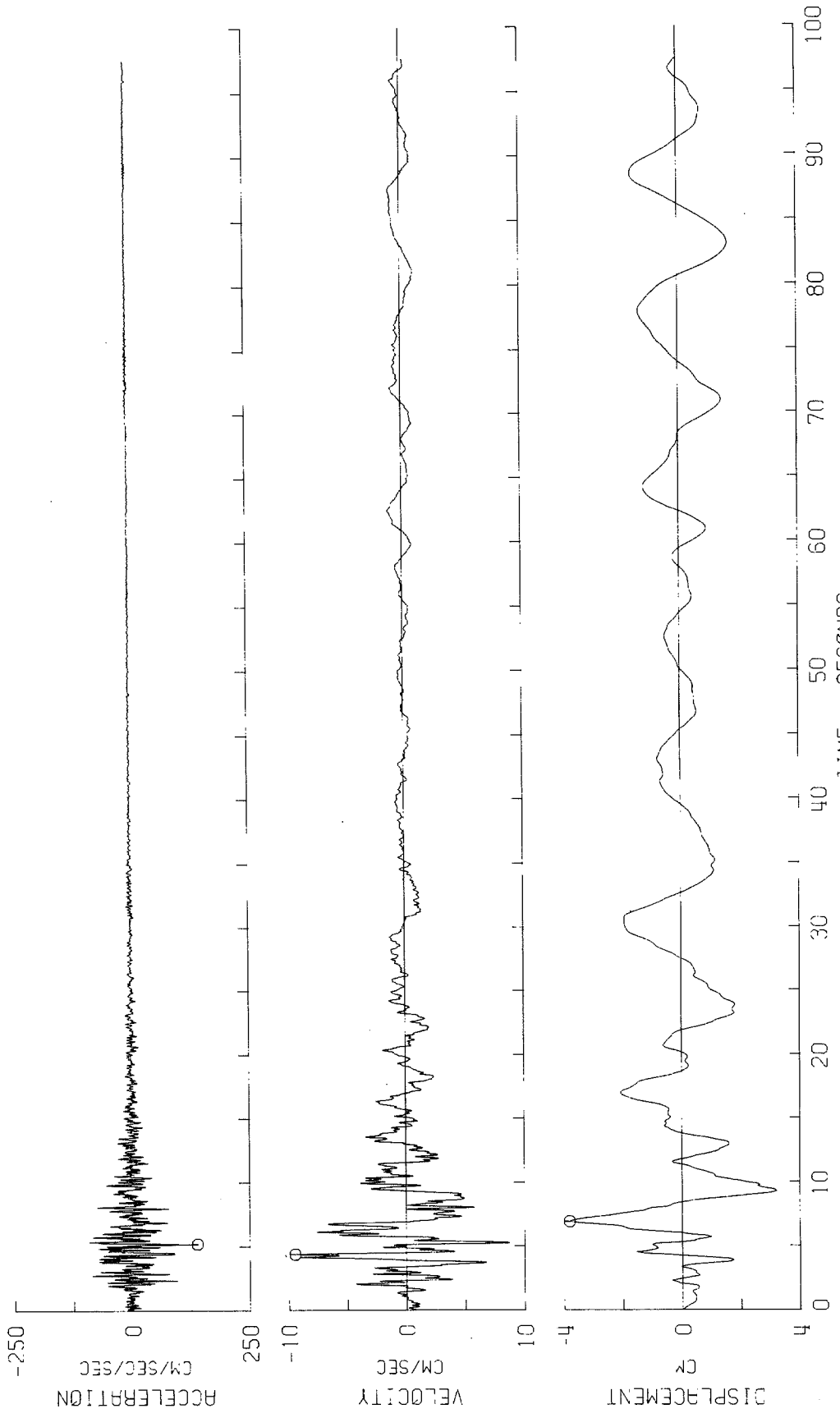
SAN FERNANDO EARTHQUAKE FEB 9, 1971 - 0600 PST
1IDH01 71.032.0 PASADENA, J.P.L., BSMI COMP S08W
Φ PEAK VALUES : ACCEL = 139.5 CM/SEC/SEC VELOCITY = -9.5 CM/SEC DISPL = -3.8 CM
ACCELERATION
CM/SEC/SEC
-250
0
250
VELOCITY
CM/SEC
-10
0
10
DISPLACEMENT
CM
-4
0
4
0
10
20
30
40
50
60
70
80
90
100
TIME - SECONDS

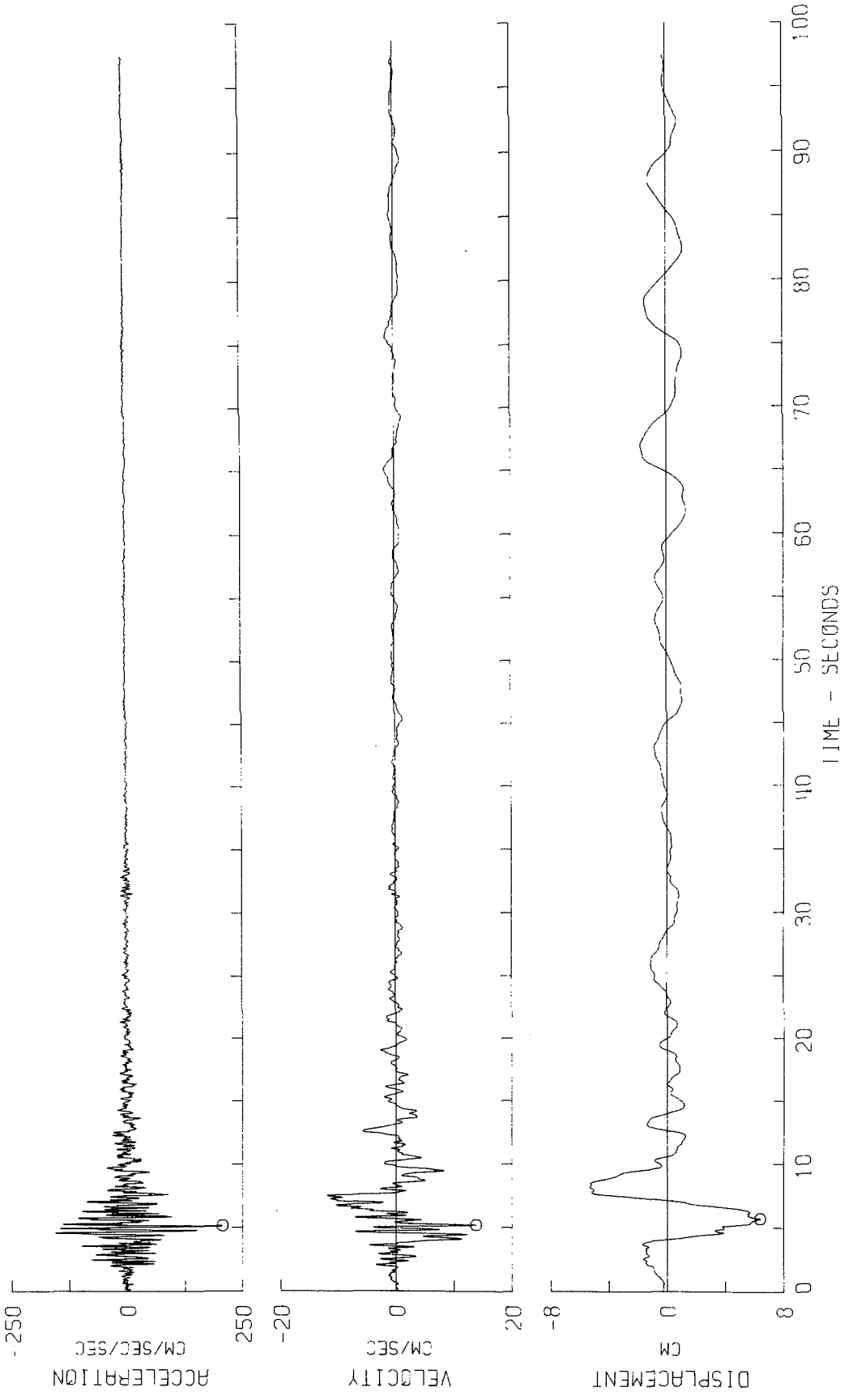
SAN FERNANDO EARTHQUAKE FEB 9, 1971 - 0600 PST
1106H01 '71.032.0 PASADENA, J.P.L., BSMT COMP S82E
PEAK VALUES : ACCEL - 207.2 CM/SEC/SEC VELOCITY - 13.8 CM/SEC DISPL = 6.4 CM
ACCELERATION
CM/SEC/SEC
-250
0
250
VELOCITY
CM/SEC
-20
0
20
DISPLACEMENT
CM
-8
0
8
0
10
20
30
40
50
60
70
80
90
100
TIME - SECONDS

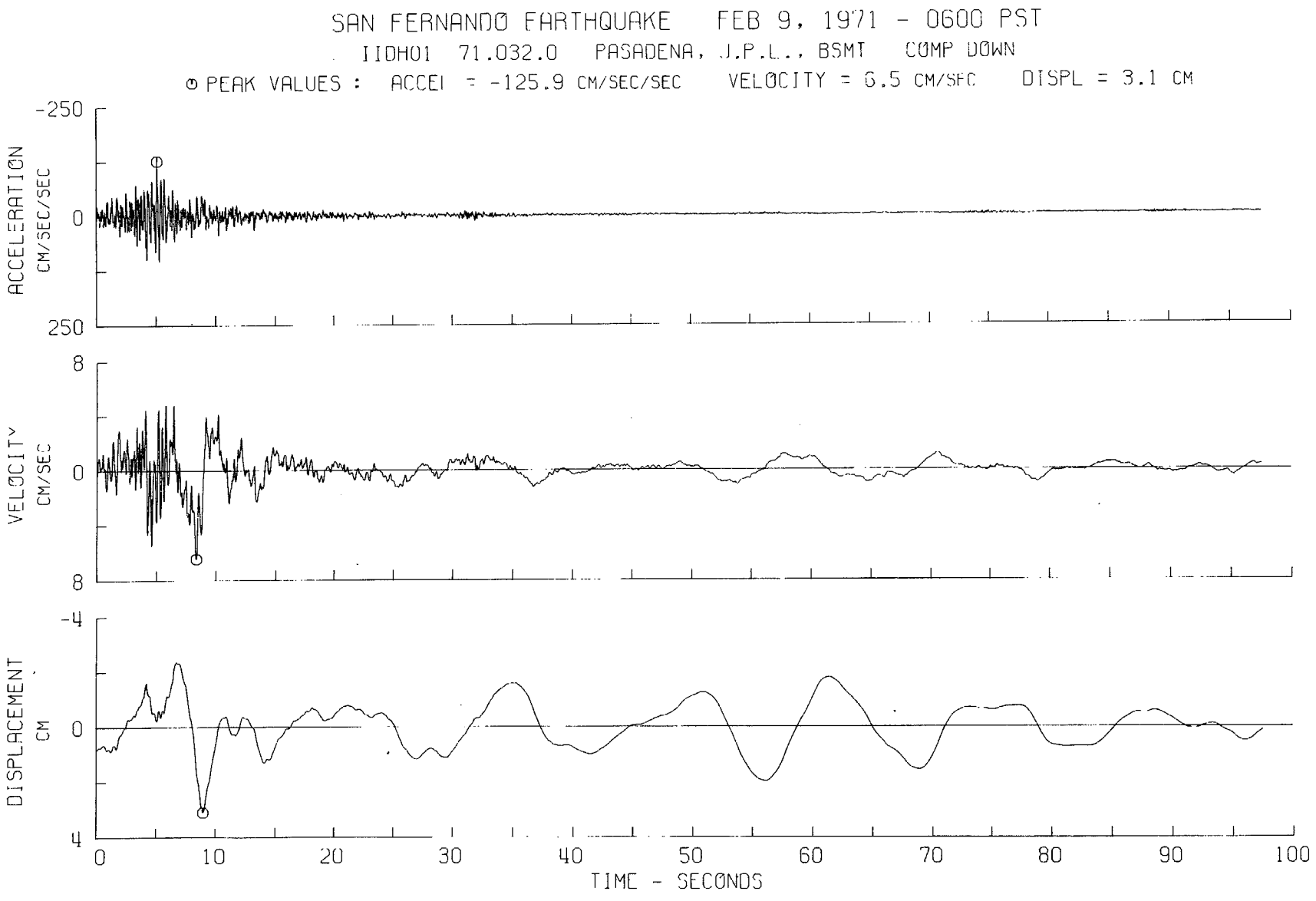
SAN FERNANDO EARTHQUAKE FEB 9, 1971 - 0600 PST
IIDH01 71.032.0 PASADENA, J.P.L., BSMT COMP DOWN
PEAK VALUES : ACCEL = -125.9 CM/SEC/SEC VELOCITY = 6.5 CM/SEC DISPL = 3.1 CM
ACCELERATION CM/SEC/SEC
-250
0
250
VELOCITY CM/SEC
8
0
-8
DISPLACEMENT CM
4
0
-4
0
10
20
30
40
50
60
70
80
90
100
TIME - SECONDS